AEDC-TR-69-179

MEASUREMENTS OF REFRACTIVE INDEX, DENSITY, AND REFLECTED LIGHT DISTRIBUTIONS FOR CARBON DIOXIDE AND WATER CRYODEPOSITS

Peter R. Müller and Walter Frost
The University of Tennessee Space Institute
and
A. M. Smith,
ARO, Inc.

September 1969

ARNOLD ENGINEERING DEVELOPMENT CENTER
AIR FORCE SYSTEMS COMMAND
ARNOLD AIR FORCE STATION, TENNESSEE

NOTICES

When U. S. Government drawings specifications, or other data are used for any purpose other than a definitely related Government procurement operation, the Government thereby incurs no responsibility nor any obligation whatsoever, and the fact that the Government may have formulated, furnished, or in any way supplied the said drawings, specifications, or other data, is not to be regarded by implication or otherwise, or in any manner licensing the holder or any other person or corporation, or conveying any rights or permission to manufacture, use, or sell any patented invention that may in any way be related thereto.

Qualified users may obtain copies of this report from the Defense Documentation Center.

References to named commercial products in this report are not to be considered in any sense as an endorsement of the product by the United States Air Force or the Government.

AEDC-TR-69-179

MEASUREMENTS OF REFRACTIVE INDEX, DENSITY, AND REFLECTED LIGHT DISTRIBUTIONS FOR CARBON DIOXIDE AND WATER CRYODEPOSITS

Peter R. Müller and Walter Frost
The University of Tennessee Space Institute
and
A. M. Smith
ARO, Inc.

FOREWORD

The research reported herein was sponsored by Headquarters, Arnold Engineering Development Center (AEDC), Air Force Systems Command (AFSC), Arnold Air Force Station, Tennessee, under Program Element 61102F, Project 8951.

The results of the research were obtained by ARO, Inc. (a subsidiary of Sverdrup & Parcel and Associates, Inc.) contract operator of AEDC, AFSC, under Contract F40600-69-C-0001. The participation of Peter R. Müller, a citizen of the Federal Republic of Germany, and Walter Frost was provided under ARO Subcontract 70-25-TS/OMD with The University of Tennessee Space Institute. The work was performed under ARO Project Nos. SW5803 and SW5906 during the period from October 1967 through December 1968. The manuscript was submitted for publication on July 17, 1969.

This technical report has been reviewed and is approved.

Michael G. Buja
2nd Lt, USAF
Research Division
Directorate of Plans
and Technology

Harry L. Maynard
Colonel, USAF
Director of Plans
and Technology

ABSTRACT

By using interference techniques, the density and the refractive index as a function of the wavelength of water and carbon dioxide cryodeposit formed at a temperature of 77°K and a deposition pressure of about 4×10^{-4} mm Hg have been measured. It is shown that the Lorenz-Lorentz constant

$$\frac{\mu^2-1}{\mu^2+2} \cdot \frac{1}{\rho} = \text{const}(\lambda)$$

at a certain wavelength computed from the refractive index and density of the cryodeposit is equal to that of the same substance at different temperature and phase, but at the same wavelength. Biangular distributions of the radiation reflected from water and carbon dioxide deposit formed at 77°K on polished copper and black paint substrates have been obtained for various deposit thicknesses and monochromatic light of $\lambda = 0.7\mu$ to 1.0μ. The influence of the deposition rate and of the wavelength of the radiation on the biangular distributions and also on the off-specular shift of the peak of the reflected radiation are investigated. Thus conclusions are drawn about the roughness of the vacuum-deposit interface of the cryodeposit. It is found that water forms a quite smooth interface, while the interface of carbon dioxide is rather rough.

TABLE OF CONTENTS

LIST OF FIGURES

FIGURE PAGE

FIGURE PAGE

FIGURE PAGE

NOMENCLATURE

A	Area of cryoplate
dA	Illuminated area of cryoplate
E	Rate of energy reflected from surface into solid angle $\Delta\omega_r$
de_i	Rate of energy incident on the surface per unit area for a collimated or focussed beam
de_r	Rate of energy reflected from the surface per unit area into a solid angle of 2π steradians
$\vec{e}$	Electric field vector
I	Intensity of reflected radiation defined by Equation (3)
k	Constant of proportionality
$\dot{m}$	Mass flow rate of gas
p	Pressure
p^*	Carbon dioxide reservoir pressure
R	Gas constant
T	Temperature
t	Time
Δt	Time between two interference maxima
Δt^*	Time between initial and final pressure measurements in carbon dioxide flow rate measurement
V	Volume

Greek Letters

α	Leak constant defined in Equation (18)
β	Constant of Proportionality
γ	Phase shift angle between electric field vector of radiation reflected off the interface and the substrate
μ	Refractive index
λ	Wavelength
τ	Thickness of deposit
$\dot{\tau}$	Deposition rate
ρ	Density
ρ_{ah}	Angular-hemispherical reflectance
ψ	Angle of incidence
θ	Viewing angle
ε	Phase shift angle
$\Delta\theta$	Off-specular shift as defined in Equation (2)
κ	Absorption coefficient
$\Delta\omega_r$	Solid angle of reflected radiation
ω	Circular frequency

Subscripts

1	Interface
2	Substrate
a,b	Different measurements
Br	Brewster angle
max	Value at interference maximum or magnitude of peak of biangular distribution
min	Value at interference minimum
p	Parallel to the plane of the incident radiation
s	Perpendicular to the plane of the incident radiation

CHAPTER I

INTRODUCTION

Most present day space simulation chambers employ cryogenic pumping. Thus the test vehicle is surrounded by panels which are cooled to 77°K with LN_2 coolants. In order to minimize the reflection of radiation from the panels they are painted black. During the period of testing, however, cryodeposits form on the cold panels changing the radiative surface properties and in turn altering the thermal heat balance on the test vehicle. In order to be able to correct the resulting thermal balance test data, it is necessary to investigate the influence of cryodeposits on the reflection of radiation from the cold panels. This includes angular-hemispherical reflectance measurements[1] and measurements of the biangular distribution of the reflected radiation. In order to obtain the thickness of the cryodeposits in these tests, the refractive index and density are needed.

Wood et al. [1][2] report detailed angular-hemispherical reflectance measurements which have been obtained

---

[1]The surface is irradiated angularly, and the hemispherically reflected radiation is measured.

[2]Numbers in brackets refer to similarly numbered references in the bibliography.

for carbon dioxide and water cryodeposits on copper and black paint substrates. Biangular distribution measurements of white light reflected from carbon dioxide deposit formed on copper and black paint substrates were performed by Tempelmeyer et al. as reported in [2]. The biangular measurement technique is illustrated in Figure 1. The deposit is illuminated with a collimated beam of light at a certain angle of incidence ψ, and the rate of energy $E(\psi,\theta,\tau)$ reflected into the solid angle $\Delta\omega_r$ is measured at different angles θ within the plane of the incident light. The resulting distributions show how cryodeposits affect the angular distribution of radiation reflected from cold panels in space chambers. It was found that cryodeposits have a diffusing effect on the radiation reflected from specular substrates so that with increasing deposit thickness the specularly reflected component decreases and finally disappears. Moreover, the following phenomena were observed:

1. Thin film interference at the specular angle
2. Scattering interference
3. Backscattering
4. Off-specular shifts

Scattering interference was investigated in detail by Tempelmeyer et al. and reported in [3] and [4], and a theory was developed which relates the maxima and minima of the reflected radiation at certain viewing angles θ

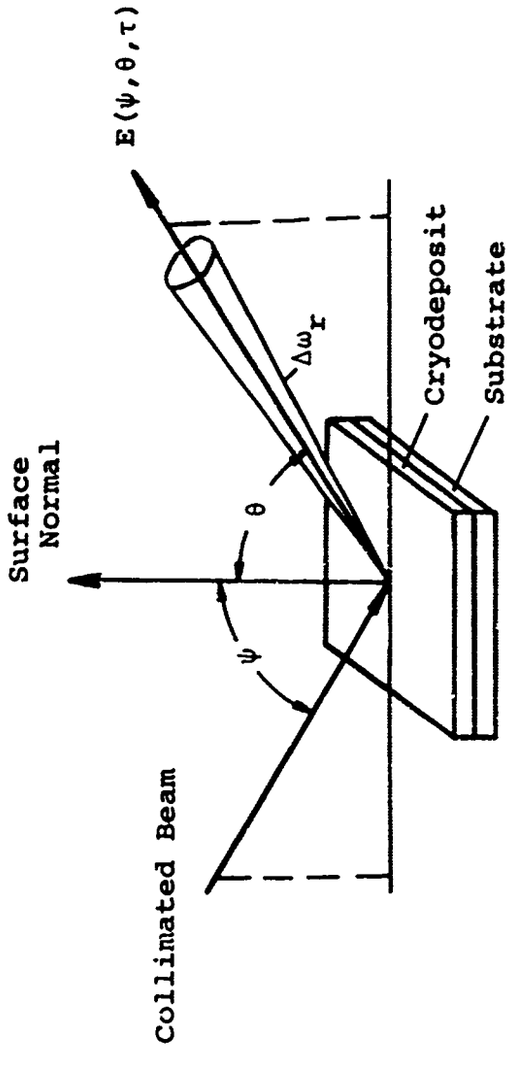

Figure 1. Coordinates for incident and reflected radiation.

to constructive and destructive interference of the ray reflected from the cryodeposit and the ray reflected from the substrate. Using this theory the thickness of the deposit can be calculated which enables computation of the density of the deposit if the mass of the condensed gas is known. This technique to measure the density was used by Tempelmeyer et al., and values of the density of carbon dioxide deposit are reported in [3], as well as the refractive index of carbon dioxide deposit at different wavelengths. The refractive index was measured by another interference technique employing the thin film interference which will be explained in detail in Chapter II. However, these reported values do not satisfy the Lorenz-Lorentz law:

$$\frac{\mu^2-1}{\mu^2+2} \cdot \frac{1}{\rho} = \text{constant} \qquad (1)$$

which is generally valid even if the substance changes its phase. The value of the constant is compared for various substances in the gaseous and liquid phase by Born and Wolf in [5], and it is found that the change of the constant due to the change of phase is very small.

The Lorenz-Lorentz constant of the carbon dioxide cryodeposit calculated with the refractive index and density of 1.35 gr/cm^3 at a deposition pressure of 10^{-4} mm Hg reported in [3] is 0.203 cm^3/gr at a wavelength of 0.589μ, while the magnitude of the constant for liquid carbon dioxide at a temperature of 15°C = 59°F and at

0.589μ calculated from data given in [6] is 0.153 cm^3/gr. It is therefore felt that the measured density is in error.

Caren et al. [7] measured the density of carbon dioxide and water cryodeposits at thicknesses on the order of 1 mm. The density reported for water deposit at 77°K is 0.51 to 0.64 gr/cm^3 at a deposition pressure of 4.6×10^{-4} mm Hg; and for carbon dioxide deposit at 77°K, the density is 1.28 to 1.63 gr/cm^3 at a deposition pressure of 3.8×10^{-3} mm Hg. The density of carbon dioxide deposit on a 90°K surface was reported by Mass and Barnes in [8] as 1.674 gr/cm^3. These results show considerable scatter; and it is therefore necessary to perform new measurements of the refractive index and density of carbon dioxide and water cryodeposits.

A further objective of the following investigation is to present measurements of biangular distributions of the radiation reflected from carbon dioxide and water cryodeposits formed on polished copper and black paint substrates at a deposition pressure of approximately 4×10^{-4} mm Hg for both deposits. These measurements will be performed with filtered light of various wavelengths between 0.7μ and 1.0μ. The angle of incidence of the light beam irradiating the cryodeposit will range from 0° to 66°, and the reflected radiation will be measured in the plane of incidence. These distributions are a first step to obtain correction factors for thermal

balance tests. However, it is not intended in this work to investigate these correction factors.

The emphasis of this work will be placed on phenomena observed from the biangular distributions of the reflected radiation. The off-specular shift of the peak of the distribution and the magnitude of the peak of the distribution of the reflected radiation as a function of deposit thickness will be investigated in detail including the influence of wavelength and deposition rate. In addition the amount of radiation reflected from the vacuum-deposit interface of the cryodeposit compared to the total amount of radiation reflected from the cryodeposit will be estimated. The investigations are intended to obtain an idea about the roughness of the interface of carbon dioxide and water cryodeposits and thus about the structure of the deposit formed at the deposition pressure and temperature used in this work. Results of other investigators using x-ray diffraction techniques to determine the structure of the deposit at various deposition pressures and temperatures, are compared with the findings of this investigation. However, no definite conclusion can be drawn from the measurements of this investigation about the exact structure of the deposit obtained in this work.

An additional remark is necessary concerning the definition of the off-specular shift. In this entire work the off-specular shift is defined as

$$\Delta\theta = \theta\Big|_{E_{max}} - \psi \tag{2}$$

where $\theta\Big|_{E_{max}}$ is the angle θ at which $E(\psi,\theta)$, the rate of energy reflected from the sample into a certain solid angle, has its maximum. Torrance et al. [9], who investigated off-specular shifts on rough surfaces earlier, defined the off-specular shift as

$$\Delta\theta = \theta\Big|_{I_{max}} - \psi$$

where $\theta\Big|_{I_{max}}$ is the angle θ at which $I(\psi,\theta)$, the intensity of the reflected radiation, has its maximum. The intensity of the reflected radiation is defined as

$$I(\psi,\theta) = \frac{E(\psi,\theta)}{\cos\theta \cdot dA\ (\psi) \cdot \Delta\omega_r} \tag{3}$$

where $dA\ (\psi)$ is the illuminated area of the cryosurface, and $\Delta\omega_r$ is the solid angle into which the radiation $E(\psi,\theta)$ is reflected from the cryosurface. Since

$$I(\psi,\theta) \sim \frac{E(\psi,\theta)}{\cos\theta}$$

it can be concluded that $I(\psi,\theta)$ and $E(\psi,\theta)$ have their respective peaks at different angles θ. Thus the two different definitions of $\Delta\theta$ lead to different values of the off-specular shift.

In order to measure the reflected intensity directly, Torrance [9] used the "over-illumination technique." If this technique is used, the solid angle, at which the detector "sees" the illuminated area, is maintained constant. Thus the viewed area projected in the direction of θ, $A\cos\theta$, stays constant while the viewed area of the sample, A, changes with θ. The rate of energy measured by the detector with this technique corresponds to the intensity $I(\psi,\theta)$ in Equation (3). But this technique has one drawback. In order to measure the reflected intensity $I(\psi,\theta)$ properly, it is necessary that the sample be irradiated in such a manner that the incident intensity is equal at every point of the viewed area. Experience shows that it is very hard to fulfill this requirement, which can be dropped, if the reflected rate of energy $E(\psi,\theta)$ from a constant viewed area is measured, and $E(\psi,\theta)$ is in this case an average reading of the light reflected from the whole illuminated area. This technique is called the "over-detection technique" and was used in this investigation because of the following reasons:

1. It does not require uniform irradiation of the sample.
2. The detector "sees" the whole illuminated area, and thus no devices are necessary which limit the solid angle at which the detector "sees" the illuminated area.
3. The detecting system is very simple and no complicated alignment which would have to be done inside the vacuum chamber, is necessary.

CHAPTER II

MEASUREMENTS ON CRYODEPOSITS

I. THEORETICAL FOUNDATIONS FOR THE MEASUREMENT OF REFRACTIVE INDEX AND DENSITY OF A CRYODEPOSIT

The measurement of the refractive index and density of cryodeposits parallels that of Tempelmeyer et al. [3] who, after Wood et al. [1], reported interference phenomena on thin films of cryodeposits and gave a simple theory relating these to the refractive index and density of the deposits. The method is described in the following.

As shown in Figure 1, page 3, a collimated light beam strikes the cryodeposit at a certain angle of incidence ψ with respect to the normal on the surface. This beam is partially reflected at the vacuum-deposit interface and partially transmitted through the cryodeposit. The transmitted beam is reflected at the substrate and depending on the cryodeposit thickness interferes constructively or destructively with the beam reflected from the interface.

The procedure used to obtain thin film interference patterns consists of setting a light detector at the specular angle ($\theta = \psi$). Then cryofrost is continuously

deposited on the cold surface at a constant rate, and the output of the light detector is monitored as a function of time. The recorded detector output shows subsequent interference maxima and minima.

An analysis of the phase difference between the beam reflected from the interface and the beam reflected from the substrate, as reported in [3], shows that the incremental change in thickness of the deposit between the occurrence of two interference maxima is given by

$$\Delta\tau = \frac{\lambda}{2\mu\sqrt{1 - \frac{\sin^2\psi}{\mu^2}}} \tag{4}$$

and is independent of the phase change by reflection from the substrate. This equation is based on Snell's law which assumes that the deposit does not exhibit any absorption. However, if the amount of absorption is small, Snell's law will still give a good approximation.

The increase of the deposit thickness $\Delta\tau$ is related to the deposition rate $\dot{\tau}$ by

$$\Delta\tau = \dot{\tau} \cdot \Delta t \tag{5}$$

where Δt is the time between the occurrence of two interference maxima.

Equating Equations (4) and (5) gives

$$\dot{\tau} \cdot \Delta t = \frac{\lambda}{2\mu\sqrt{1 - \frac{\sin^2\psi}{\mu^2}}} \tag{6}$$

which contains $\dot{\tau}$ and μ. Be measuring Δt at two different angles of incidence ψ_a and ψ_b and constant deposition rate for a given wavelength, Equation (6) can be solved for μ and $\dot{\tau}$.

$$\mu^2 = \frac{\sin^2\psi_b - \left(\frac{\Delta t_a}{\Delta t_b}\right)^2 \sin^2\psi_a}{1 - \left(\frac{\Delta t_a}{\Delta t_b}\right)^2} \tag{7}$$

$$\dot{\tau} = \frac{1}{\Delta t_a} \cdot \frac{\lambda}{2\mu\sqrt{1 - \frac{\sin^2\psi_a}{\mu^2}}} \tag{8}$$

Where Δt_a corresponds to ψ_a, and Δt_b corresponds to ψ_b.

Equations (4) and (8) are valid for unpolarized light and a substrate of polished copper, even though the phase change of the ray reflected at the polished copper is different for parallel and perpendicular polarized radiation. This can be proven in the following way.

It is assumed that the electric field vectors of the parallel polarized component of the radiation reflected

from the vacuum deposit interface and of the radiation reflected from the substrate are $\vec{e}_{1p}$ and $\vec{e}_{2p}$ respectively; and the electric field vectors of the perpendicular polarized component of the radiation reflected from the vacuum deposit interface and of the radiation reflected from the substrate are $\vec{e}_{1s}$ and $\vec{e}_{2s}$ respectively. The phase angle between $\vec{e}_{1p}$ and $\vec{e}_{2p}$ is $\gamma_p(t) = \omega \cdot t$; the phase angle between $\vec{e}_{1s}$ and $\vec{e}_{2s}$ is $\gamma_s(t) = \omega t + \varepsilon$, where ε results from the different phase change of parallel and perpendicular polarized light reflected from the polished copper substrate. The circular frequency ω is independent of this phase change and is thus equal for parallel and perpendicular polarized radiation. Interference of $\vec{e}_{1p}$ and $\vec{e}_{2p}$ and also $\vec{e}_{1s}$ and $\vec{e}_{2s}$ yields

$$|\vec{e}_p|^2 = |\vec{e}_{1p}|^2 + |\vec{e}_{2p}|^2 - 2|\vec{e}_{1p}| \cdot |\vec{e}_{2p}| \cdot \cos \omega t \tag{9}$$

$$|\vec{e}_s|^2 = |\vec{e}_{1s}|^2 + |\vec{e}_{2s}|^2 - 2|\vec{e}_{1s}| \cdot |\vec{e}_{2s}| \cdot \cos (\omega t - \varepsilon) \tag{10}$$

where $\vec{e}_p$ is the electric field vector of the parallel polarized component of the detected signal, and $\vec{e}_s$ is the electric field vector of the perpendicular polarized component. By using

$$|\vec{e}|^2 = \beta \cdot I \tag{11}$$

where β is a constant of proportionality, and

$$\cos(\omega t-\varepsilon) = \cos\omega t\cdot\cos\varepsilon + \sin\omega t\cdot\sin\varepsilon,$$

Equations (9) and (10) can be written as

$$\beta I_p = \beta I_{1p} + \beta I_{2p} - 2\beta\sqrt{I_{1p}\cdot I_{2p}}\cdot\cos\omega t \tag{12}$$

$$\beta I_s = \beta I_{1s} + \beta I_{2s} - 2\beta\sqrt{I_{1s}\cdot I_{2s}}\cdot\cos\omega t\cdot\cos\varepsilon - 2\beta\sqrt{I_{1s}\cdot I_{2s}}\cdot\sin\omega t\cdot\sin\varepsilon \tag{13}$$

The total detected intensity is

$$I = I_p + I_s \tag{14}$$

Equations (12) and (13) are substituted in Equation (14), and it is obtained

$$I = \underbrace{I_{1p} + I_{2p} + I_{1s} + I_{2s}}_{I^*} - [\underbrace{(2\sqrt{I_{1p}\,I_{2p}} + 2\sqrt{I_{1s}\,I_{2s}}\cos\varepsilon)}_{B_1}\cos\omega t + \underbrace{2\sqrt{I_{1s}\,I_{2s}}\sin\varepsilon}_{B_2}\cdot\sin\omega t] \tag{15}$$

where I^*, B_1 and B_2 are independent of ω and t.

$$I = I^* - (B_1 \cos \omega t + B_2 \sin \omega t)$$

can be also written in the form

$$I = I^* - B^* \cdot \cos (\omega t - \varepsilon^*)$$

where ε^* is a phase shift angle which is different from the phase shift angle ε. However, the circular frequency ω of the sum of the parallel and perpendicular polarized components of unpolarized radiation is equal to ω of the polarized components; and thus the time between the occurrence of two interference maxima is equal. This shows that Equations (4) to (8) are also valid if a polished copper substrate and unpolarized radiation are used for the measurement of the refractive index μ and the deposition rate $\dot{\tau}$.

By assuming that the cryodeposit forms a film of uniform thickness over the whole cryosurface, the density of the deposit is obtained from

$$\rho = \frac{\dot{m}}{A \cdot \dot{\tau}} \qquad (16)$$

where A is the area of the cryoplate; and $\dot{m}$ is the mass flow rate of the water vapor or carbon dioxide, respectively.

II. EXPERIMENTAL APPARATUS

A. Vacuum System

The tests on cryodeposits were conducted in a 76 cm diameter spherical vacuum chamber consisting of two stainless steel hemispheres joined with an O-ring seal shown schematically in Figure 2. The interior surface of the chamber was coated with flat black paint to minimize internal reflections.

The pumping system consisted of a 400 liter/min mechanical pump and a 6 inch oil diffusion pump equipped with an LN_2 - cooled cold trap. Pressures of 1×10^{-6} mm Hg were easily obtained. As seen in Figure 2, the chamber could be valved off from the pumping system. Valves were also provided to by-pass the diffusion pump and to isolate the diffusion pump from the mechanical pump. Thus it was possible to open the chamber and pump it down from atmospheric pressure, even if the diffusion pump was hot.

The pressure inside the chamber was measured with a thermal ionization gauge at pressures below 10^{-3} mm Hg and with an alpha radiation ionization gauge at pressures above 10^{-3} mm Hg.

B. Cryosurface

The cryosurface had a diameter of 10.3 cm and was located in the center of the sphere. The construction of the cryosurface is shown in Figure 3. The cryoplate was

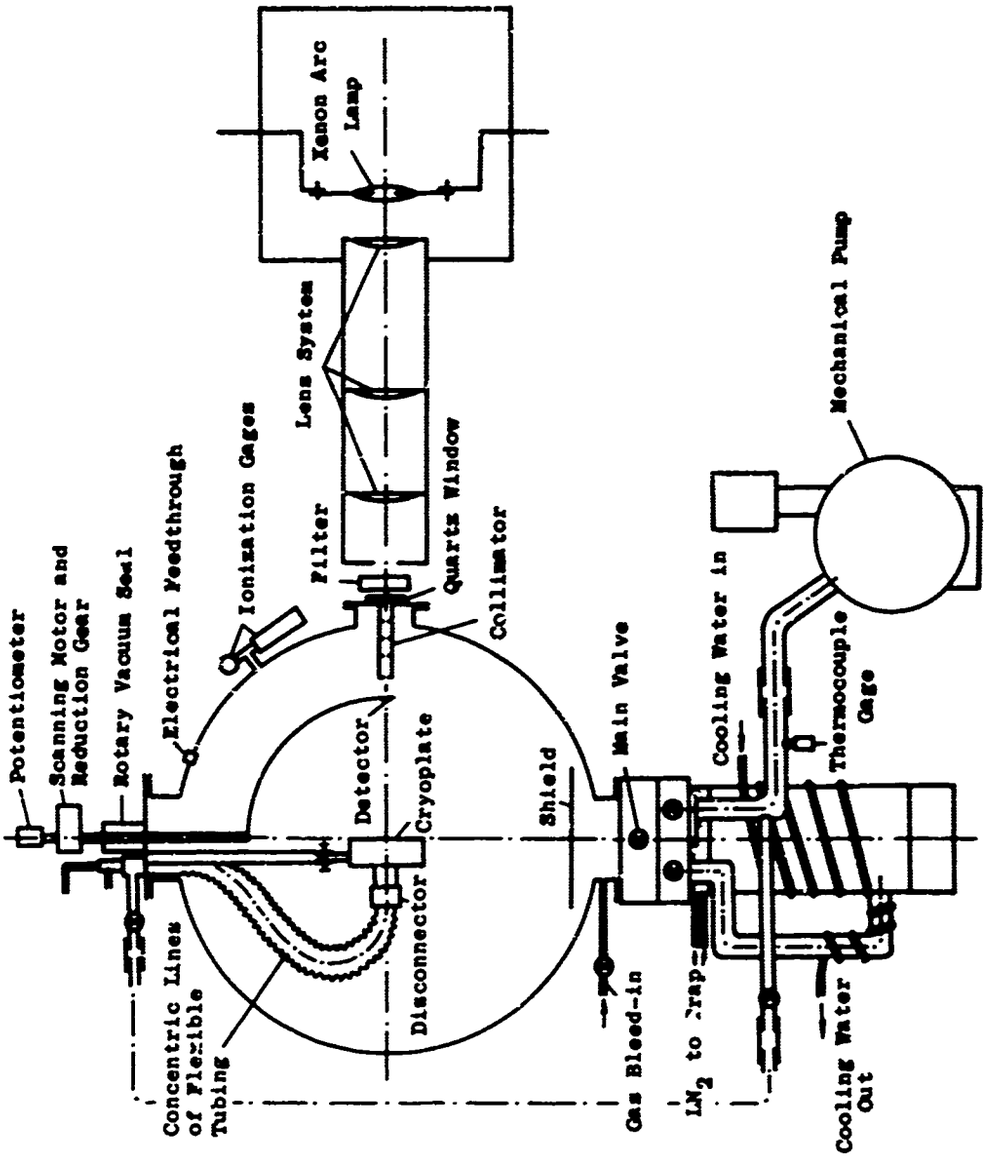

Figure 2. Experimental apparatus for measurements on cryodeposits.

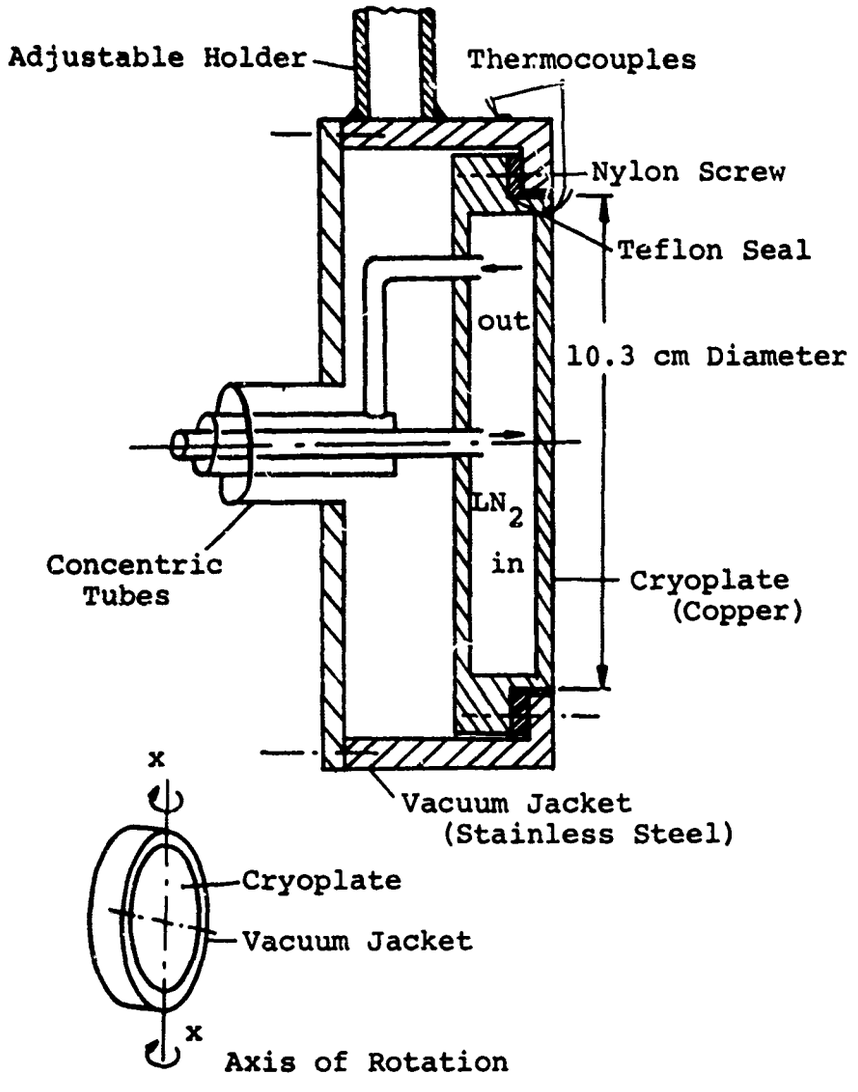

Figure 3. Construction of cryoplate.

made out of copper for good heat conduction, and the vacuum jacket surrounding it was made of stainless steel covered with a flat black paint. The cryoplate and vacuum jacket were circular, since this shape could easily be machined to close tolerances. In order to prevent unequal deposit thickness at different locations of the plate due to edge effects, the insulating jacket was flush with the front face of the plate. As shown in Figure 3, there was a gap of about 0.5 mm between the cryoplate and the jacket. Between the plate and the jacket, a teflon seal was located which was not vacuum tight, but which inhibited metallic contact and thus excessive heat conduction. Nylon screws held the cryosurface in place. The cryosurface was polished to a rms surface roughness of less than 0.01μ. In some tests it was coated with flat black epoxy paint. The temperature of the cryoplate and jacket were monitored with conventional thermocouples.

The cryosurface could be rotated about axis X-X, shown in an insert in Figure 3, to any desired angle with an accuracy of ± 0.5° using a protractor indexing device and to multiples of 11° by means of stops that permitted very accurate setting of the angle of incidence of the light beam with respect to the normal of the plate. This stop mechanism consisted of a ring with a number of holes equally spaced in intervals of 11°. The ring was mounted

in such a way that it could be easily readjusted. The LN_2 feed lines to the cryoplate were concentric flexible tubes surrounded by a vacuum jacket which could be continuously evacuated with the mechanical pump. In order to facilitate disassembly of the cryoplate and jacket the LN_2 lines were connected by copper shear seals and the jacket line by flanges.

C. Gas Addition Systems

The gas addition systems for the water vapor and the carbon dioxide are shown in Figure 4. The distilled water was kept in a reservoir which was cooled by tap water. The temperature of the tap water remains essentially constant during a given day, and thus the vapor pressure of the water inside the reservoir remained constant during a given test. Cooling the reservoir with tap water also had the advantage that no condensation occurred in the line between the reservoir and the rotameter and in the glass tube of the rotameter below the ball, since tap water is always cooler than room temperature.

Before starting a test, the gas flow was diverted to a mechanical pump until steady state flow conditions were obtained. Steady state conditions were assumed to be established when the ball in the rotameter tube became stationary. Then the gas flow rate was adjusted with a needle valve.

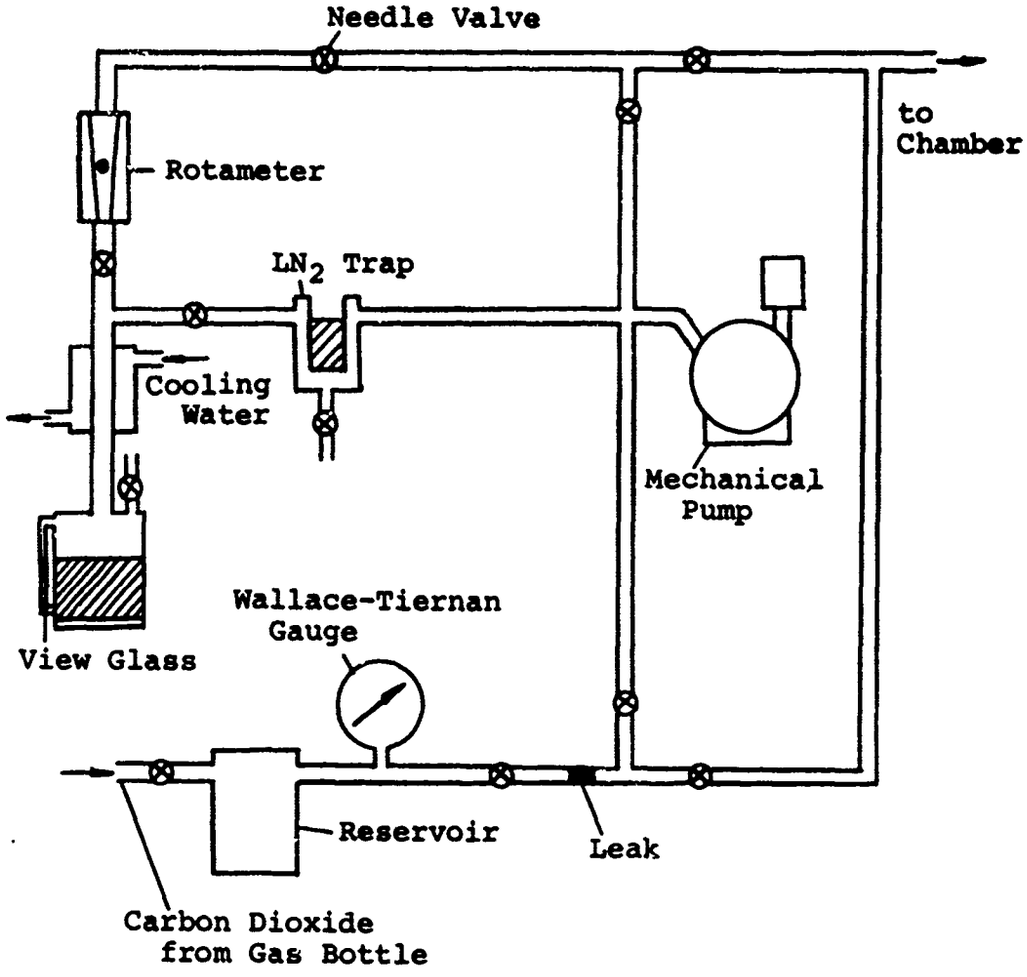

Figure 4. Gas addition system.

The level of the water inside the reservoir could be checked with a view glass as seen in Figure 4. Each time the reservoir was refilled with water, the air inside the reservoir was pumped out with a mechanical pump. An LN_2 filled cold trap prevented water from getting into the pump.

Carbon dioxide which had a purity of 99.8 percent was supplied to a reservoir which was maintained at an essentially constant pressure of 760 mm Hg as measured by a Wallace-Tiernan gauge. The gas was introduced to the vacuum chamber by means of a commercially available orifice leak.

D. Generation of Collimated Light Beam

A xenon arc lamp was used as a radiation source because the state-of-the-art solar simulators employ high power xenon arc lamps as radiation sources. The light output of a xenon arc lamp as a function of the wavelength is shown in Figure 5. Strong emission lines are observed between 0.8μ and 1.0μ which indicates that the characteristic wavelength of the unfiltered light is about 0.9μ.

The collimated beam is obtained by means of a lens system and a collimator tube built into the vacuum chamber port as shown in Figure 2, page 17. It is also

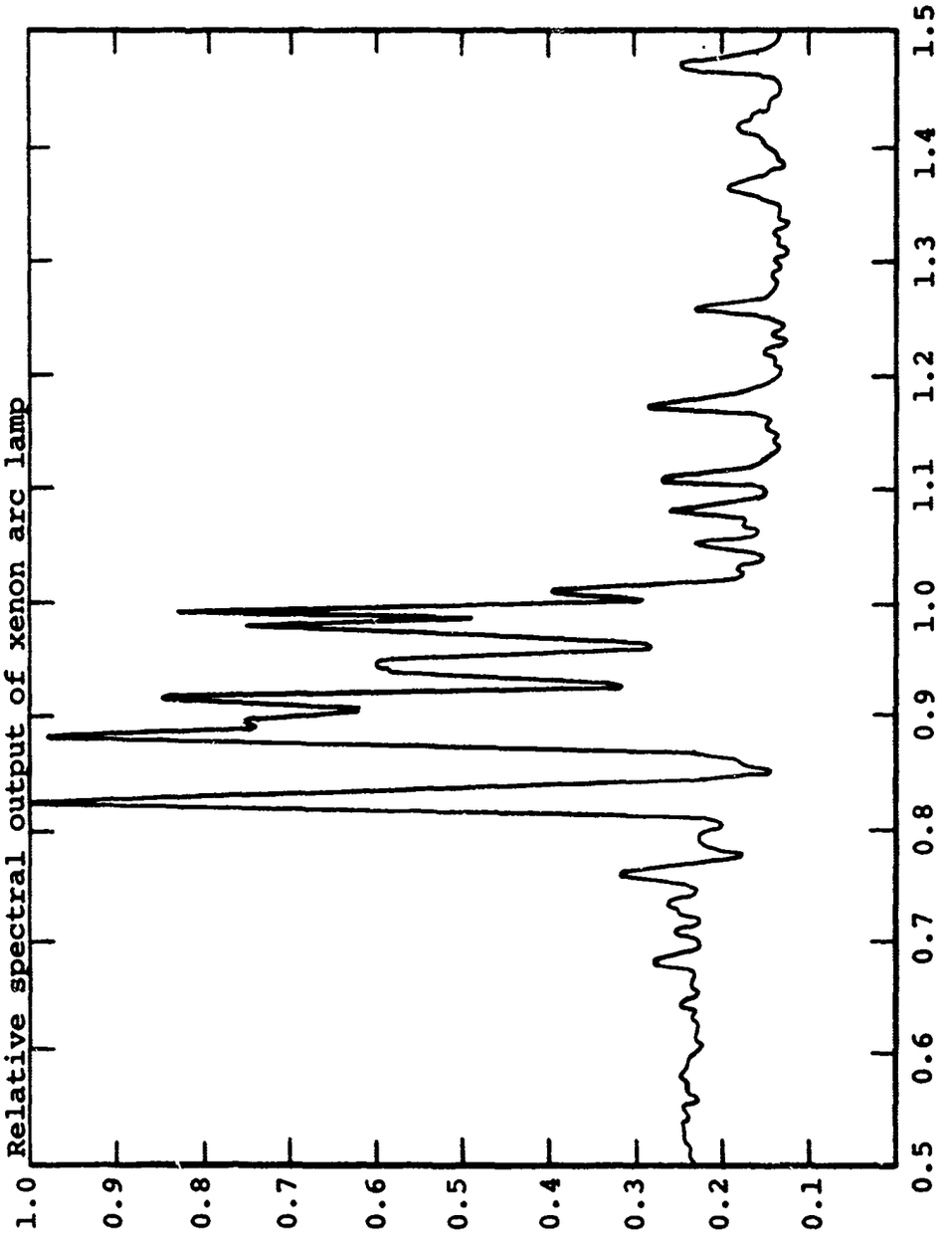

Figure 5. Relative spectral output of xenon arc lamp.

seen that interference-type filters could be inserted into the light beam to obtain monochromatic irradiation of the cryosurface.

E. Detection of Reflected Radiation and Recording

A silicon solar cell (8 mm × 3 mm) served as a light detector. It was mounted on a remotely controlled arm which could be rotated at a constant angular velocity through a range from $\theta = -90°$ to $\theta = +90°$. The axis of rotation of the detector was the vertical centerline of the cryosurface; and the detector stayed within the plane of the incident light. The distance between detector and cryosurface was 25 cm.

To insure good linearity of the recorded signal, the detector output was loaded with a resistor of 100 ohms. The voltage at the resistor was recorded with either an X-Y plotter with a lowest full scale of 5 mV or a conventional strip-chart recorder with a lowest full scale of 0.1 mV.

III. TEST PROCEDURE

A. Measurements of Refractive Index and Deposition Rate for Water and Carbon Dioxide Cryodeposit

The procedure for measuring the refractive index μ and the deposition rate $\dot{\tau}$ of the cryodeposit was essentially the same for water and carbon dioxide. These measurements were performed only on a substrate of polished copper.

Initially the chamber was pumped down to a pressure of about 1×10^{-6} mm Hg in order to have very little foreign deposit formed on the cryosurface when cooling it down to a temperature of 77°K. The temperature of the cryoplate was monitored with a thermocouple attached to the plate. After the plate reached 77°K, the xenon arc lamp was turned on. Experience showed that after about five minutes the lamp light output reached equilibrium. This could be observed by measuring the time variation of the radiation reflected from the cryoplate at constant viewing angle θ and for constant angle of incidence ψ. Equilibrium was assumed to be established when the detector output became constant with time.

As discussed before the gas addition system also was started about five minutes prior to the test in order to establish a constant gas flow rate which was essential for these measurements. The gas flow during these five minutes was diverted to a mechanical pump.

At an angle of incidence of 0°, the biangular distribution of the reflected radiation is symmetrical about $\theta = 0°$. The setting for this angle of incidence was easily found and the stop mechanism, which sets the angle of incidence accurately to multiples of 11°, was readjusted at this angle of incidence. After this readjustment the plate was set to an angle of incidence of 33°, and the detector was positioned in the specular direction

($\theta = \psi$). An interference-type filter was inserted into the beam incident on the cryosurface. After valving off the chamber from the pumping system, a cryodeposit was formed on the cold surface with a constant deposition rate $\dot{\tau}$ by bleeding water vapor or carbon dioxide at a constant mass flow rate $\dot{m}$ into the chamber.

The radiation reflected from the cryodeposit in the specular direction was monitored continuously with a strip-chart recorder. The time between each two interference maxima was checked. Since this time remained constant, one was further assured that the gas flow rate remained constant. The flow was stopped after six to ten interference maxima which were a sufficient number to give an accurate average value of the time between two interference maxima Δt.

The pressure of the residual noncondensible gases did not exceed 2×10^{-4} mm Hg. This gas was subsequently pumped out of the chamber. Then the cryoplate was set to an angle of incidence of 55° and the detector at the specular angle. In the same manner as before interference maxima and minima were obtained for the new angle of incidence.

By using Equation (7) and the measured values of Δt_a and Δt_b at the angles of incidence ψ_a and ψ_b the refractive index μ is obtained and the deposition rate $\dot{\tau}$ is computed from Equation (8).

B. Measurement of the Flow Rate of Water Vapor

In a separate test immediately following the previous experiment, the flow rate $\dot{m}$ of the water vapor used for the measurement of the refractive index and deposition rate was measured by condensing the water in a glass vessel cooled with LN_2. From the measurement of the weight of the glass vessel initially and after a specified time (normally 15 minutes) the gas flow rate $\dot{m}$ could be computed. The weight was measured on an analytical balance with an accuracy of 10^{-3} gr. The glass vessel was allowed to reach room temperature prior to the weighing in order to prevent convection currents between the glass surface and the atmosphere from effecting the accuracy of the measurement.

C. Measurement of the Flow Rate of Carbon Dioxide

The flow rate $\dot{m}$ of carbon dioxide was measured by monitoring the gas pressure in the reservoir valved off from the gas supply while bleeding gas through the leak into the chamber (see Figure 4, page 21). This pressure changed sufficiently slowly that equilibrium could be assumed at every instant.

The chamber pressure was maintained at a pressure of approximately 4×10^{-4} mm Hg. This pressure corresponded to the deposition pressure which was established during the measurement of the refractive index and the

deposition rate. Since the chamber pressure was equal during this previous measurement and the following measurement of the flow rate, it was assumed that the flow rate through the leak was equal in both measurements. This chamber pressure of 4×10^{-4} mm Hg was obtained by pumping with the mechanical pump and the cold trap. The diffusion pump was switched off.

The reservoir was filled with carbon dioxide to the normal operating pressure $p^* = 760$ mm Hg. Then the gas supply was valved off and the valve to the leak opened. The gas pressure inside the reservoir was read initially as p^* and at time Δt^* as p_a.

The gas flow rate $\dot{m}$ at the normal operating reservoir pressure p^* is obtained by differentiating the equation of state

$$p \cdot V = m \cdot R \cdot T$$

with respect to time so that

$$\dot{m} = \frac{V_R}{R_{CO_2} \cdot T} \cdot \left.\frac{dp}{dt}\right|_{p^*} \tag{17}$$

where V_R is the volume of the reservoir. T is the temperature of the gas inside the reservoir which is equal to room temperature of 300°K. To derive an expression for $\left.\frac{dp}{dt}\right|_{p^*}$, it can be assumed that the flow rate is proportional

to the gas pressure p. Since the flow rate is also proportional to $\frac{dp}{dt}$, as seen in Equation (17), it can be stated that $\frac{dp}{dt}$ is proportional to p. This can also be written as

$$\frac{dp}{dt} = \alpha \cdot p \tag{18}$$

where α is a constant depending on the leak. Integrating Equation (18) leads to

$$\ln p = \alpha \cdot t + C_1$$

The boundary conditions are

$$p = p^* \quad \text{at} \quad t = 0$$

and

$$p = p_a \quad \text{at} \quad t = \Delta t^*$$

so that

$$\ln p^* = C_1 \tag{19}$$

$$\ln p_a = \alpha \, \Delta t^* + C_1 \tag{20}$$

Equations (19) and (20) are solved for α,

$$\alpha = \frac{1}{\Delta t^*} \ln \frac{p_a}{p^*} \tag{21}$$

and α is introduced into Equation (18). It is thus obtained at $p = p^*$

$$\left.\frac{dp}{dt}\right|_{p^*} = \frac{1}{\Delta t^*} \cdot \ln \frac{p_a}{p^*} \cdot p^* \tag{22}$$

In order to compute the reservoir volume V_R, the reservoir was evacuated to a pressure of about 10^{-3} mm Hg and connected with a vessel of known volume V_C filled with carbon dioxide at a pressure p_c of about 760 mm Hg. The gas was then allowed to flow into the evacuated vessel. After equilibrium pressure was reached, the common pressure p_e was read. The reservoir volume was computed from

$$p_c \cdot V_C = p_e \, (V_C + V_R) \tag{23}$$

which can be solved for V_R

$$V_R = \frac{p_c - p_e}{p_e} \cdot V_C \tag{24}$$

The volume V_C was found by filling the vessel slowly with distilled water so that no air bubbles formed inside. The weight of the water divided by its density is equal to the volume of the vessel.

By introducing Equation (22) for $\left.\frac{dp}{dt}\right|_{p^*}$ and Equation (24) for V_R into Equation (17), the gas flow rate at normal

operating reservoir pressure p^* is obtained

$$\dot{m} = \frac{p_c - p_e}{p_e} \cdot \frac{V_c}{R_{CO_2} \cdot T} \cdot \frac{1}{\Delta t^*} \cdot \ell n \frac{p_a}{p^*} \cdot p^* \quad (25)$$

D. Measurement of Biangular Distributions of the Reflected Radiation

The measurement of biangular distributions of the radiation reflected from carbon dioxide and water cryodeposits was carried out by forming the deposits on either polished copper or black paint substrates at a deposition pressure of approximately 4×10^{-4} mm Hg. This was done in the following way.

After the vacuum chamber had been evacuated to a pressure of about 10^{-6} mm Hg, the xenon lamp was turned on, and biangular distributions of the radiation reflected from the bare substrate, either polished copper or black paint, were measured for various angles of incidence ψ.

Next, the cryoplate was cooled to 77°K. The plate was set at an angle of incidence of 22°, the detector was positioned in the direction of the specular angle, and an interference-type filter with a peak transmission at a certain wavelength λ was inserted into the beam as shown in Figure 2, page 17. After valving off the chamber from the pumping system, either water vapor or carbon dioxide was introduced into the chamber, and the detector

output was monitored on a strip-chart recorder. The time between two maxima of the arising interference pattern was measured, and the deposition rate $\dot{\tau}$ was computed from Equation (8) using the refractive index which was measured before.

Cryodeposits of specified thickness were then formed by flowing either water vapor or carbon dioxide into the chamber for a specified time. After the flow was stopped, biangular distributions of the reflected radiation were recorded for various values of ψ. Then gas was added again to the chamber, so that another cryodeposit layer formed on the first; and the radiation measurements were repeated. This procedure was continued, and measurements of the reflected radiation were made for each resulting cryodeposit thickness.

Biangular distributions could be conveniently recorded on the X-Y plotter where one coordinate was the detector output $E(\psi,\theta,\tau)$, and the other coordinate indicated the position of the detector arm.

Also the strip-chart recorder which has a much better sensitivity than the X-Y plotter, was used for the measurement of biangular distributions. This was possible since the detector arm rotated at constant angular velocity. The recorded distribution was referenced to the points $\theta = -90°$ and $\theta = +90°$ where $E(\psi,\theta,\tau)$ is zero.

As a check point $\theta = -\psi$ was used, since at this angle the detector passes in front of the incident light beam and the detector output is zero. This is the reason why the biangular distributions reported later are interrupted at this angle.

IV. RESULTS AND DISCUSSION

A. Measurements of Refractive Index and Density

The measured refractive index is shown in Figure 6 for a water cryodeposit and in Figure 7 for a carbon dioxide cryodeposit. Also displayed in Figure 7 is a curve reported by Tempelmeyer in [3]. The same technique as used in this work was used by Tempelmeyer, and his measurements were reproducible only at a wavelength of 0.7μ. It is observed that the value of the refractive index at a wavelength of 0.567μ shows considerable scatter. Tempelmeyer assumed this to be the actual value while it will be shown in the following discussion that this value is not the true value of the refractive index. The discussion will also show the accuracy one can obtain with this technique at various wavelengths.

In order to obtain monochromatic light, interference-type filters were used. These filters have very good spectral resolution at a wavelength of 0.5μ, but with increasing wavelength, the spectral resolution decreases. This is especially noticeable above a wavelength of 0.8μ.

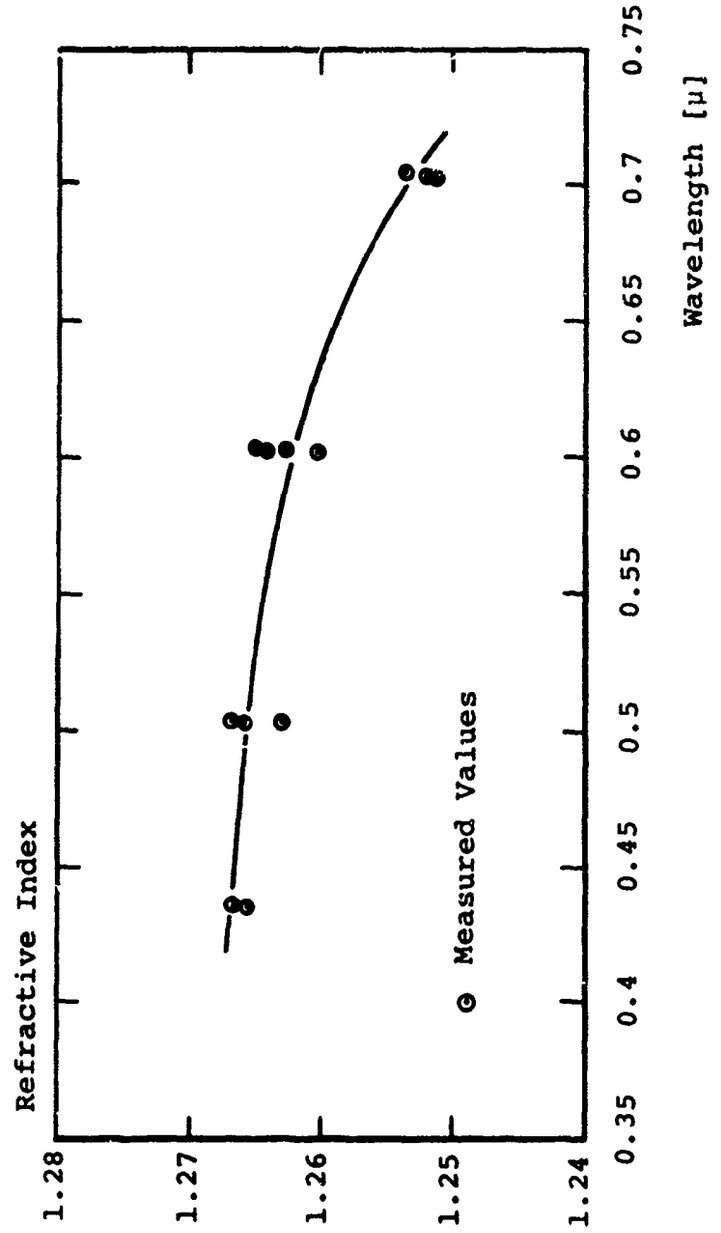

Figure 6. Refractive index of water cryodeposit.

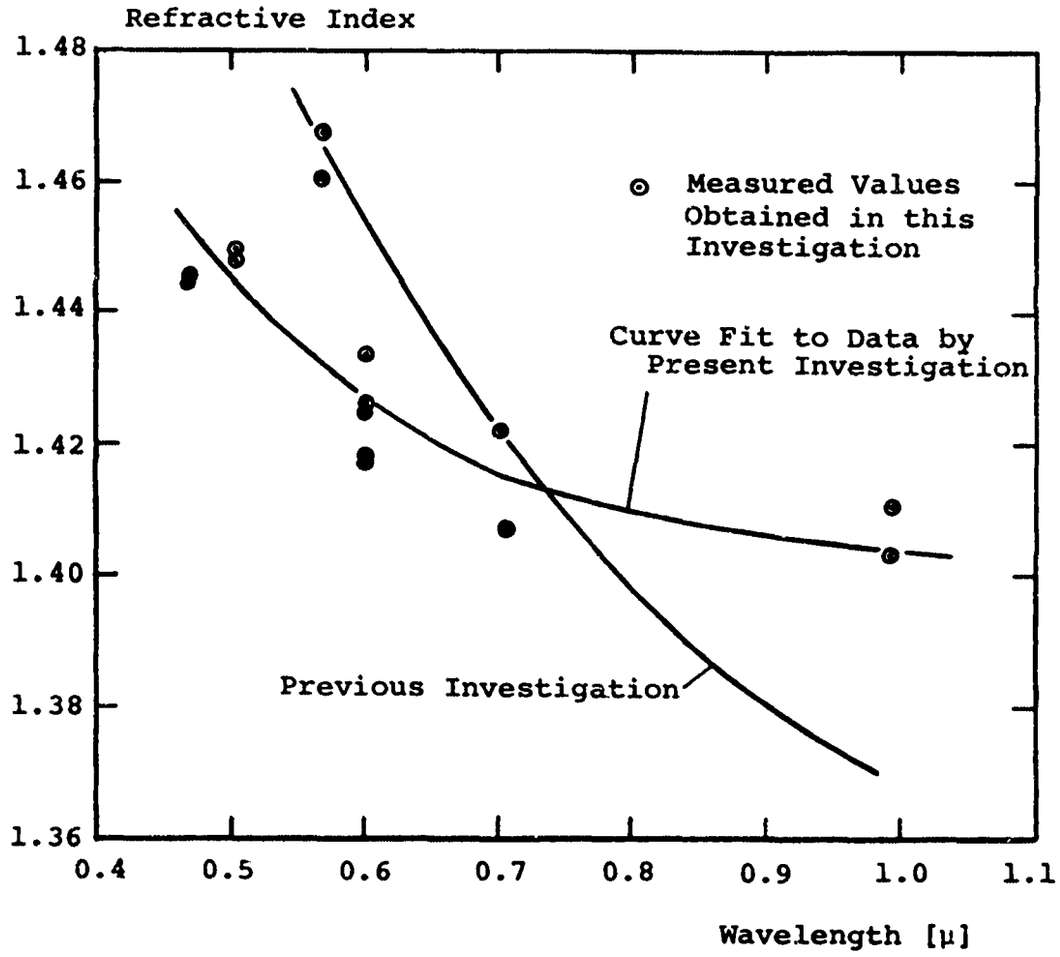

Figure 7. Refractive index of carbon dioxide cryodeposit.

The representative wavelength for the transmission band of the filter is normally assumed to be the wavelength at which the maximum transmission occurs. If the light transmitted through the filter is reflected off a substrate like polished copper, which was used for the measurements of the refractive index and density, the maximum of the detected light flux does not occur at the representative wavelength for the filter, since the reflectance of polished copper changes with wavelength. The relative reflectance[3] of polished copper measured by Wood [10] is shown in Figure 8 as a function of the wavelength and the angle of incidence. It is observed that at 0.57μ the reflectance of copper increases rapidly with increasing wavelength causing the peak of the detected light flux to shift to a greater wavelength than that corresponding to maximum transmission of the filter. It can be reasoned that the greater the slope in Figure 8, the greater will be the shift of the wavelength.

For the calculation of the refractive index, it is not necessary to know the exact wavelength at which the peak of the detected light flux occurs. However, it is assumed that this wavelength is equal at the two different angles of incidence ψ_a and ψ_b, which is probably not true

---

[3]Relative reflectance is the reflectance with respect to magnesium oxide.

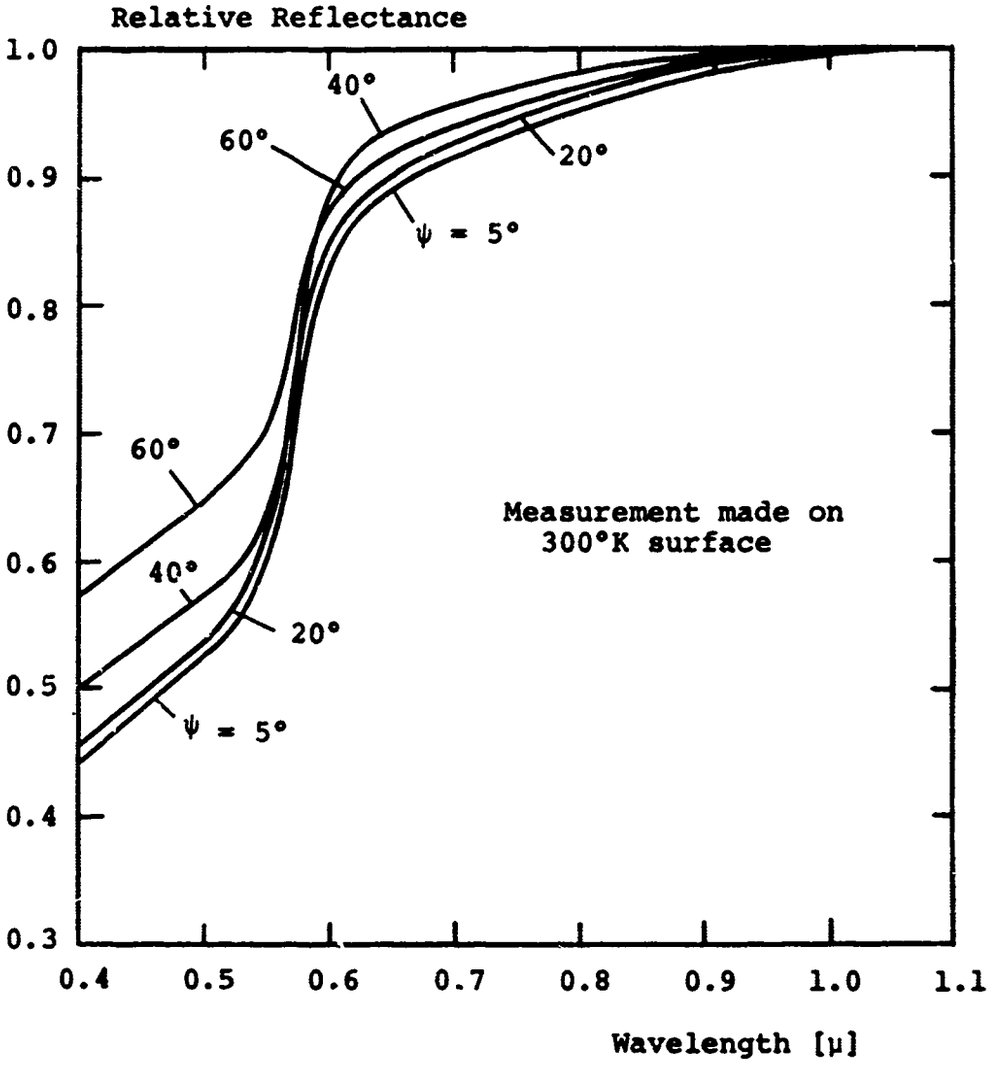

Figure 8. Relative reflectance of polished copper.

at a wavelength of 0.57μ and leads to the inconsistent measurements of the refractive index at a wavelength of 0.57μ in Figure 7, page 35. At wavelengths below 0.55μ, it can be assumed that the shift of the wavelength is small at different angles of incidence, so that the refractive index obtained at these wavelengths is accurate. Since there is no shift at wavelengths above 0.6μ, it is believed that the measurements at wavelengths of 0.6μ and 0.7μ reported in Figure 6, page 34, and Figure 7, page 35, are the most accurate.

It is noted in Figure 6, page 34, that the refractive index of water cryodeposit was measured only below a wavelength of 0.7μ, since the measurement above this wavelength did not produce meaningful results. This can be explained in the following way.

The absorption coefficient of water steadily increases with increasing wavelength after passing through a minimum at a wavelength of 0.4μ as shown by Dunkle and Bevans in [11]. Around 0.9μ a weak absorption band occurs which was also observed for cryodeposits by Wood et al. reported in [1]. Because an absorption band leads to anomalous dispersion, the refractive index of water cryodeposit for wavelengths near 0.9μ should show the behavior sketched in Figure 9.

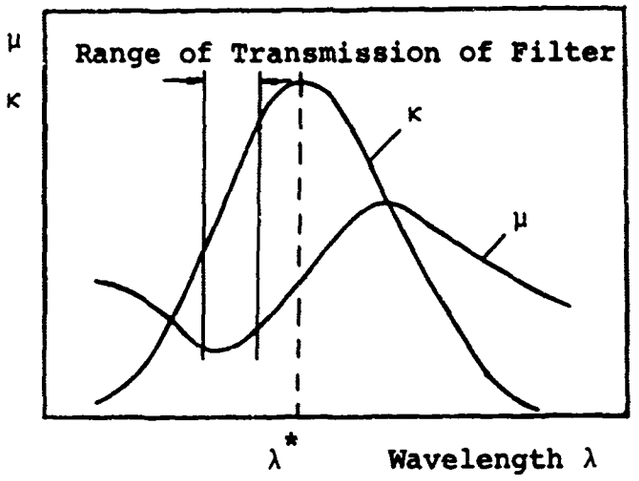

Figure 9. Spectral variation of refractive index and absorption coefficient near an absorption band.

Although the absorption coefficient of water below a wavelength of 1.0μ is still small enough that Snell's law (the basis of this measurement technique) can be applied without appreciable error, tests above a wavelength of 0.7μ were not successful. It is felt that this lack of meaningful results for wavelengths above 0.7μ was due to the spectral resolution of the interference-type filters which is not sufficient at these wavelengths for accurate measurements of the refractive index.

The influence of the shift of wavelength (from the characteristic wavelength of filter transmission to the wavelength at which the maximum rate of energy is detected, which is the characteristic wavelength of the combination

of filter transmission and reflection from the polished copper substrate) mentioned before is more severe on the measurement of the density than on the measurement of the refractive index because for the calculation of the density the characteristic wavelength of the combination of filter transmission and reflection from the polished copper substrate must be known, since

$$\dot{\tau} \sim \lambda$$

and

$$\rho \sim \frac{1}{\dot{\tau}}$$

At a wavelength of 0.7μ essentially no shift of wavelength should occur, since the relative reflectance of copper is flat with respect to wavelength in this spectral region. Hence the characteristic wavelength of the transmission of this filter can be used to evaluate the deposition rate $\dot{\tau}$, which leads to the density of the deposit. Since $\dot{\tau}$ remains equal at different wavelengths, provided the flow rate of the gas addition system is kept constant, the characteristic wavelength of the combination of filter transmission and reflection from the polished copper substrate can be calculated for filters at different wavelengths. For two different filters using the same substrate, the characteristic wavelengths are:

1. Characteristic wavelength of transmission and reflection from polished copper for two filters 0.612μ 0.522μ
2. Characteristic wavelength of the two filters as given by the manufacturer 0.567μ 0.502μ

It is noted that the exact characteristic wavelength of the filters as given by the manufacturer was used in the calculations of the deposition rate.

The density of carbon dioxide cryodeposit formed at 77°K and at a deposition pressure of 4×10^{-4} mm Hg is 1.67 ± 0.03 gr/cm^3. The refractive index is obtained from Figure 7, page 35, as 1.428 at a wavelength of 0.589μ, and the Lorenz-Lorentz constant computed from Equation (1) at this wavelength is 0.154 cm^3/gr.

The refractive index of liquid carbon dioxide and its density is given in [6]. The Lorenz-Lorentz constant of liquid carbon dioxide at 15°C (59°F) and at a wavelength of 0.589u is 0.153 cm^3/gr. This value is in close agreement with the value obtained from the cryodeposit. The measured density of carbon dioxide deposit compares favorably with the measurement of Mass [8] who obtained 1.674 gr/cm^3.

The density of water cryodeposit formed at 77°K and a deposition pressure of 4×10^{-4} mm Hg is 0.81 ± 0.02 gr/cm^3, and the value of the refractive index of 1.264 at a wavelength of 0.589μ, obtained from Figure 6, page 34. The Lorenz-Lorentz constant becomes 0.205. Dorsey [12] gives a value of 0.21 for ice at this wavelength which is in close agreement with the value obtained for the cryodeposit.

Another approach to the measurement of the refractive index of water cryodeposit employed a polarization technique. The polarization filters used were glass laminated plastic filters. In order to determine in what wavelength range these filters polarize light, two polarization filters were placed in series in such a way that the plane of polarization of one filter was perpendicular to the plane of polarization of the other filter (so that no visible light was transmitted). The radiation transmitted through both filters was then measured. By changing the wavelength of the light transmitted through both polarization filters it was found that up to a wavelength of 0.7μ essentially no radiation was transmitted. At 0.75μ the transmission increased rapidly which showed that the polarization filters do not polarize the radiation above a wavelength of 0.7μ. The lower limit

of the wavelength range in which the polarization filters work properly was not investigated.

Because both the light output of the xenon arc lamp and the detector output increase with increasing wavelength up to 0.9μ, a wavelength just below the limiting wavelength of the polarization filter, 0.7μ, was used for the measurement of the refractive index of water cryodeposit by the polarization technique explained in the following.

The refractive index of a material with a polished surface can be found by measuring the Brewster angle ψ_{Br} at which light polarized parallel to the plane of incidence is not reflected. This angle is related to μ by

$$\mu = \tan \psi_{Br} \tag{26}$$

If the surface is rough or if the polished material has absorption, a certain amount of parallel polarized light incident on the material at the Brewster angle is reflected.

In order to obtain a value which characterizes the reflective properties for polarized light of any surface departing from a polished surface of a non-absorbing material, the "degree of polarization" was introduced.

As defined by Torrance [9] , the "degree of polarization" is

$$\frac{I(\psi,\psi)_s - I(\psi,\psi)_p}{I(\psi,\psi)_s + I(\psi,\psi)_p} = \frac{E(\psi,\psi)_s - E(\psi,\psi)_p}{E(\psi,\psi)_s + E(\psi,\psi)_p} \qquad (27)$$

where E_s is perpendicular polarized radiation and E_p is parallel polarized radiation. Equation (27) approaches a value of 1.0 as the angle of incidence approaches the Brewster angle of a polished non-absorbing medium. The "degree of polarization" of absorbing media and also of non-absorbing media with rough surfaces as shown in [9] has a maximum which is smaller than 1.0. It is also reported in [9], that the maximum of the "degree of polarization" decreases with increasing surface roughness, and that the angle ψ, where the maximum value occurs, shifts to greater angles with increasing surface roughness.

In Figure 10 the "degree of polarization" of black paint and of water cryodeposit formed on a black paint substrate at a thickness of 150μ is displayed as a function of the angle of incidence ψ. The maximum of 0.86 obtained with the black paint occurs at $\psi = 56° \pm 0.5°$. If it is assumed that the maximum in the "degree of polarization" of the black paint is smaller than 1.0 due to the surface roughness of the paint only, and not due to the effect of absorption, a refractive index of 1.48 ± 0.03 is obtained for the black paint.

The maximum value of the "degree of polarization" of the radiation reflected from the water deposit is not

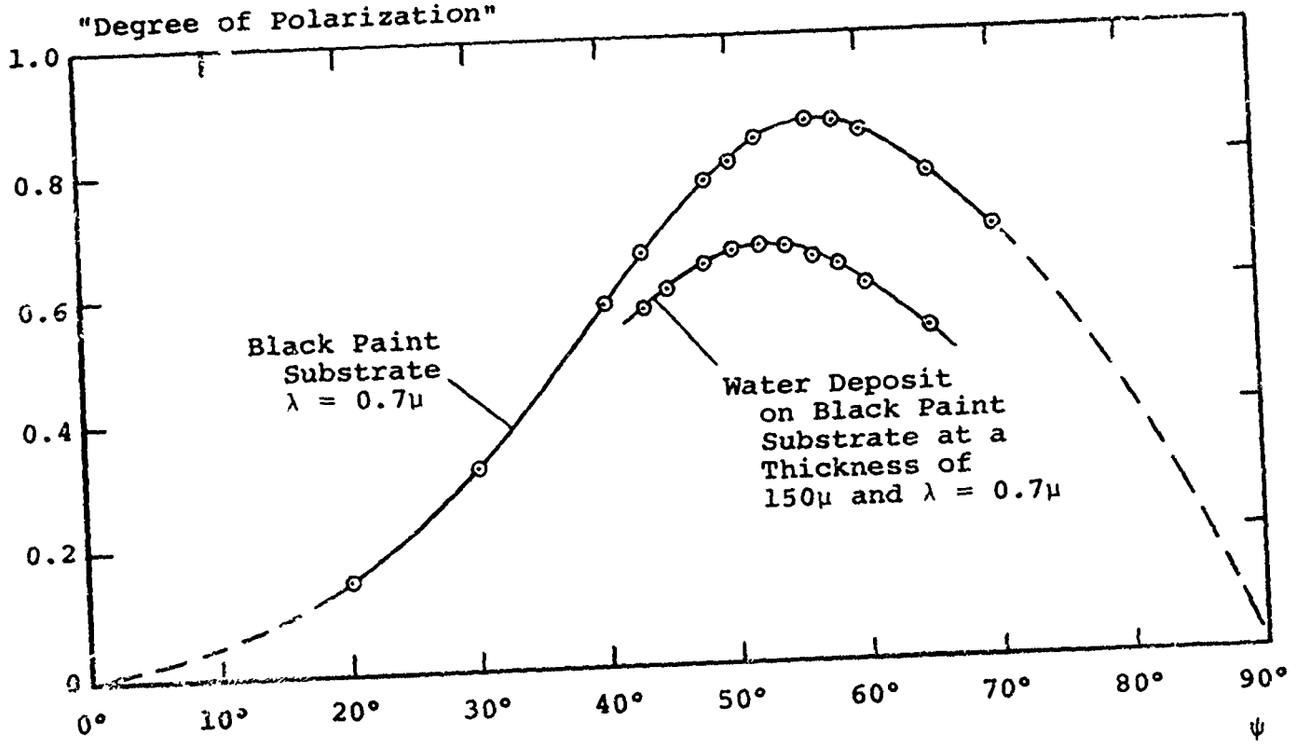

Figure 10. "Degree of polarization" of the black paint substrate and water deposit.

only due to the reflection from the vacuum-deposit interface which is required for this measurement technique, but also due to radiation being reflected from the cryodeposit by reflection from the substrate and by internal scattering inside the deposit. However, it will be shown subsequently from the measurements of the biangular distributions of the radiation reflected from cryodeposits that water deposit at a thickness of 150μ is almost a specular reflector which is attributed to a very smooth interface. Thus it can be reasoned that $E(\psi,\psi)_s$ and $E(\psi,\psi)_p$, the rate of energy reflected in specular direction, is mostly due to reflection from the vacuum-deposit interface which justifies the use of this method of measuring the refractive index.

It is observed in Figure 10 that the maximal "degree of polarization" of the radiation reflected from the water deposit is 0.67 at an angle $\psi = 52° \pm 0.5°$. This leads to a refractive index of 1.28 ± 0.025 which compares favorably with the value of 1.253 obtained at a wavelength of 0.7μ by the interference technique.

B. Thin Film Interference Pattern

In order to estimate the rate of energy reflected from the vacuum-deposit interface and from the substrate at low deposit thickness, the initial thin film interference maximum and minimum is used. Since the electric

field vectors of the radiation reflected from interface and substrate interfere, the measured rate of energy has to be converted into the magnitude of the electric field vector.

For a water deposit on a black paint substrate at a wavelength of 0.7μ and at an angle of incidence ψ and a viewing angle θ of 22°, the first measured interference maximum is $E_{max} = 45.3$ and the first minimum is $E_{min} = 1.7$ expressed in arbitrary, but consistent rate of energy units. The intensity of the reflected radiation is given in Equation (3)

$$I(\psi,\theta) = \frac{E(\psi,\theta)}{\cos\theta \cdot dA(\psi) \cdot \Delta\omega_r}$$

Since θ, $dA(\psi)$, and $\Delta\omega_r$ are constant, $I(\psi,\theta)$ is proportional to $E(\psi,\theta)$. Thus Equation (3) can be written in the form

$$I = k^2 \cdot E$$

where

$$k^2 = \frac{1}{\cos\theta \cdot dA(\psi) \cdot \Delta\omega_r}$$

is the proportionality constant. Thus the maximum and minimum intensity of the reflected radiation is

$$I_{max} = k^2 \cdot E_{max}$$

$$I_{min} = k^2 \cdot E_{min}$$

The relation connecting the magnitude of the electric field vector with the intensity was given in Equation (11)

$$|\vec{e}|^2 = \beta \cdot I$$

so that

$$|\vec{e}_{max}| = \sqrt{\beta \cdot I_{max}} = k \cdot \sqrt{\beta E_{max}}$$

$$|\vec{e}_{min}| = \sqrt{\beta \cdot I_{min}} = k \cdot \sqrt{\beta E_{max}}$$

By using the measured values of E_{max} and E_{min}, the preceding relations yield

$$|\vec{e}_{max}| = k \cdot 6.74 \sqrt{\beta}$$

$$|\vec{e}_{min}| = k \cdot 1.303 \sqrt{\beta}$$

Interference occurs between the electric field vector of the radiation reflected from the interface and that of the radiation reflected from the substrate, $\vec{e}_1$ and $\vec{e}_2$. The magnitude of these electric field vectors is obtained from

$$|\vec{e}_1| = \frac{|\vec{e}_{max}| + |\vec{e}_{min}|}{2} \qquad (28)$$

$$|\vec{e}_2| = \frac{|\vec{e}_{max}| - |\vec{e}_{min}|}{2} \tag{29}$$

where $|\vec{e}_1|$ and $|\vec{e}_2|$ are interchangeable. The intensity of the radiation reflected from the interface and the substrate is computed from $\beta \cdot I = |\vec{e}|^2$. Thus, the intensities

$$\left[\frac{|\vec{e}_{max}| + |\vec{e}_{min}|}{2}\right]^2 = 12.3 \cdot k^2\beta \tag{30}$$

$$\left[\frac{|\vec{e}_{max}| - |\vec{e}_{min}|}{2}\right]^2 = 7.36 \cdot k^2\beta \tag{31}$$

are obtained, but it is not yet known which of these two values represents the intensity of the radiation reflected from the interface, I_1, and which represents the intensity of the radiation reflected from the substrate, I_2. In order to decide this, the relative intensity of the radiation[4] reflected from the interface and from the substrate has to be estimated.

The refractive index of water deposit obtained by interference techniques is 1.253 at a wavelength of 0.7μ. The black paint shows a maximum of the "degree of polarization" at an angle of 56° which is displayed in Figure 10, page 45. It was discussed before that this angle

---

[4]Relative intensity of the reflected radiation $= I_{reflected}/I_{incident}$.

corresponds to a refractive index of 1.48 at a wavelength of 0.7μ, if absorption of the paint is neglected.

At an angle of incidence of 22° with unpolarized light, the following simple equation for an angle of incidence of 0° is approximately correct

$$\frac{I_{reflected}}{I_{incident}} = \left(\frac{\mu-1}{\mu+1}\right)^2 \tag{32}$$

This relation is obtained from the Fresnel equations given in [13]. Substituting the value of μ for water, given above, into Equation (32), a value of 0.0126 is obtained. The same calculation for the substrate using the relative refractive index[5] of 1.184 leads to a value of 0.00709. Thus, the ratio of the intensities of the radiation reflected from the interface and from the substrate, as obtained from the estimate is

$$\frac{I_1}{I_2} = \frac{0.0126}{0.00709} = 1.78$$

The ratio of the intensities in Equations (30) and (31) computed from the measurements of the interference maximum and minimum is

[5]Relative refractive index = refractive index of substrate/refractive index of deposit.

$$\frac{12.3}{7.36} = 1.67$$

It is observed that this value is essentially equal to the ratio of the intensities of the radiation reflected from the interface and from the substrate. This indicates that Equation (30) represents the intensity of the radiation reflected from the interface, and Equation (31) represents the intensity of the radiation reflected from the substrate.

The same procedure can be used with a thin film interference pattern obtained from a carbon dioxide cryodeposit on a black paint substrate at a wavelength of 0.9μ and an angle of incidence of 22°. In this case the first interference maximum is $E_{max} = 57.7$, and the first minimum is $E_{min} = 32.5$ expressed in arbitrary, but consistent rate of energy units. Following the same procedure as before it is obtained

$$\left[\frac{|\vec{e}_{max}| + |\vec{e}_{min}|}{2}\right]^2 = 44.2 \cdot k^2\beta \tag{33}$$

$$\left[\frac{|\vec{e}_{max}| - |\vec{e}_{min}|}{2}\right]^2 = 0.89 \cdot k^2\beta \tag{34}$$

The refractive index of carbon dioxide cryodeposit is 1.406 at a wavelength of 0.9μ which was obtained before by interference techniques. Thus, the relative intensity

of the radiation reflected from the interface is 0.0285, and the relative intensity of the radiation reflected from the substrate is 0.000665 where a relative refractive index of 1.053 is used. The ratio of the intensities of the radiation reflected from the interface and from the substrate, as obtained from the estimate, is

$$\frac{I_1}{I_2} = \frac{0.0285}{0.000665} = 42.9$$

The ratio of the intensities in Equations (33) and (34), computed from the measurements of the interference maximum and minimum, is

$$\frac{44.2}{0.89} = 49.7$$

From the approximate equality of these two ratios it can be concluded that Equation (33) represents the intensity of the radiation reflected from the interface, and Equation (34) represents the intensity of the radiation reflected from the substrate. Since I_2 is very small compared to I_1, essentially all radiation reflected from the thin cryodeposit is due to reflection from the interface.

A cryodeposit on a polished copper substrate can be investigated in the same manner. The thin film interference pattern of water cryodeposit at a wavelength of 0.6μ shows a first measured interference maximum $E_{max} = 7.2$

and a first minimum $E_{min} = 4.25$. Using the same procedure as before

$$\left[\frac{|\vec{e}_{max}| + |\vec{e}_{min}|}{2}\right]^2 = 5.60 \cdot k^2\beta \tag{35}$$

and

$$\left[\frac{|\vec{e}_{max}| - |\vec{e}_{min}|}{2}\right]^2 = 0.096 \cdot k^2\beta \tag{36}$$

is obtained. It is apparent that Equation (35) represents the intensity of the radiation reflected from the substrate, and Equation (36) represents the intensity of the radiation reflected from the interface.

The intensities of the radiation reflected from interface and substrate are computed from measurements taken on a very small deposit thickness (in the order of the wavelength of the radiation). With increasing deposit thickness the amplitude of the pattern decreases which can be attributed to the following factors. Interference-type filters were used which transmit not only one wavelength but also sidebands. These sidebands generate constructive and destructive interference at different deposit thicknesses. This obscures the interference pattern.

Templemeyer et al. [3] report a similar attenuation of the amplitude of the pattern, although their data were taken using a He-Ne laser which has a much better spectral resolution than the filter. This suggests

that the interference pattern is further influenced by deviations of the rays transmitted through the deposit from the assumption of a collimated transmitted beam which was made in the theory mentioned earlier. These rays possess different path lengths inside the deposit and are thus out of phase when interfering with the ray reflected on the interface. This results in an attenuation of the amplitude of the interference pattern. Rays deviating from the collimated transmitted beam are caused by scattering inside the deposit and by scattering at the rough interface of the transmitted beam.

C. Distributions of the Reflected Radiation from Carbon Dioxide and Water Cryodeposits

1. Results of measurements. Biangular distributions of the reflected radiation were obtained for carbon dioxide and water cryodeposits using substrates of polished copper and black epoxy paint. The deposition rate for water was 0.044μ/sec, and for carbon dioxide it was 0.016μ/sec. The deposition pressure was approximately 4×10^{-4} mm Hg in both cases.

Using a polished copper substrate, biangular distributions of the reflected radiation at various deposit thicknesses are displayed in Figures 11 to 14 for carbon dioxide deposit and in Figures 15 to 18 for water deposit. These distributions are normalized with respect to the magnitude

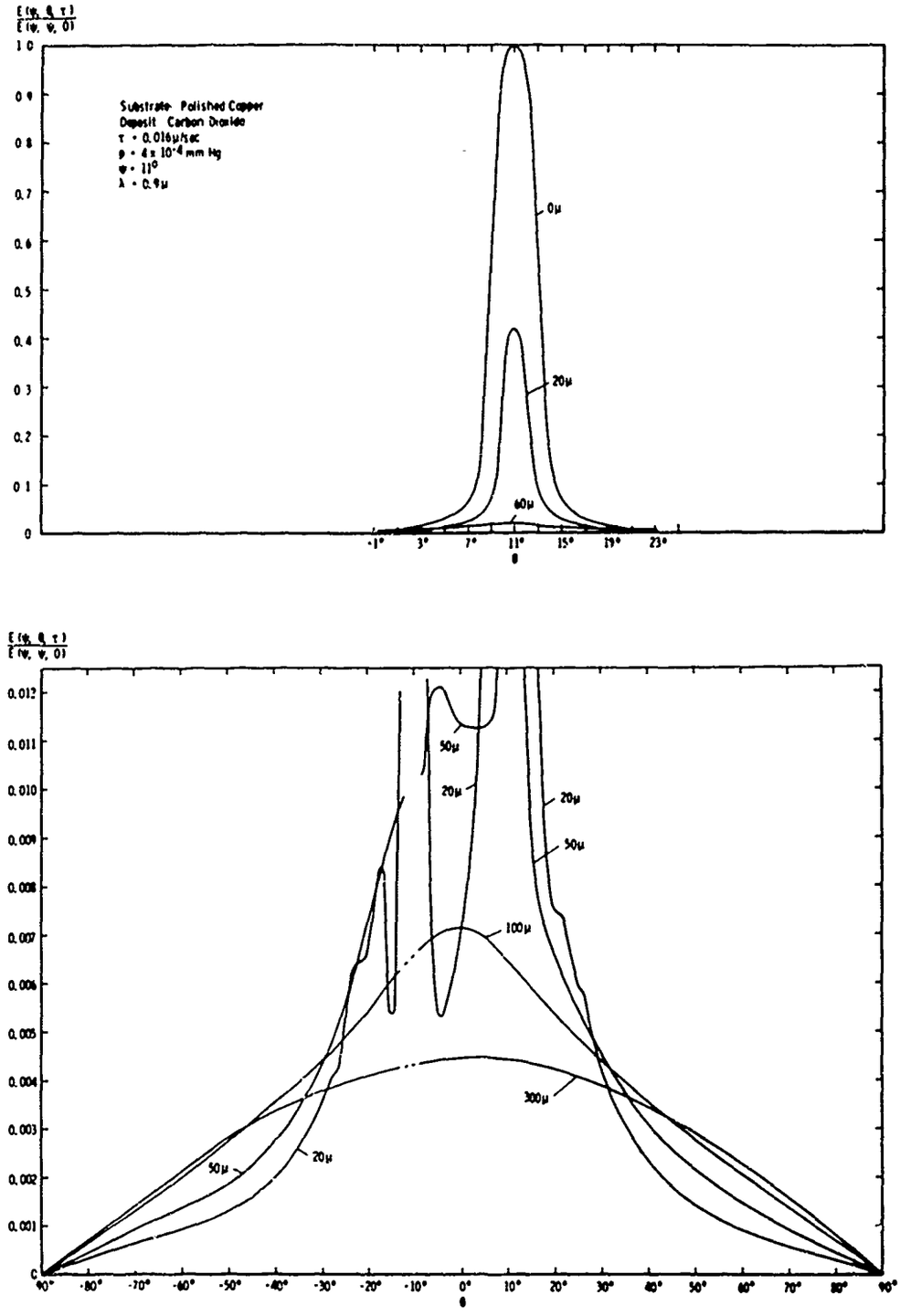

Figure 11. Normalized biangular distributions of $\lambda = 0.9\mu$ radiation reflected from various thicknesses of carbon deposit formed on polished copper, $\psi = 11°$.

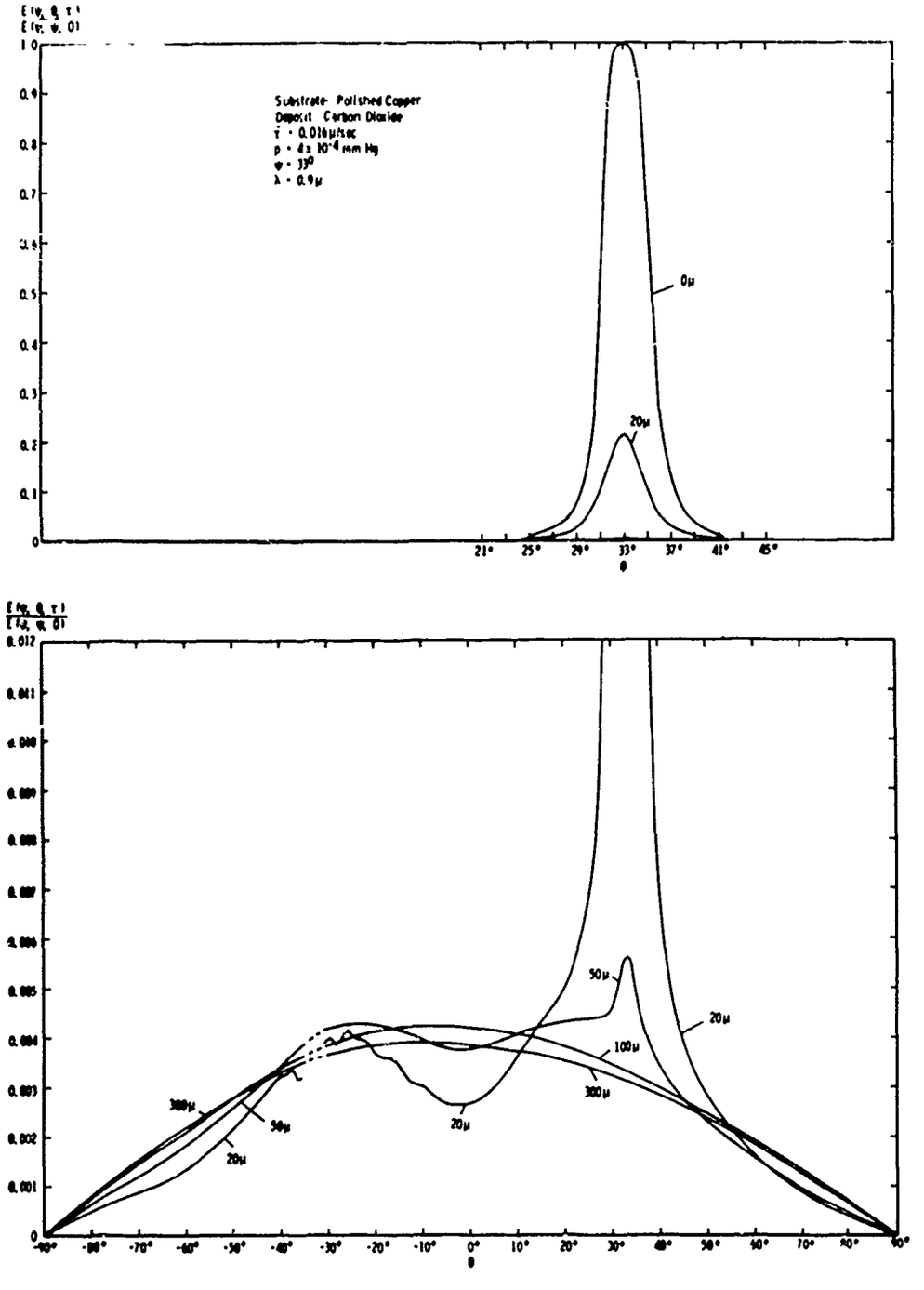

Figure 12. Normalized biangular distributions of $\lambda = 0.9\mu$ radiation reflected from various thicknesses of carbon dioxide deposit formed on polished copper, $\psi = 33°$.

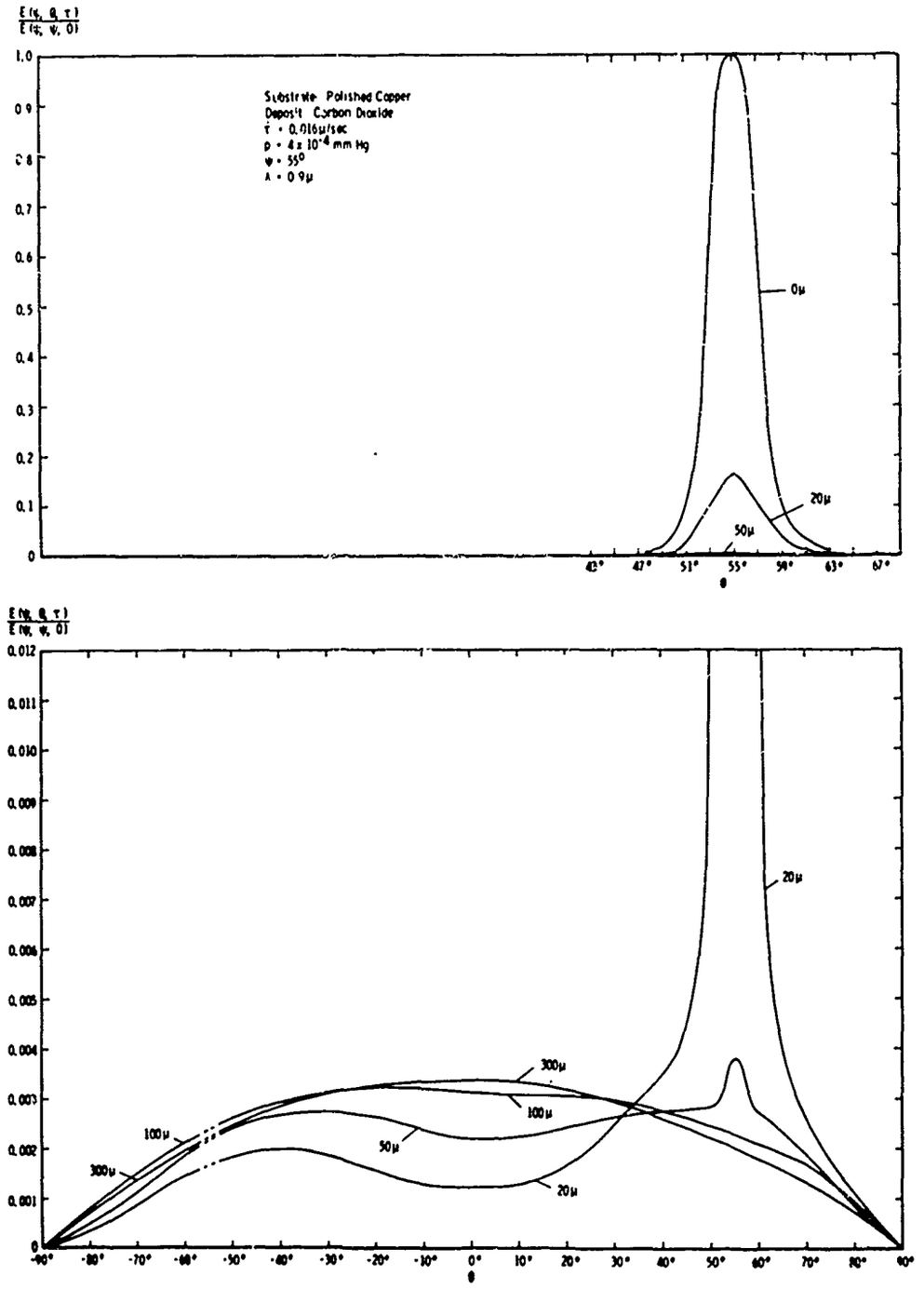

Figure 13. Normalized biangular distributions of $\lambda = 0.9\mu$ radiation reflected from various thicknesses of carbon dioxide deposit formed on polished copper, $\psi = 55°$.

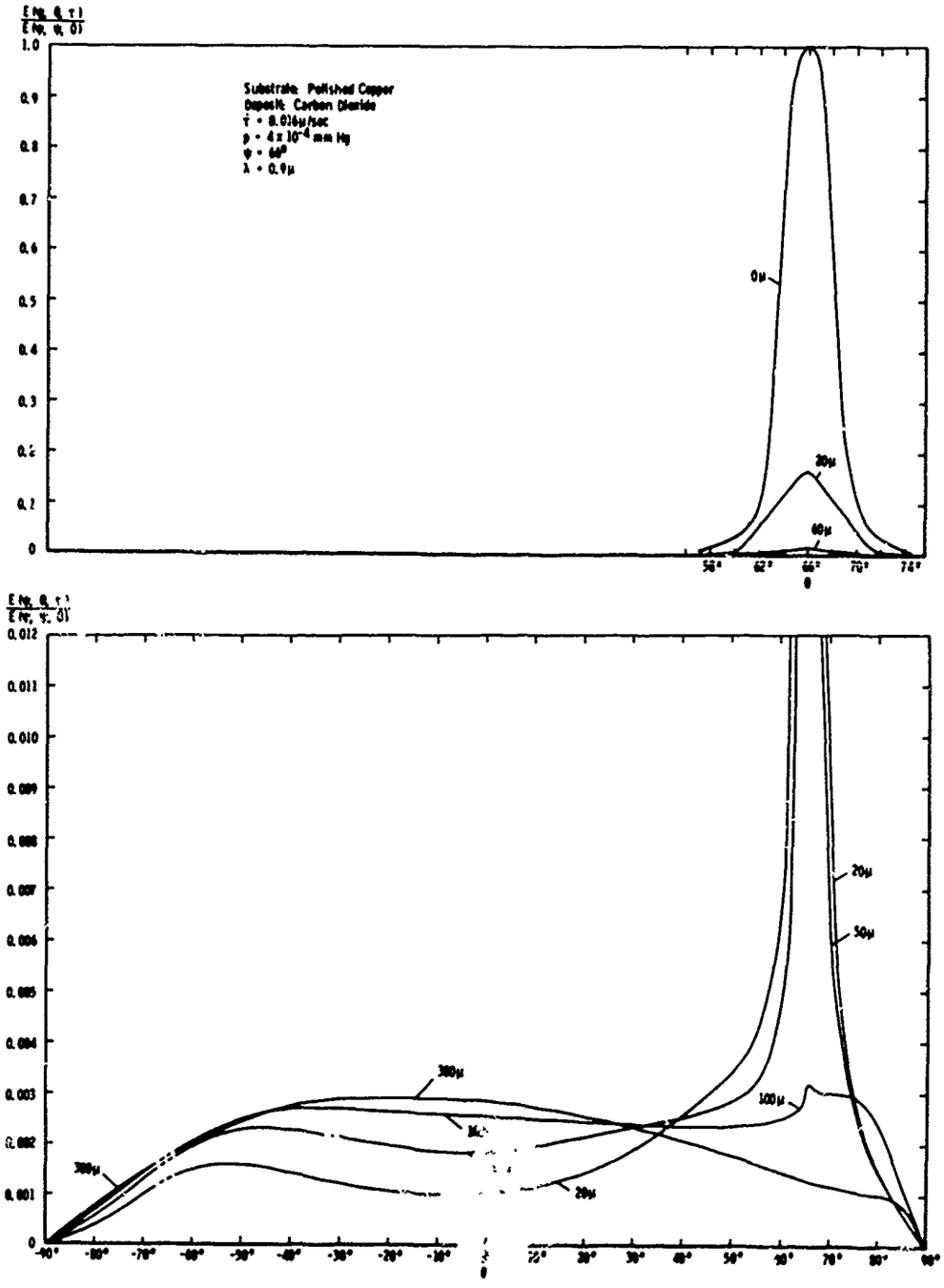

Figure 14. Normalized angular distributions of $\lambda = 0.9\mu$ radiation reflected from various thicknesses of carbon dioxide deposit formed on polished copper, $\psi = 66°$.

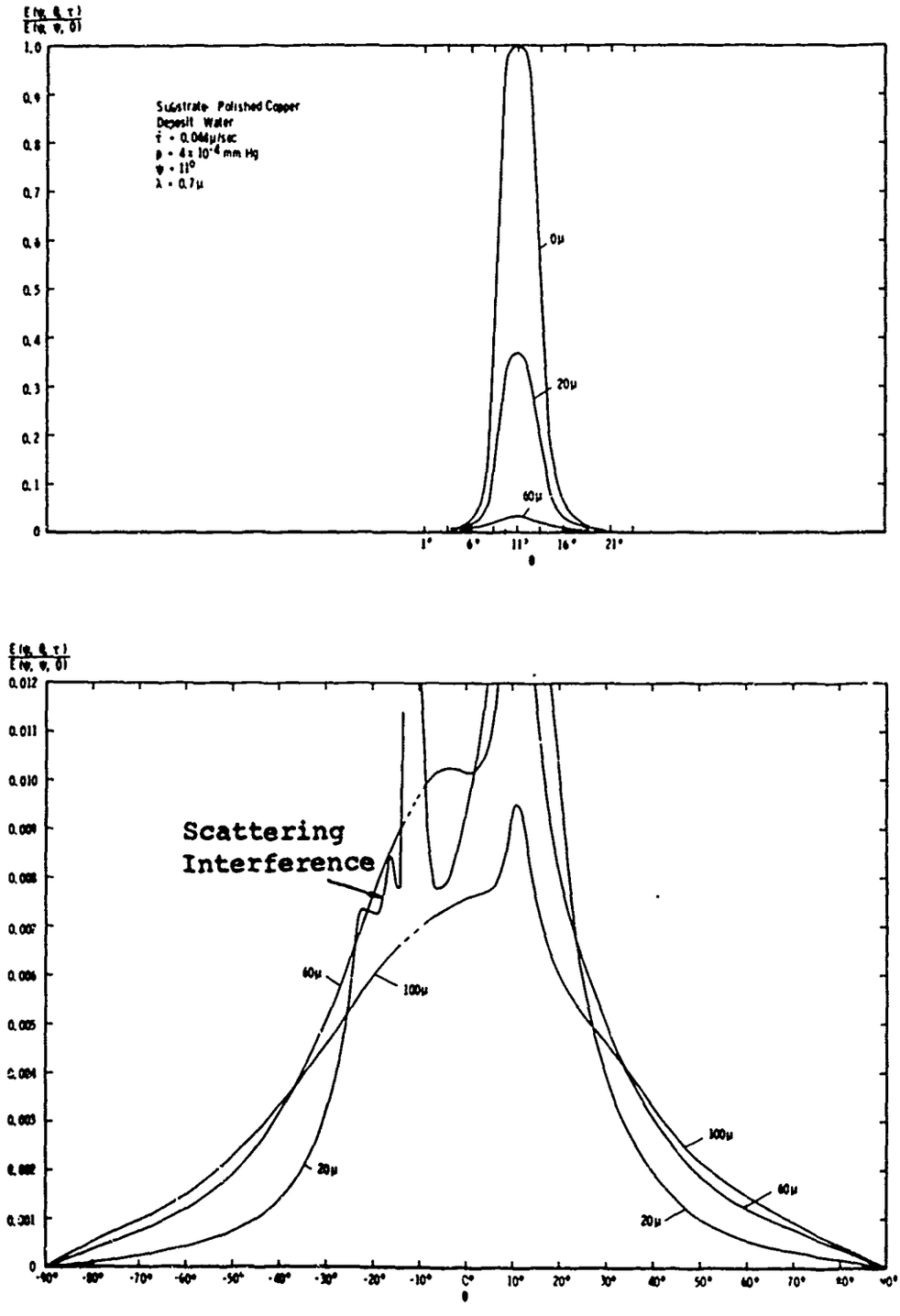

Figure 15. Normalized biangular distributions of $\lambda = 0.7\mu$ radiation reflected from various thicknesses of water deposit formed on polished copper, $\psi = 11°$.

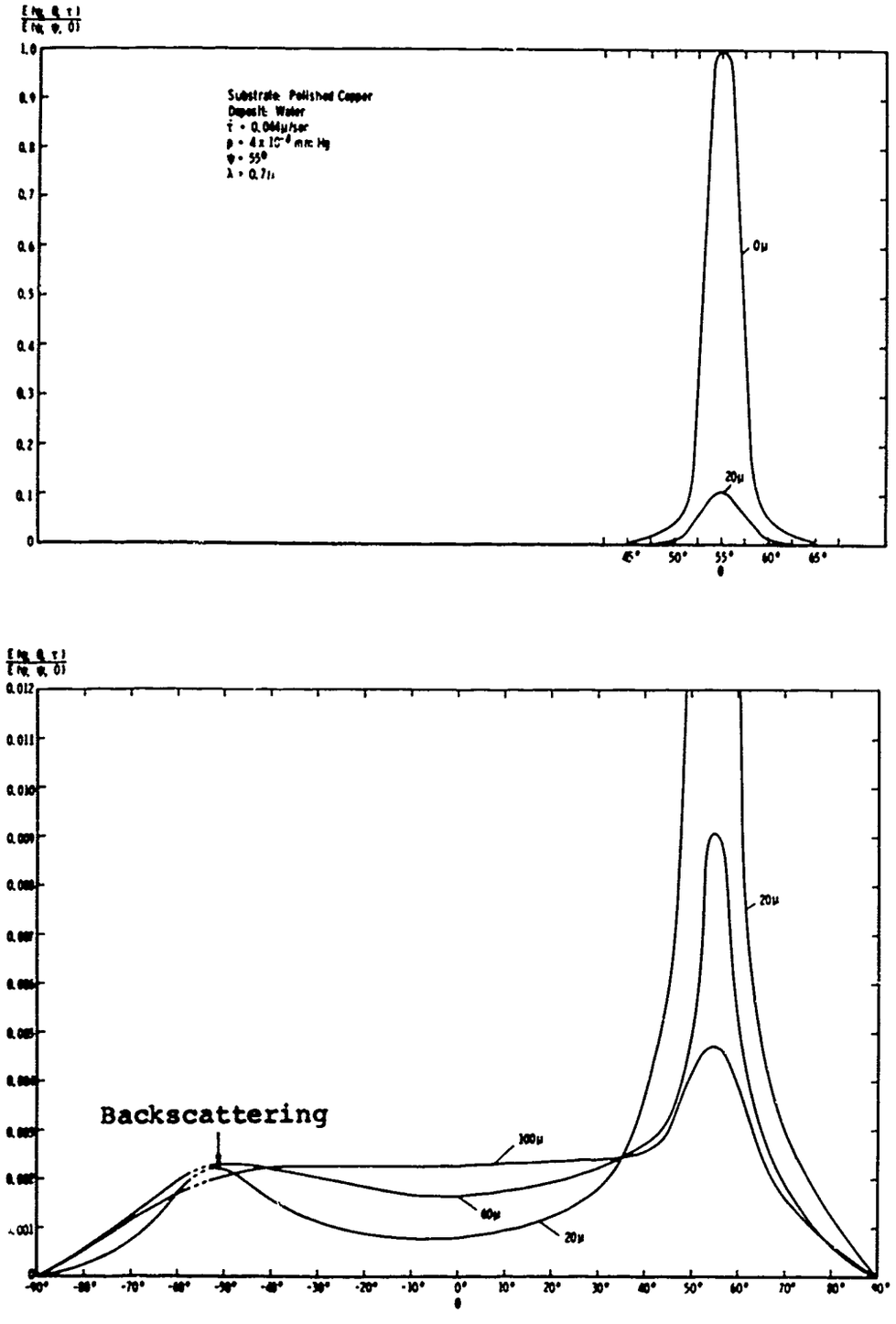

Figure 16. Normalized biangular distributions of $\lambda = 0.7\mu$ radiation reflected from various thicknesses of water deposit formed on polished copper, $\psi = 55°$.

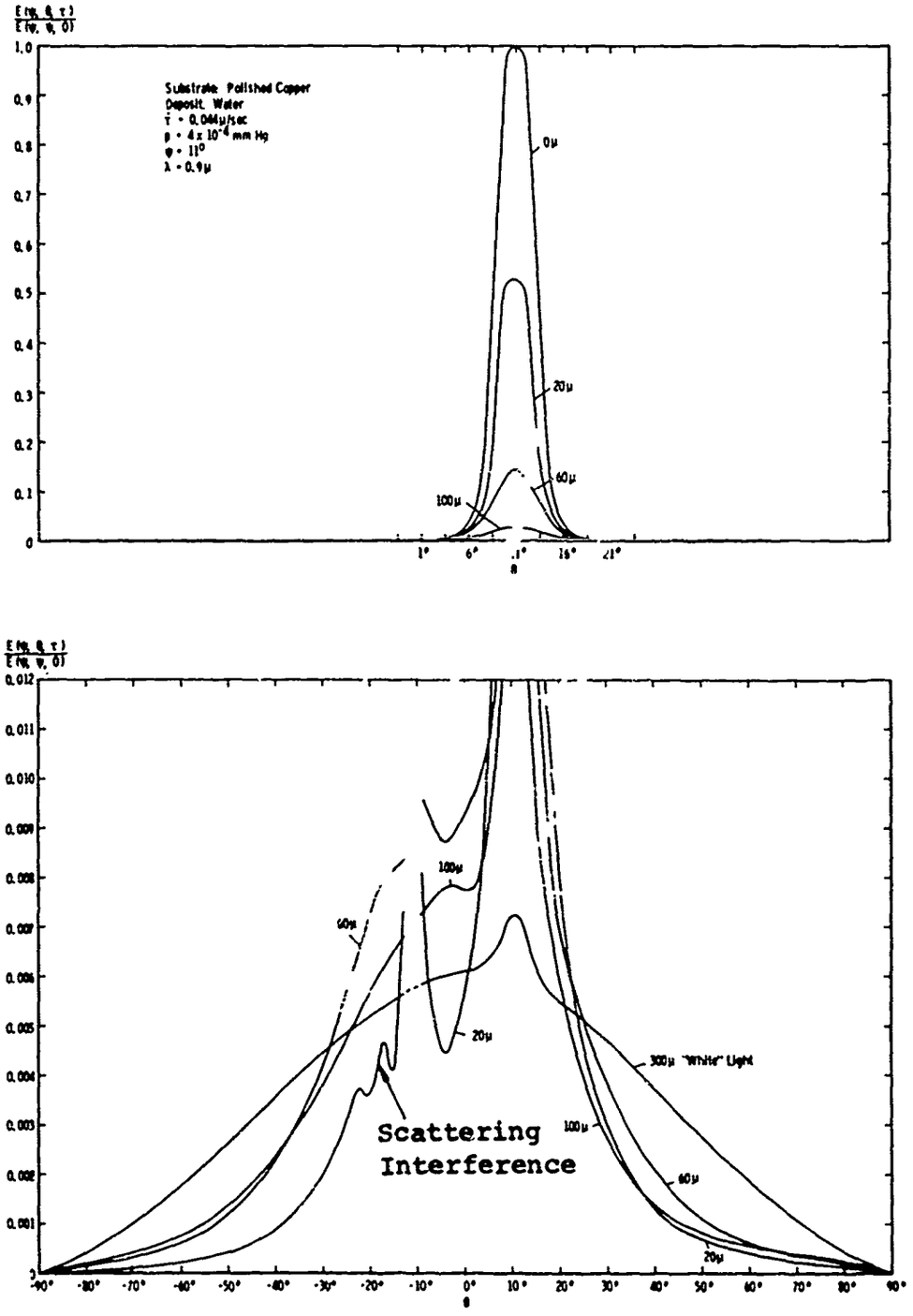

Figure 17. Normalized biangular distributions of $\lambda = 0.9\mu$ radiation reflected from various thicknesses of water deposit formed on polished copper, $\psi = 11°$.

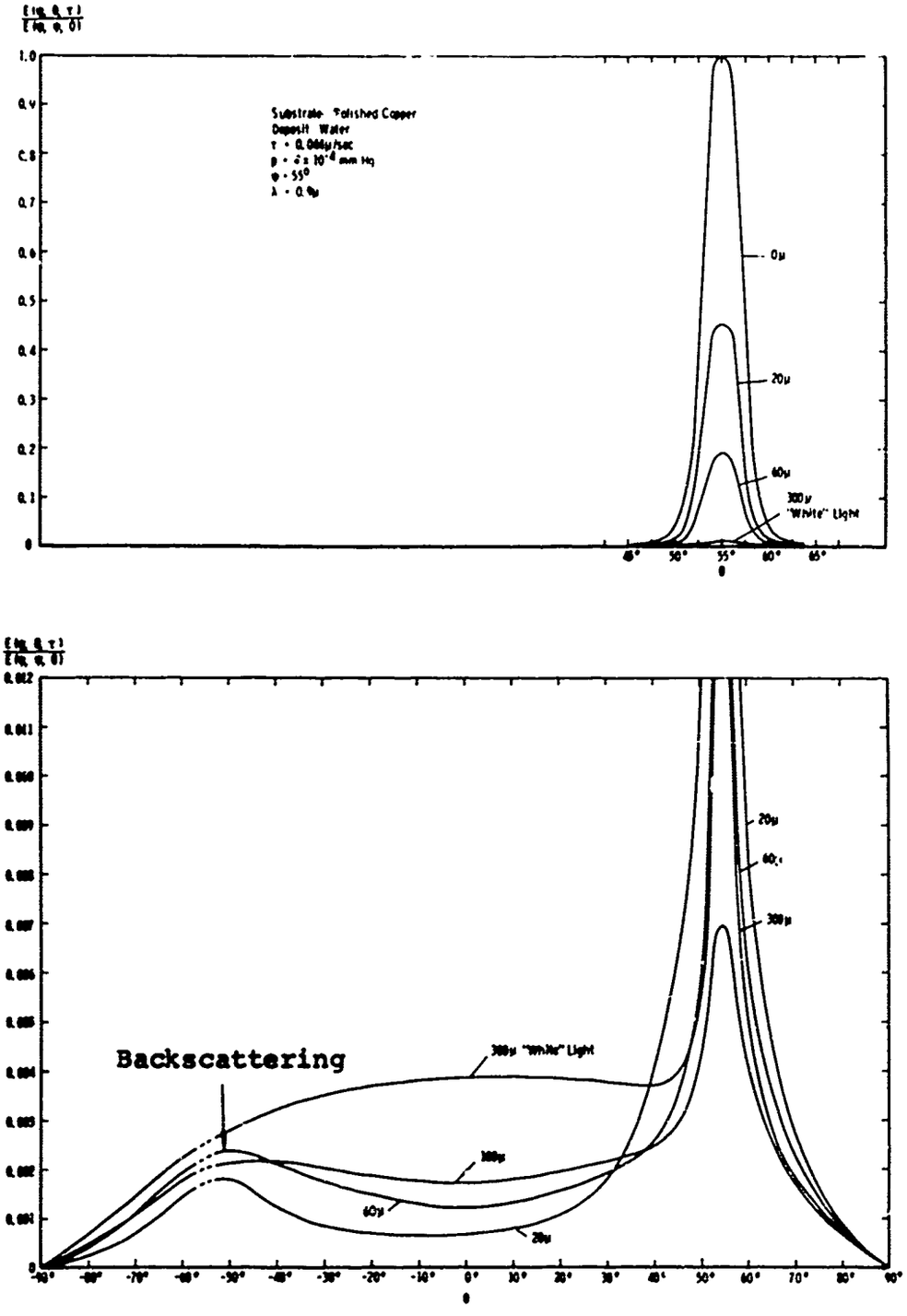

Figure 18. Normalized biangular distributions of $\lambda = 0.9\mu$ radiation reflected from various thicknesses of water deposit formed on polished copper, $\psi = 55°$.

of the radiation reflected from the bare substrate at the specular angle. The normalization is discussed later in detail.

Monochromatic light of the wavelengths $\lambda = 0.7\mu$ and 0.9μ was employed. In order to show the behavior of the distributions at angles θ where the reflected rate of energy is very small compared to that at the specular peak, two plots are displayed where the lower plot has a greatly increased scale.

The bare black paint has a small total reflectivity of 4 to 8 percent. Therefore, biangular distributions for this substrate were measured with irradiation by unfiltered "white" light. This resulted in a greater detector output which insures good measurement accuracy. Results for angles of incidence of 0°, 33°, 55°, and 66° are reported in Figures 19 through 26. These distributions are normalized in two different ways:

1. with respect to the magnitude of the peak of the distribution of the radiation reflected from the bare substrate at the same angle of incidence,
2. with respect to the magnitude of the radiation reflected from the bare substrate at the specular angle.

The normalization is discussed later in detail.

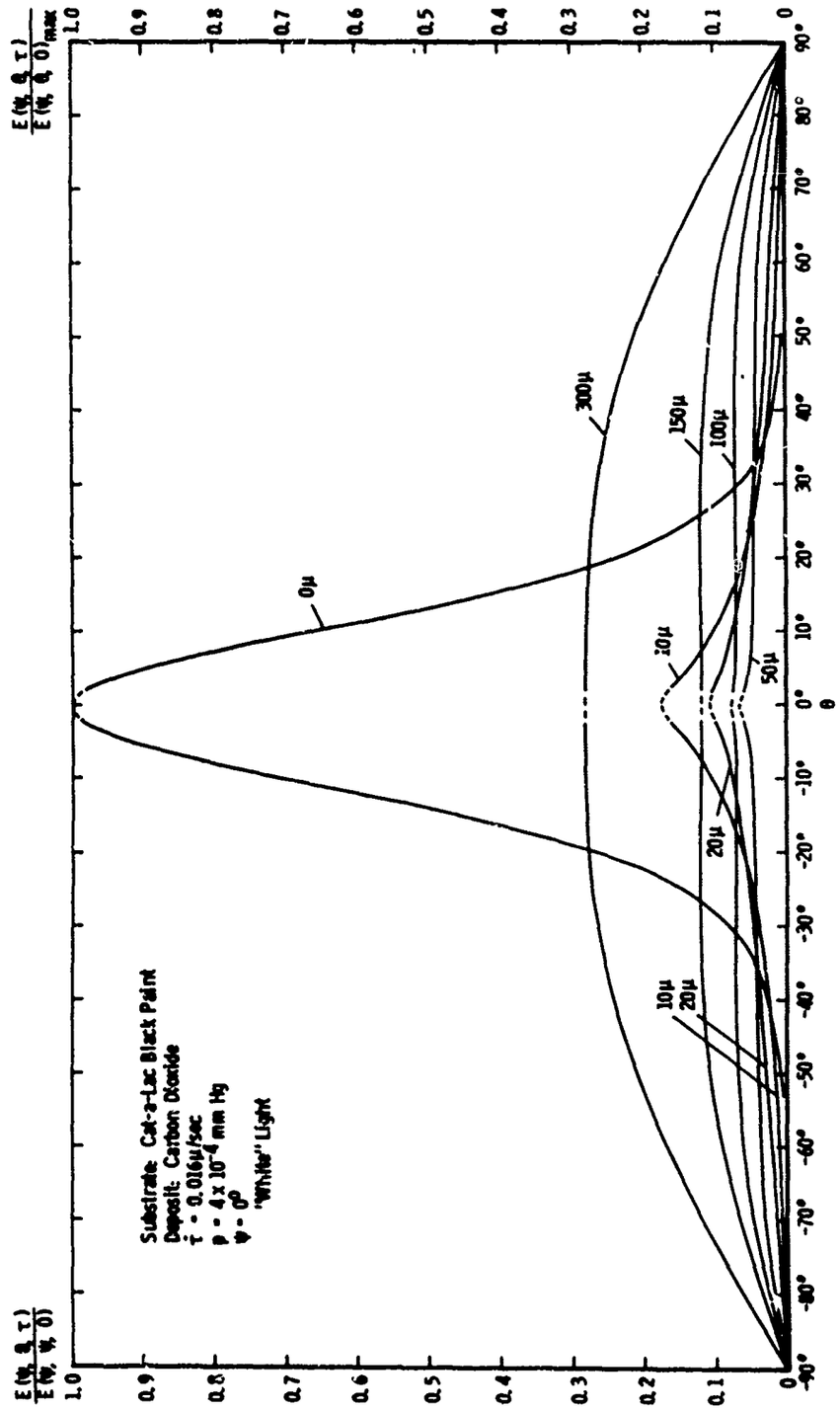

Figure 19. Normalized biangular distributions of "white" light radiation reflected from various thicknesses of carbon dioxide deposit formed on a black paint substrate, $\psi = 0°$.

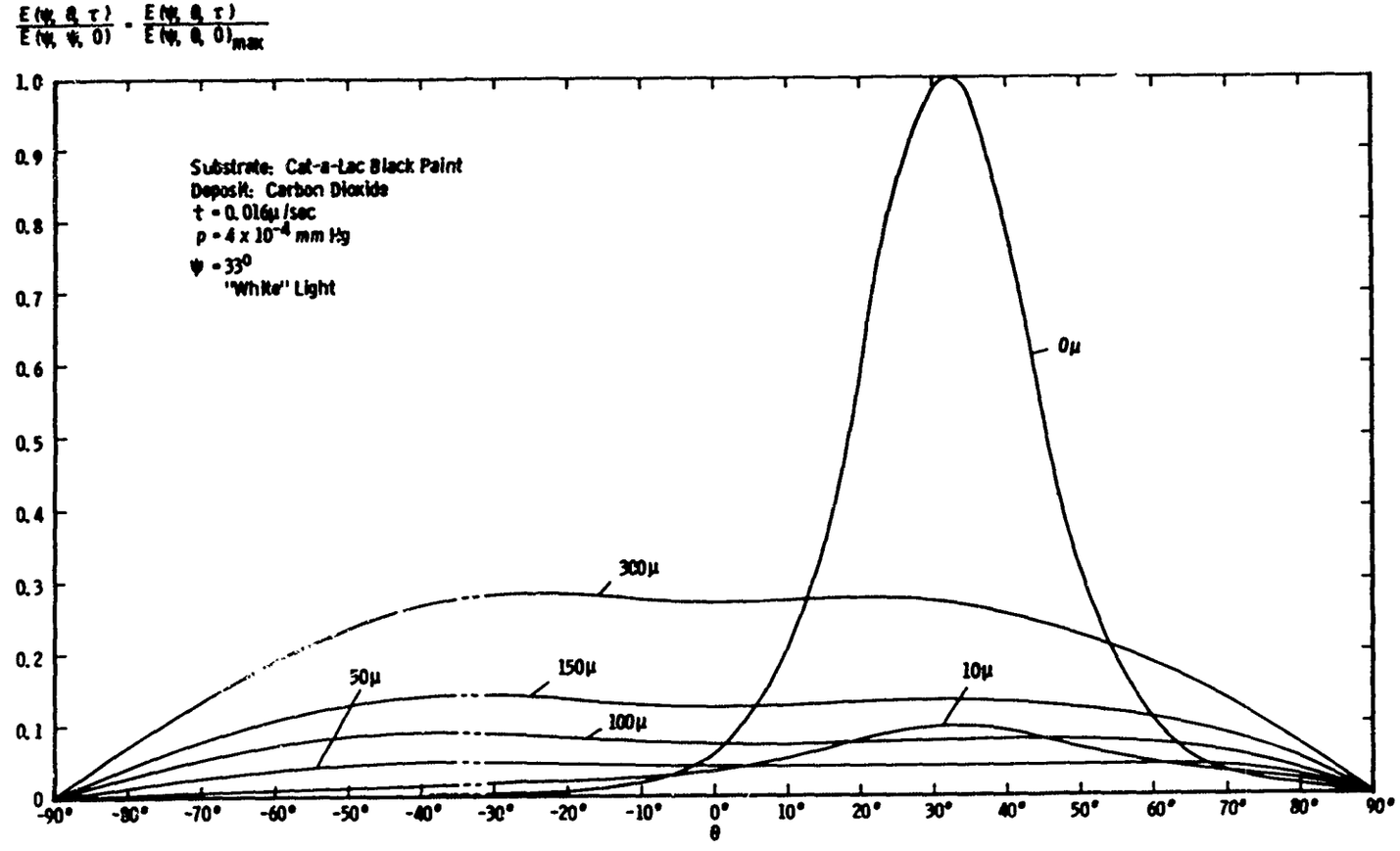

Figure 20. Normalized biangular distributions of "white" light radiation reflected from various thicknesses of carbon dioxide deposit formed on a black paint substrate, $\psi = 33°$.

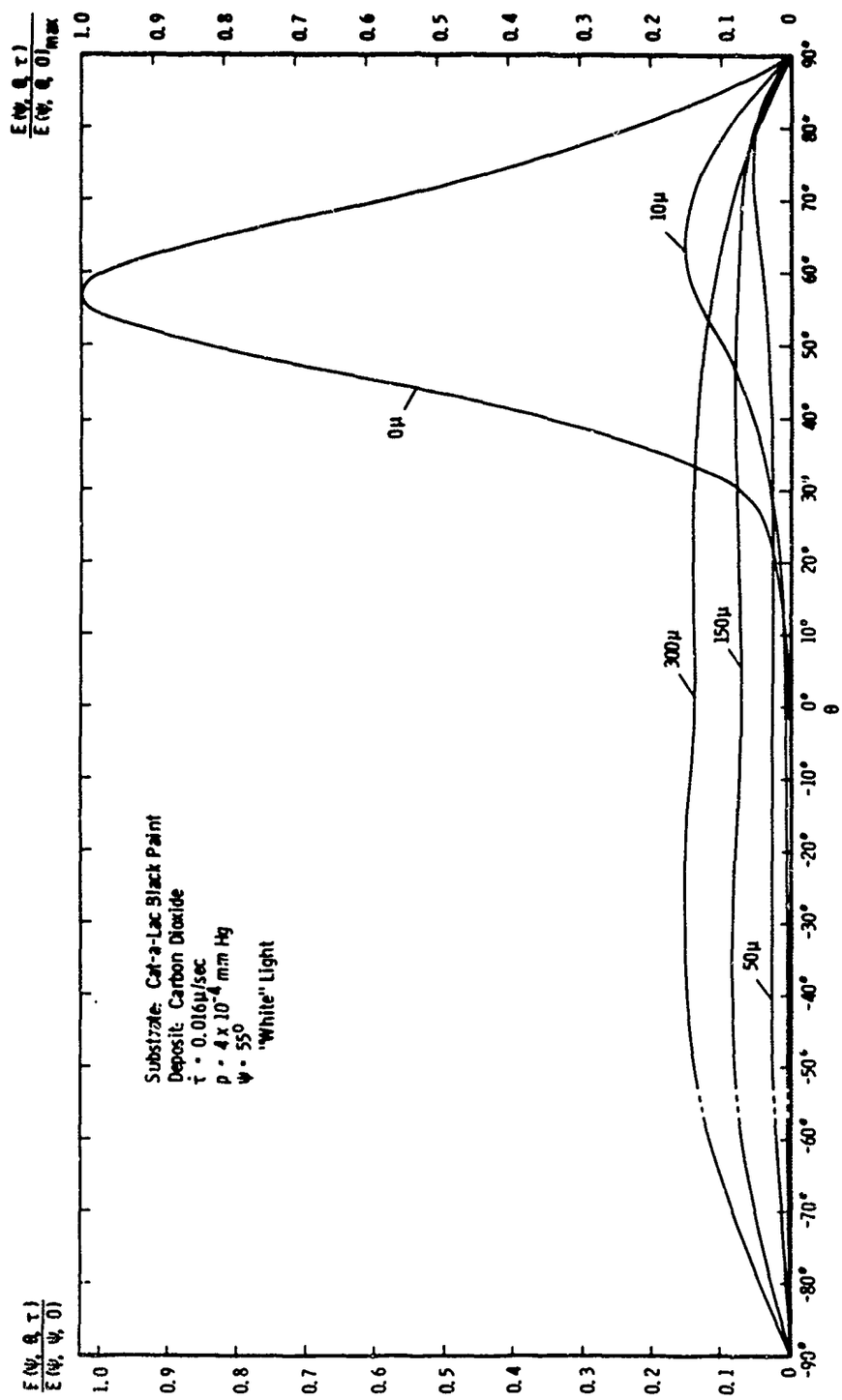

Figure 21. Normalized biangular distributions of "white" light radiation reflected from various thicknesses of carbon dioxide deposit formed on a black paint substrate, $\psi = 55°$.

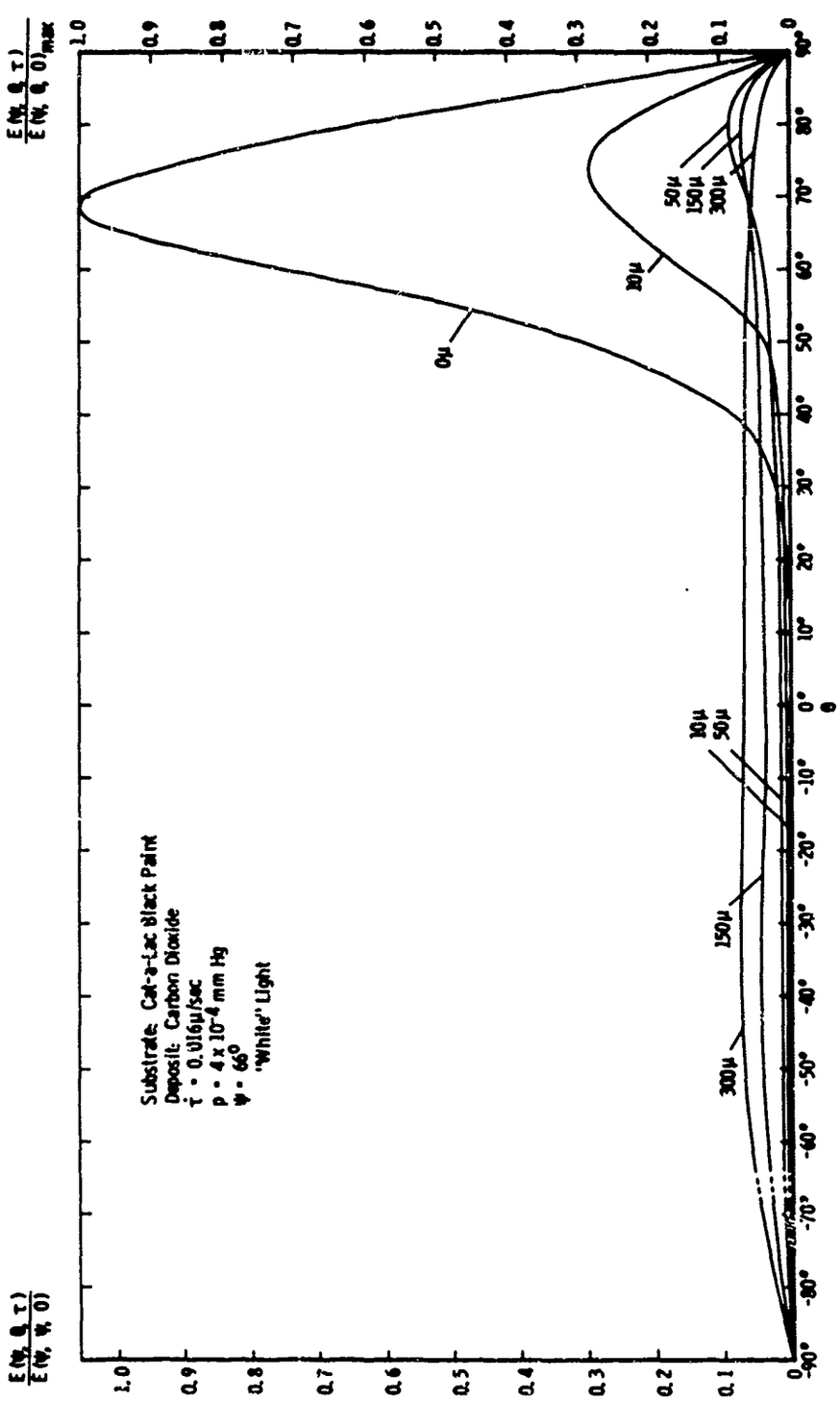

Figure 22. Normalized biangular distributions of "white" light radiation reflected from various thicknesses of carbon dioxide deposit formed on a black paint substrate, $\psi = 66°$.

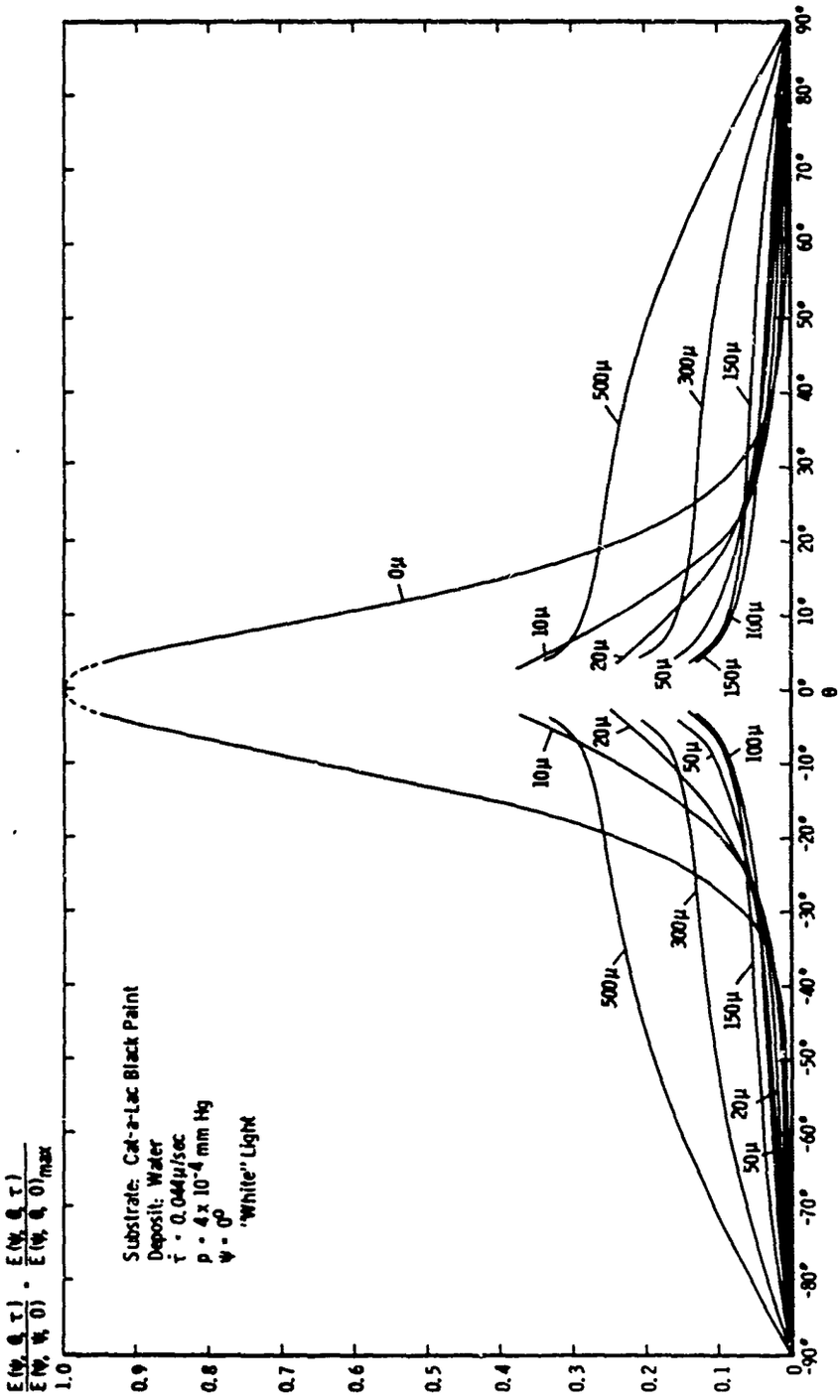

Figure 23. Normalized biangular distributions of "white" light radiation reflected from various thicknesses of water deposit formed on a black paint substrate, ψ = 0°.

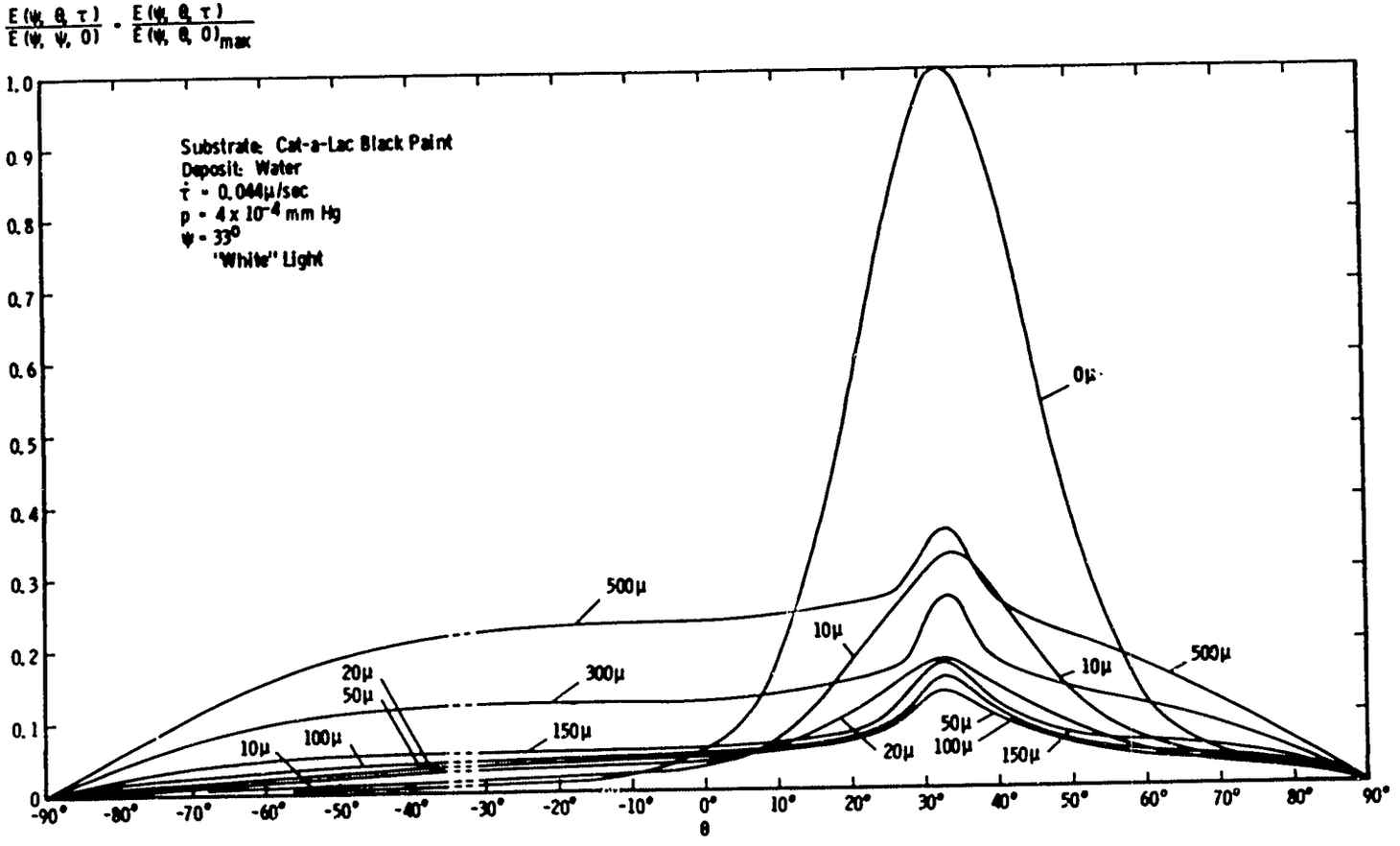

Figure 24. Normalized biangular distributions of "white" light radiation reflected from various thicknesses of water deposit formed on a black paint substrate, $\psi = 33°$.

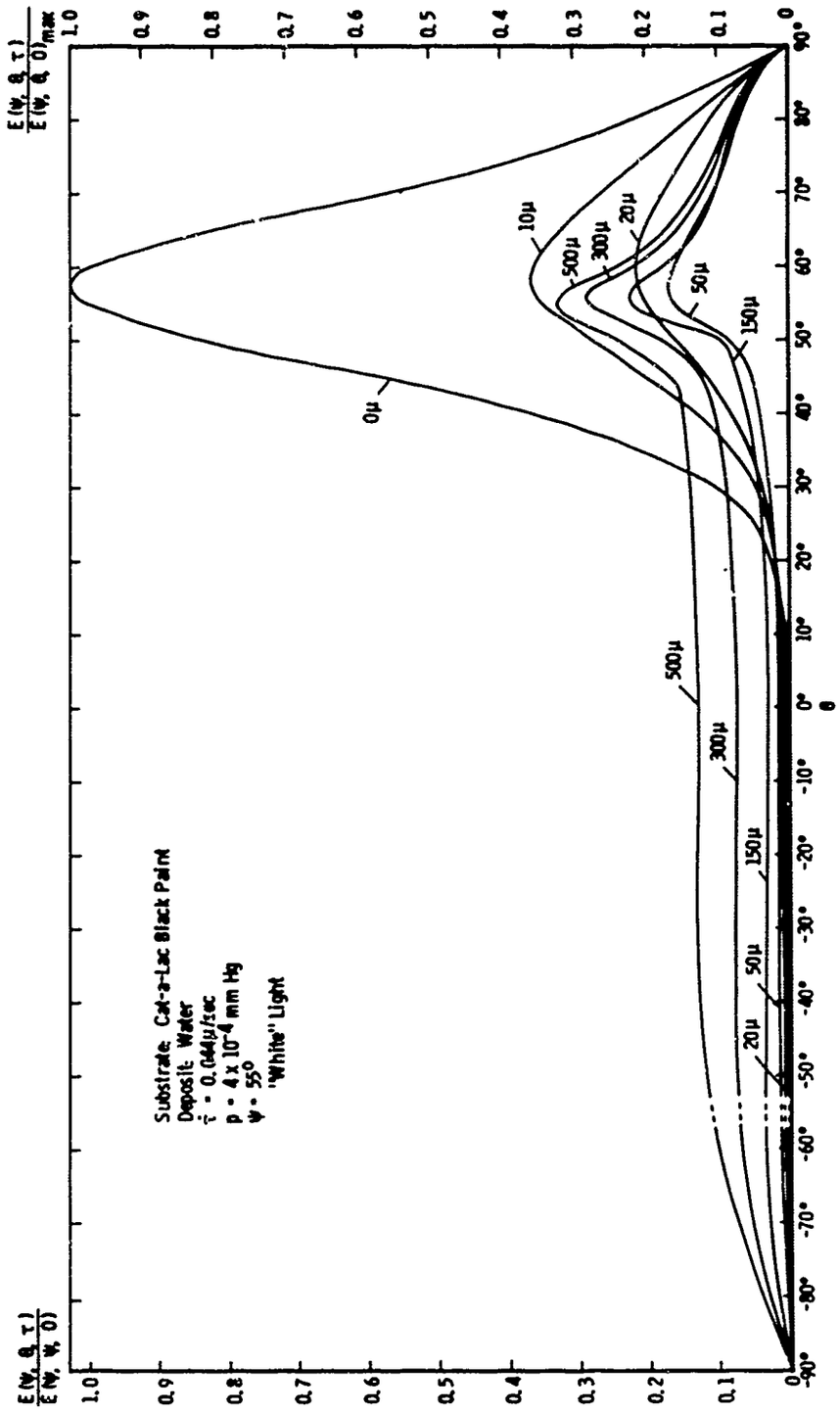

Figure 25. Normalized biangular distributions of "white" light radiation reflected from various thicknesses of water deposit formed on a black paint substrate, ψ = 55°.

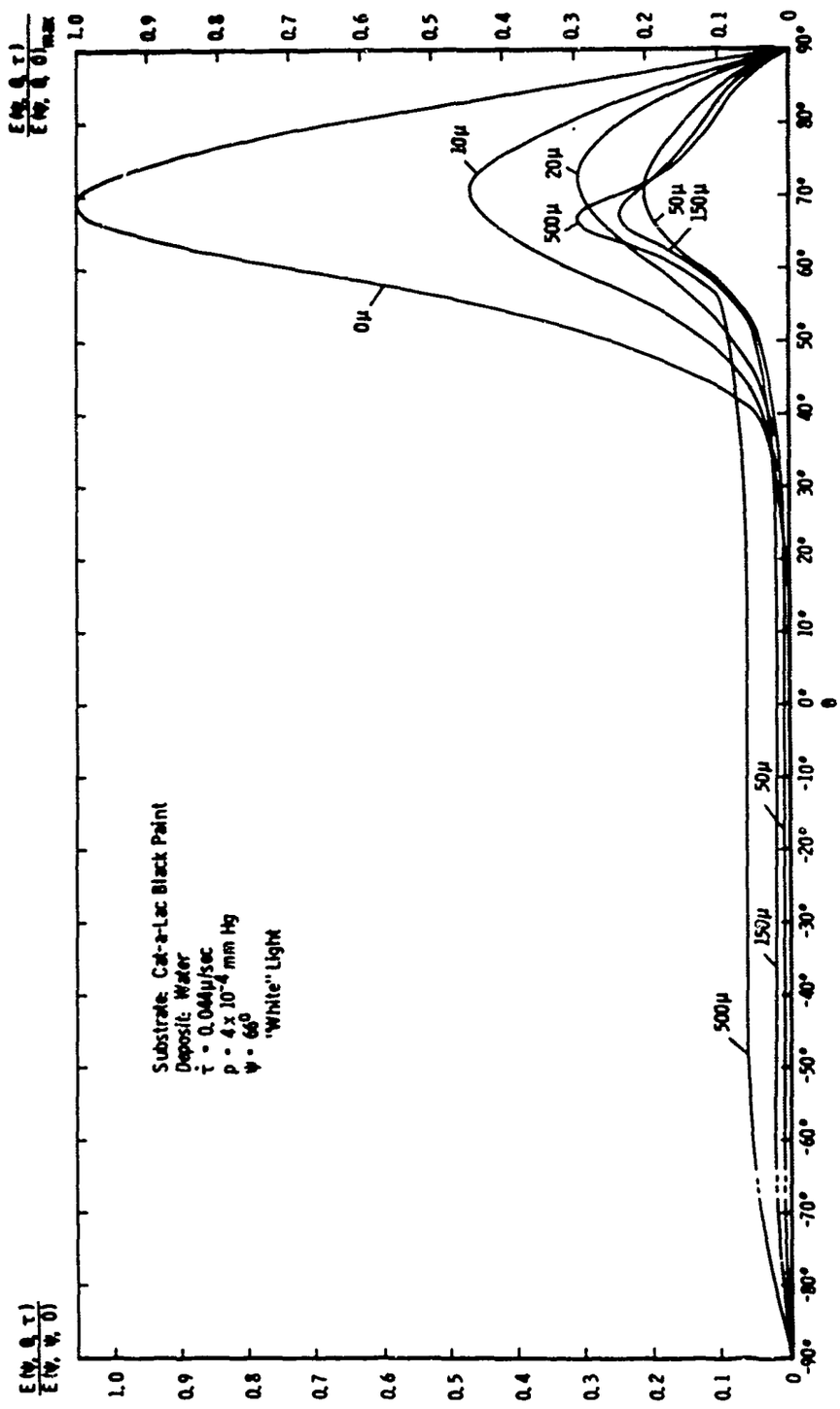

Figure 26. Normalized biangular distributions of "white" light radiation reflected from various thicknesses of water deposit formed on a black paint substrate, ψ = 66°.

The influence of the wavelength on the distributions is shown in Figures 27 through 30 for carbon dioxide deposit and in Figure 31 for water deposits. These distributions were obtained at a constant deposit thickness and a constant angle of incidence at wavelengths $\lambda = 0.7\mu$, 0.8μ, 0.9μ, and 1.0μ. Irradiation of the cryodeposit with filtered light results in very small detector outputs (below 0.1 mV at the recorder). Hence, these measurements are less accurate than the distributions obtained with "white" light, since the noise level of the silicon light detector and transfer line was approximately 0.004 mV which is 4 percent of the maximum recorded signal. This noise voltage was measured at zero irradiation as the difference in voltage read on the recorder between having the recorder terminals shorted and having the light detector and transfer line connected.

As was discussed before the distributions are interrupted in the region $\theta = -\psi$ because at this angle the detector passes in front of the incident beam of radiation. Therefore, $E(0°,0°,0)$, the normalization factor for distributions obtained at an angle of incidence $\psi = 0°$, could not be measured. $E(5°,5°,0)$ is substituted for $E(0°,0°,0)$ which should be approximately correct considering that $E(\psi,\psi,0)$ is essentially equal at $\psi = 5°$ and $\psi = 10°$.

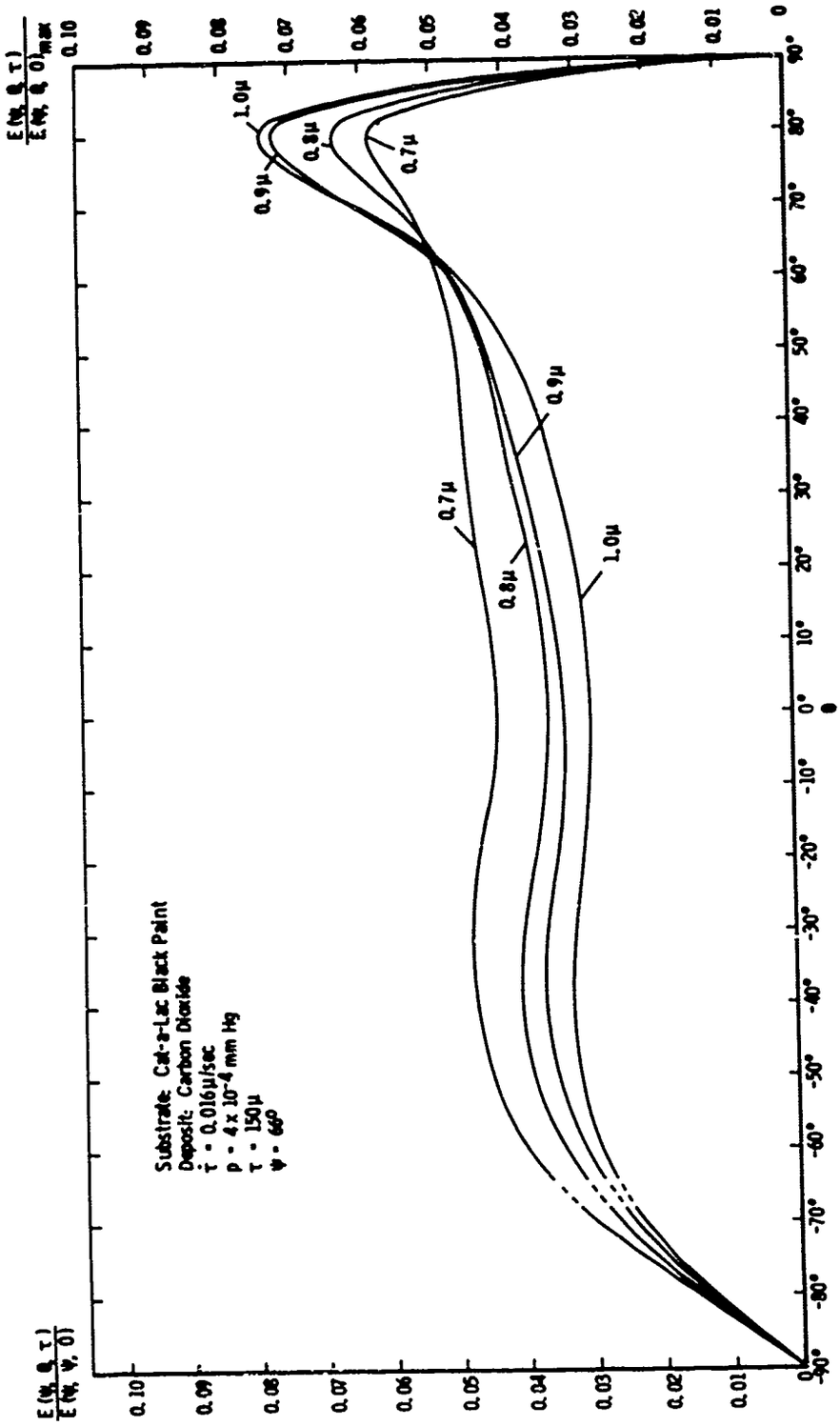

Figure 27. Normalized biangular distributions of radiation of various wavelengths reflected from a 150μ thick carbon dioxide deposit formed on a black paint substrate, ψ = 66°.

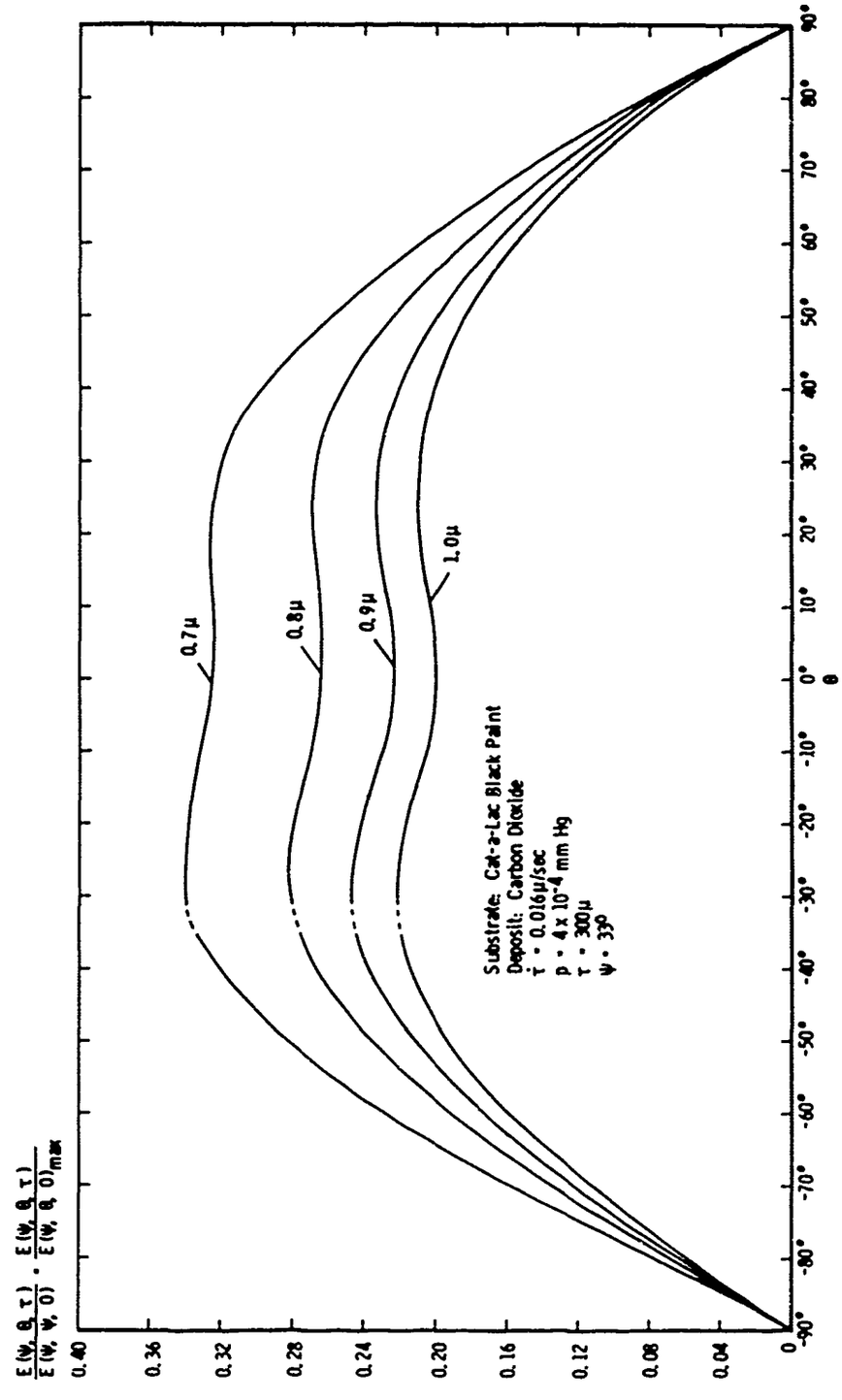

Figure 28. Normalized biangular distributions of radiation of various wavelengths reflected from a 300μ thick carbon dioxide deposit formed on a black paint substrate, ψ = 33°.

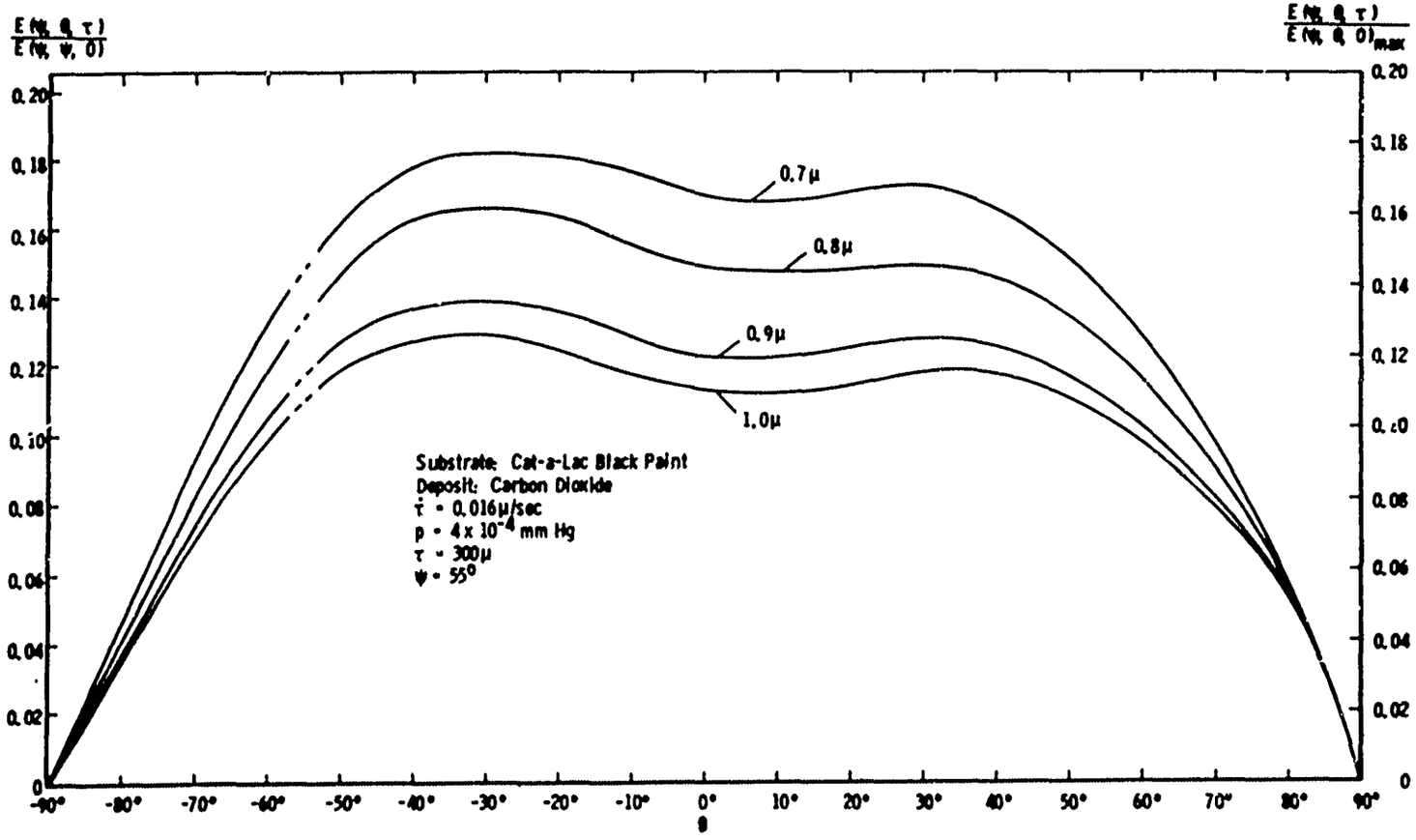

Figure 29. Normalized biangular distributions of radiation of various wavelengths reflected from a 300μ thick carbon dioxide deposit formed on a black paint substrate, ψ = 55°.

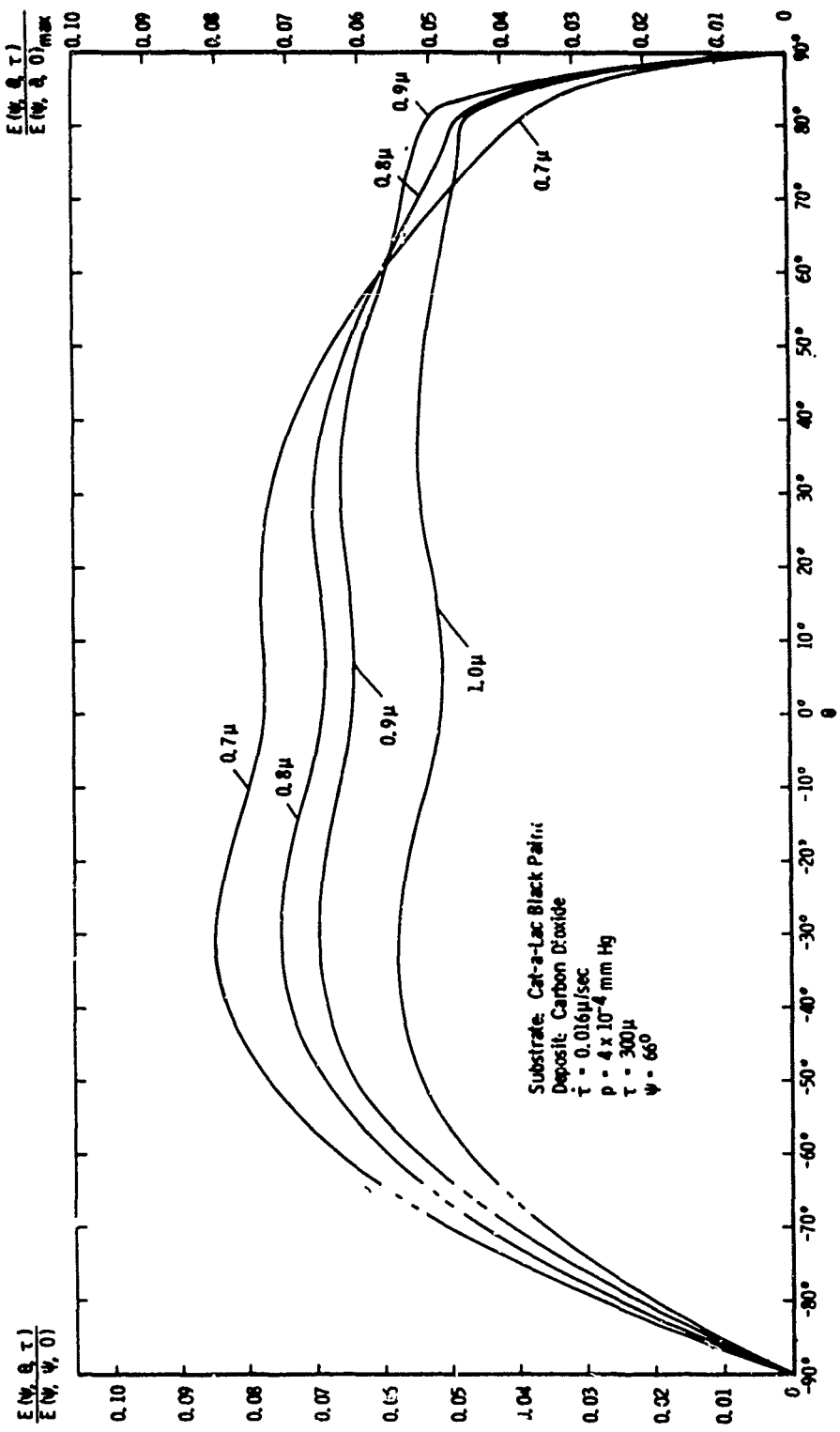

Figure 30. Normalized biangular distributions of radiation of various wavelengths reflected from a 300μ thick carbon dioxide deposit formed on a black paint substrate, ψ = 66°.

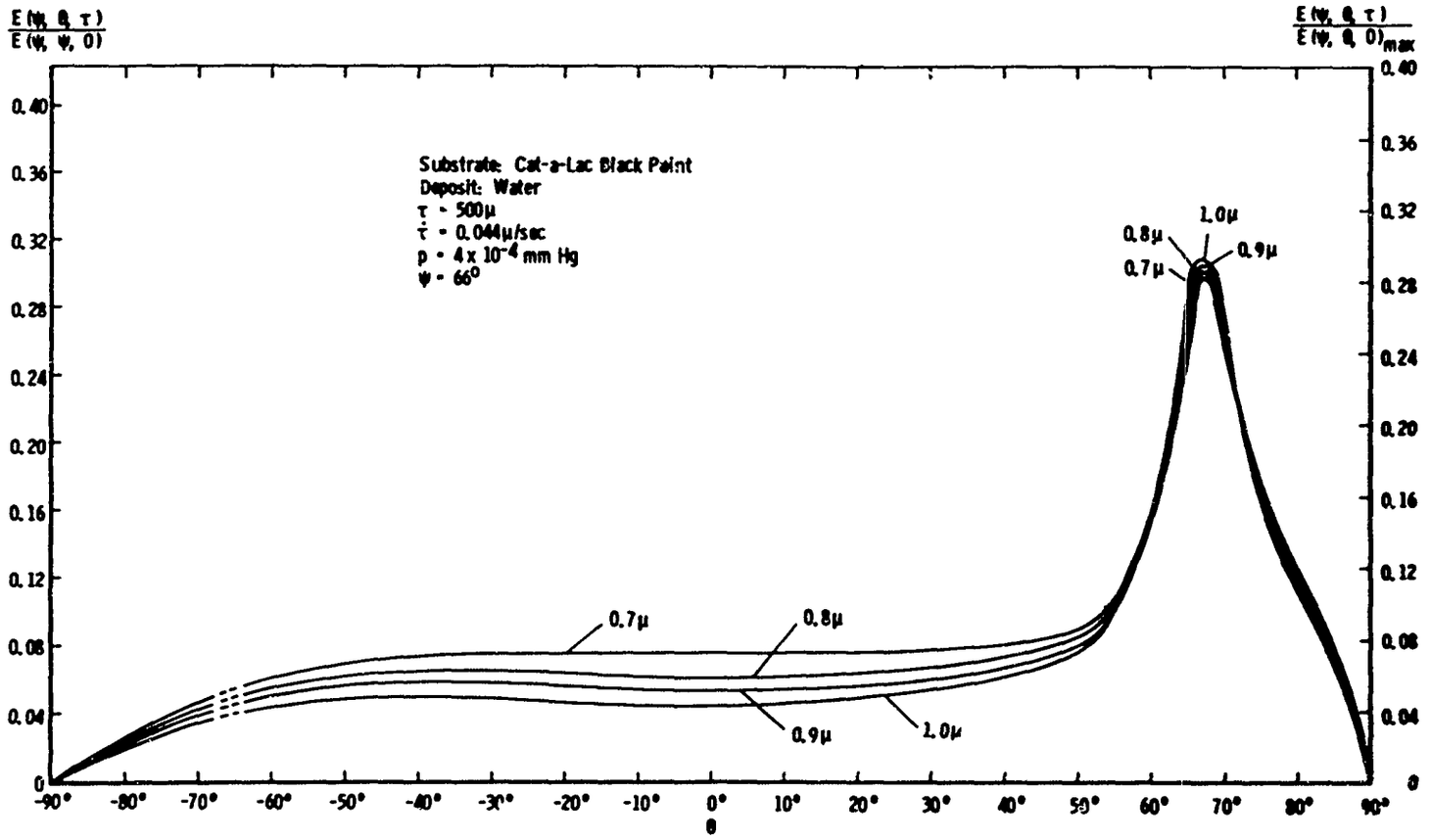

Figure 31. Normalized bi[illegible]lar distributions of radiation of various wavelengths reflected [illegible] a 500μ thick water deposit formed on a black paint substrate, ψ = 66°.

2. The normalization of the biangular distributions. The biangular distributions of the radiation reflected from cryodeposits can be normalized with respect to either the magnitude of the peak of the reflected radiation $E(\psi,\theta,0)_{max}$ or to the amount of the radiation reflected from the bare substrate at the specular angle $E(\psi,\psi,0)$. When no off-specular shift of the radiation reflected from the bare substrate occurs, both normalization factors are equal. This is the case for the polished copper substrate in general and the black paint substrate at an angle of incidence of 0° and 33°. The radiation reflected from the black paint, if it is irradiated at an angle of incidence of 55° and 66°, shows an off-specular shift, and thus the normalization factors are different. Therefore, two scales are provided in the figures which report biangular distributions obtained on a black paint substrate at angles of incidence of 55° and 66°. No preference was given to either of the two normalization factors. Normalization with respect to the reflectance at the specular angle, similar to normalizing with $E(\psi,\psi,0)$, was used by Torrance [9]. However, it is felt advantageous to use $E(\psi,\theta,0)_{max}$ as the normalization factor since it leads to better reproducibility of results with different batches of the black paint substrate. Experience shows that the black paint substrates prepared in different batches result in different

off-specular shifts at the same angle of incidence. While $E(\psi,\psi,0)$ may change appreciably for off-specular shifts as great as 3°, $E(\psi,\theta,0)_{max}$ remains essentially independent of off-specular shifts. Also the use of $E(\psi,\theta,0)_{max}$ as normalization factor has the advantage that it can be more accurately measured than $E(\psi,\psi,0)$.

Normalized distributions obtained at different wavelengths are compared quantitatively. Therefore, the normalization factor has to be proportional to the light flux incident on the cryodeposit. In order to demonstrate that this is true, a crude analysis of the light flux incident on the cryodeposit is carried out in the following.

The incident light flux can be calculated from the measurement of the distribution of the radiation reflected from the bare substrate at an angle of incidence of 0°. The entire amount of energy reflected per unit time and unit area from the illuminated area dA of the substrate is obtained from

$$de_r = 2\pi \cdot \int_0^{\pi/2} I(\theta) \cdot \cos\theta \cdot \sin\theta \, d\theta \qquad (37)$$

given in [14]. The intensity of the reflected radiation $I(\theta)$ is computed from Equation (3), where for $\psi = 0°$

$$I(\theta) = \frac{E(0°,\theta,0)}{dA\ \Delta\omega_r \cos\theta} \tag{38}$$

The energy incident on the substrate per unit time and unit area is approximately

$$de_i = \frac{1}{\rho_{ah}} \cdot de_r$$

where ρ_{ah} is the angular-hemispherical reflectance of the substrate. The relative reflectance of polished copper with respect to magnesium oxide is very close to one if the wavelength is greater than 0.7μ (see Figure 8, page 37). The evaluation of the integral in Equation (37) by a graphical technique, however, becomes very inaccurate since polished copper is a specular reflector. The integral can be evaluated very well for the black paint since the paint is not nearly as specular as polished copper. But de_r cannot be obtained accurately with this paint because ρ_{ah} of this paint varies between 4 and 8 percent for paint prepared in different batches. The relative reflectance of black paint with respect to magnesium oxide, as measured by Wood et al. and reported in [1], remains essentially constant between a wavelength of 0.5μ and 1.0μ. Thus de_i is proportional to de_r between these wavelengths, and by using Equations (37) and (38), it can further be concluded that

$$de_i \sim \int_0^{\pi/2} \frac{E(0°,\theta,0)}{\cos\theta} \cdot \cos\theta \cdot \sin\theta \, d\theta \qquad (39)$$

In Table 1, the incident light flux on the cryodeposit per unit area at a certain wavelength and at an angle of incidence of 0°, as computed from Equation (39), is compared with the directly measured rate of energy reflected from the cryodeposit at the same wavelength and angle of incidence of 5°. The value at a wavelength of 0.9μ serves as a reference.

TABLE 1

COMPARISON OF THE LIGHT FLUX INCIDENT ON THE DEPOSIT AND THE NORMALIZATION FACTOR AT AN ANGLE OF INCIDENCE OF 0° AND VARIOUS WAVELENGTHS

λ	$\frac{de_{i_\lambda}}{de_{i_{0.9\mu}}}$	$\frac{E(5°,5°,0)_\lambda}{E(5°,5°,0)_{0.9\mu}}$ black paint
0.7μ	0.389	0.402
0.8μ	0.690	0.681
0.9μ	1.0	1.0
1.0μ	0.804	0.794
"white" light	26.7	26.8

Since both values agree well at each wavelength, it can be concluded that the normalizing factor E(5°,5°,0) is proportional to the light flux incident on the cryodeposit.

It is shown in Table 2 that

$$\frac{E(66°,\theta,0)_{max}}{E(5°,5°,0)}$$

of the black paint is essentially equal at different wavelengths. Thus, at an angle of incidence of 66°, the normalizing factor $E(66°,\theta,0)_{max}$ is also proportional to the light flux incident on the cryodeposit.

TABLE 2

COMPARISON OF THE NORMALIZATION FACTOR FOR THE BLACK PAINT AT AN ANGLE OF INCIDENCE OF 5° AND 66° AND AT VARIOUS WAVELENGTHS

λ	$\left.\frac{E(66°,\theta,0)_{max}}{E(5°,5°,0)}\right\|_{\text{black paint}}$
0.7μ	5.34
0.8μ	5.49
0.9μ	5.49
1.0μ	5.58
"white" light	5.44

A significant increase of the normalization factor with the angle of incidence is observed from Table 2. Therefore, it is not possible to compare directly normalized distributions at different angles of incidence. This

applies also to the polished copper substrate, where in this case $\frac{E(66°,\theta,0)_{max}}{E(5°,5°,0)}$ is between 1.2 and 1.5.

Since this normalization factor is different at different angles of incidence, the normalized distributions obtained at different angles of incidence cannot be compared directly. Thus, in order to show quantitatively the influence of the angle of incidence on the distributions, the distributions obtained at different angles of incidence should be normalized with respect to the same normalization factor. In Figure 32, distributions are displayed which were obtained from carbon dioxide deposit formed on the black paint substrate at the same deposit thickness and wavelength but at different angles of incidence. These distributions are normalized with respect to the same normalization factor E(5°,5°,0). It is observed that the amount of radiation reflected from the cryodeposit is increasing with increasing angle of incidence. However, by comparing Figures 19 through 22, pages 64 through 67 directly, a wrong conclusion would have been drawn. The behavior of the curves in Figure 32 will be explained in detail later.

3. Phenomena observed from the biangular distributions of the reflected radiation. The biangular distributions of the radiation reflected from cryodeposits show

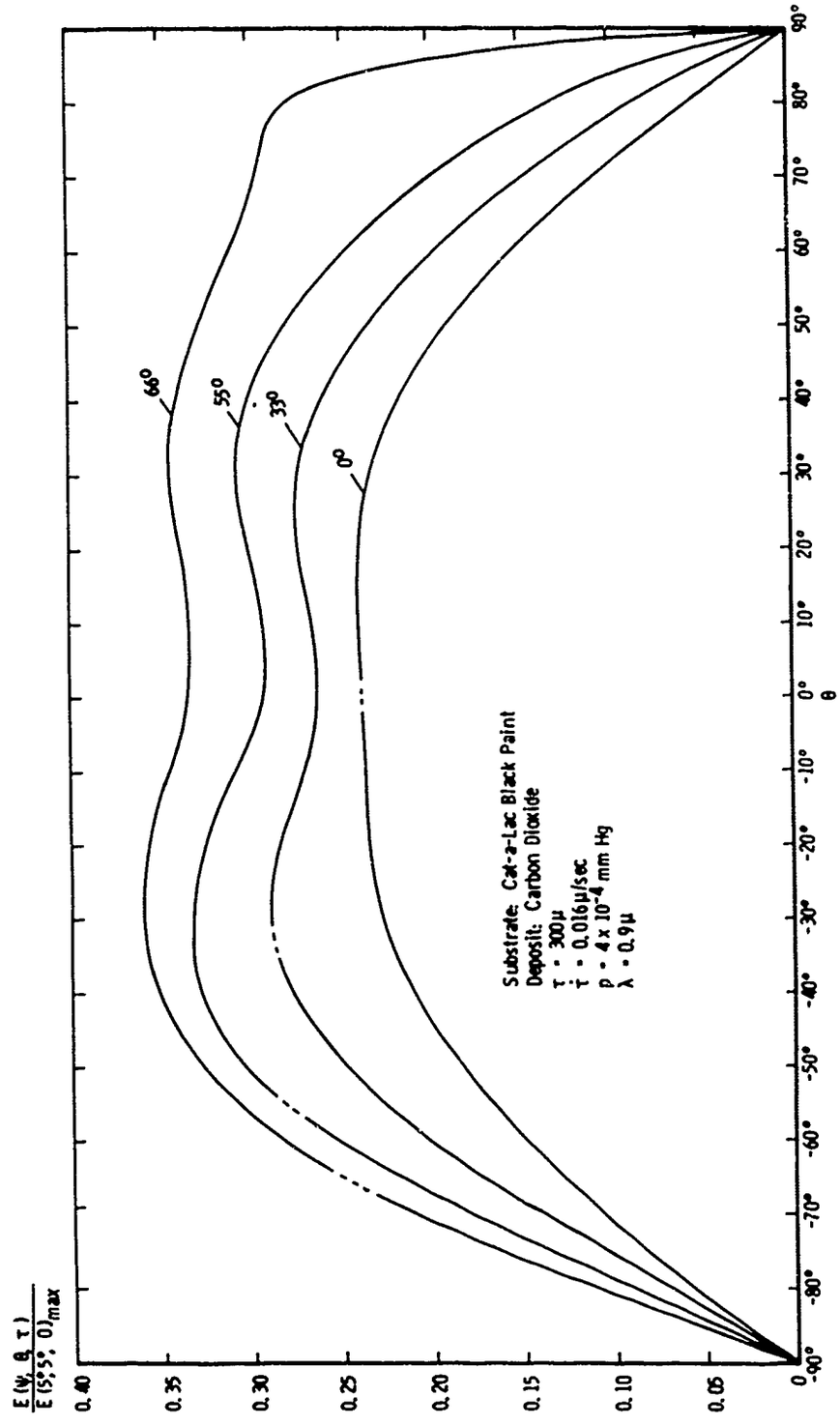

Figure 32. Biangular distributions of λ = 0.9μ radiation reflected from carbon dioxide deposit formed on a black paint substrate for various angles of incidence with constant normalization factor.

the following phenomena which were observed before by other investigators mentioned in Chapter I.

1. The magnitude of the peak of the distribution is decreasing with increasing deposit thickness
2. Scattering interference patterns
3. Backscattering
4. Off-specular shift of the peak of the distribution

It is observed from all reported distributions that the magnitude of the peak of the distribution decreases with increasing deposit thickness so that the radiation reflected from cold panels covered by cryodeposits becomes more diffuse with increasing deposit thickness. It is also noticed that a greater decrease of the magnitude of the peak of the distribution results from carbon dioxide depcsits than from water deposit at the same deposit thickness.

Scattering interference patterns are observed and indicated in Figure 15, page 59, and in Figure 17, page 61. These scattering interference patterns are not investigated in this work since they were analyzed in detail in [3] for carbon dioxide deposit.

Backscattering is in this investigation defined as a peak in the reflected radiation which occurs at negative viewing angles θ. Backscattering is observed

and indicated in Figure 16, page 60, and in Figure 18, page 62. This phenomenon is not investigated in this work.

Off-specular shifts of the peaks of the distributions of the reflected radiation (as defined in Chapter I) are observed in many of the reported biangular distributions. These off-specular shifts, as well as the magnitudes of the peaks of the distributions, are investigated in detail in the following: first, for carbon dioxide and water cryodeposits formed on a black paint substrate and secondly from carbon dioxide and water cryodeposits formed on a polished copper substrate.

4. Carbon dioxide deposit formed on a black paint substrate. The off-specular shift of the radiation reflected from carbon dioxide cryodeposit at an angle of incidence of 55° and 66° and at wavelengths of 0.7μ and 0.9μ is shown in Figure 33. It is observed that for an angle of incidence of 66° the carbon dioxide deposit shows an off-specular shift increasing with the deposit thickness until the off-specular shift reaches a maximum value of 14° at a deposit thickness of 50μ. If the angle of incidence is 55°, the shift reaches a maximum value of 19.9° at the same thickness. At an angle of incidence of 33° and 0°, no off-specular shift was observed as shown in Figures 19 and 20, pages 64 and 65. Above a

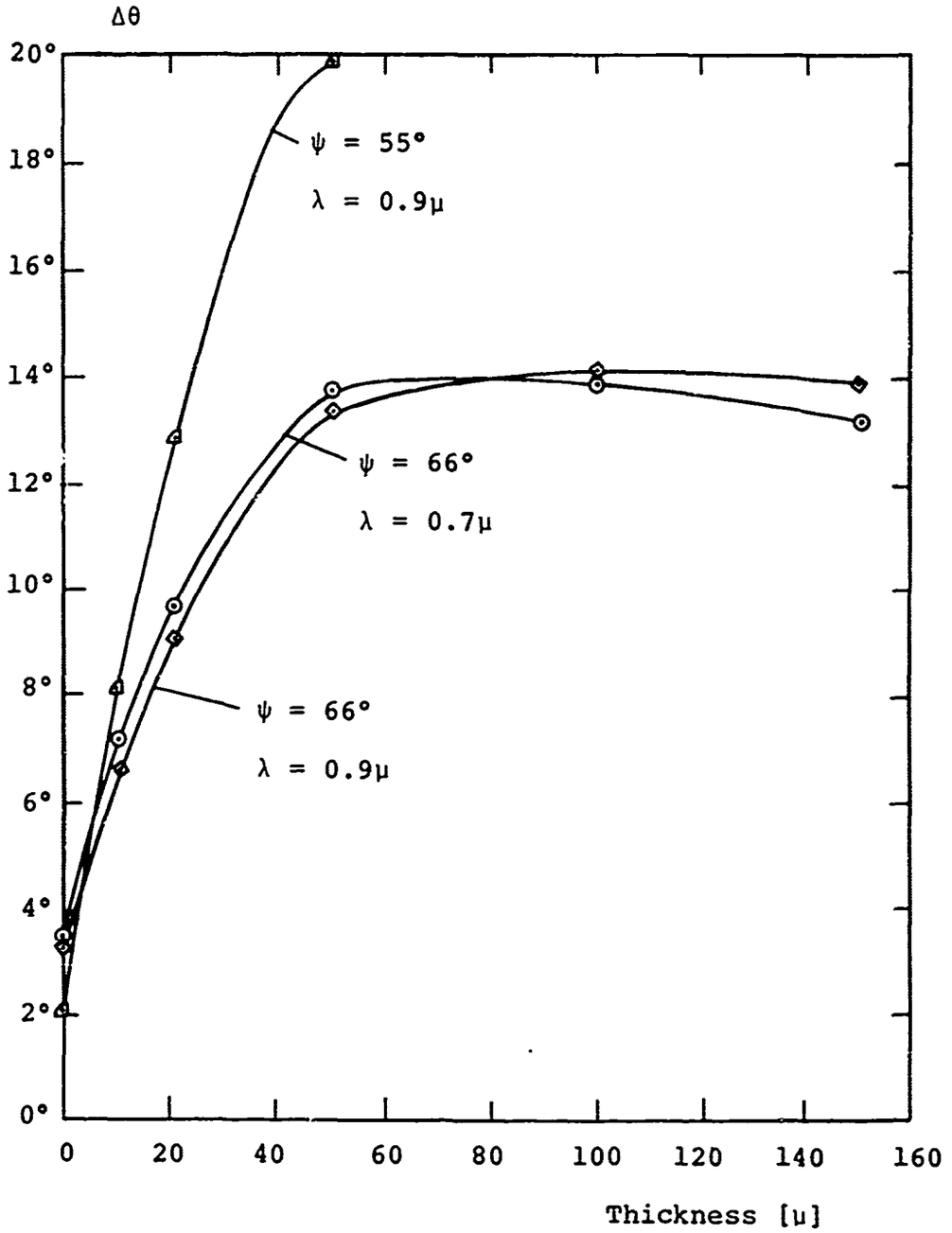

Figure 33. Off-specular shift of radiation reflected from carbon dioxide deposit formed on a black paint substrate.

deposit thickness of 50μ for an angle of incidence of 55° and above a thickness of 150μ for an angle of incidence of 60°, inspection of Figures 21 and 22, pages 66 and 67, shows that the distribution of the reflected radiation becomes diffuse. Thus, the off-specular shift is not definable. While no systematic influence of the deposition rate $\dot{\tau}$ on the off-specular shift was apparent from the measurements, ($0.0011\mu/\text{sec} \leq \dot{\tau} \leq 0.016\mu/\text{sec}$; 6×10^{-5} mm Hg $\leq p \leq 4 \times 10^{-4}$ mm Hg), an investigation of the influence of the wavelength of the off-specular shift indicated that at an angle of incidence of 66°, the off-specular shift decreases with increasing wavelength below a deposit thickness of 100μ. Above this thickness of 100μ the shift increases with increasing wavelength. The change of the off-specular shift with wavelength is only very small, and this change is smaller than the accuracy of this measurement. However, it is felt that the indicated change of the off-specular shift with wavelength is real since these measurements of the off-specular shift at different wavelengths were obtained in the same test run, and thus with the same deposit and at the same setting of the angle of incidence. The observed influence of the wavelength on the off-specular shift at a deposit thickness below 100μ (decreasing off-specular shift with increasing wavelength) is explained in the following paragraph. Afterwards, an explanation

is given for the influence of the wavelength on the off-specular shift at a deposit thickness above 100 (increasing off-specular shift with increasing wavelength).

As shown before the light flux reflected from the substrate in the case of carbon dioxide cryodeposit is very small compared to that reflected from the interface. If the deposit is thin and the internal scattering inside the deposit can be neglected, most of the detected radiation is due to reflection from the interface, and thus it can be assumed that the off-specular shift is solely due to the influence of the surface roughness of the vacuum-deposit interface on the reflected radiation. The off-specular shift from the thin deposit and the off-specular shift obtained from roughened glass surfaces is influenced by the wavelength in the same manner, as can be shown from measurements on roughened glass surfaces reported my Müller in (15). It was found that below a roughness of $\sigma = 1.77\mu$, decreasing off-specular shift occurs with increasing wavelength (σ/λ becomes smaller with increasing λ), which explains the decreasing off-specular shift with increasing wavelength observed at a deposit thickness below 100μ.

It is also observed in Figure 33, page 87, that the off-specular shift increases with increasing deposit thickness. This suggests that the interface roughness is increasing with increasing deposit thickness. This

increased roughness tends towards more diffuse reflection which can be concluded from measurements on roughened glass surfaces reported in Chapter III. In addition to the surface roughness, however, internal scattering tends to influence the distribution.

The exact amount of radiation reflected due to internal scattering cannot be obtained from the distribution of the reflected radiation because also the interface reflects light into angles θ aside from the specular direction, and hence, the reflection from the interface cannot be distinguished from that scattered internally. However, one can reason that the reflected radiation measured at angles far from the specular direction is due to internal scattering since the magnitude at these angles increases about linearly with the deposit thickness as seen from the measured distributions in Figures 19 through 22, pages 64 through 67. Using this argument it can be concluded from Figure 28, page 74, that the amount of internally scattered radiation increases with decreasing wavelength. This leads to an explanation for the increasing off-specular shift with increasing wavelength at a deposit thickness above 100μ.

The amount of internally scattered radiation increases with decreasing wavelength, so that the magnitude of the peak of the radiation reflected from the interface becomes relatively smaller at decreasing wavelength as

compared to the reflected radiation due to internal scattering. If this radiation, which shows an essentially diffuse distribution at a deposit thickness of 100μ, is added to the radiation reflected from the interface, the sum of the two components will possess less off-specular shift than the component of the reflection on the interface alone. This effect will be stronger if the component due to interface reflection is relatively smaller as compared to the component due to internal scattering. Thus the off-specular shift will be smaller for a smaller wavelength which explains the influence of the wavelength on the off-specular shift at a deposit thickness above 100μ.

If the angle of incidence is 55°, a greater off-specular shift is observed at a deposit thickness of 50μ than at an angle of incidence of 66°. It is shown by Müller in (15) that also the reflection of radiation from roughened glass surfaces shows this behavior. On the other hand the off-specular shift disappears at a lower thickness for an angle of incidence of 55°. This is a result of the smaller magnitude of the peak of the radiation reflected from the interface for an angle of incidence of 55° as indicated by the Fresnel equations. The relative intensity of unpolarized radiation computed with the Fresnel equations is smaller at an angle of incidence of 55° than at an angle of incidence of 66°. Hence, the

radiation reflected from the interface is obscured by reflected radiation due to internal scattering at a smaller deposit thickness for $\psi = 55°$ than for $\psi = 66°$.

5. Water deposit formed on a black paint substrate. In order to investigate the influence of the deposition rate and deposit thickness on the formation of the water cryodeposit, the off-specular shift of the radiation reflected from the cryodeposit on a black paint substrate was measured, and this shift is shown in Figure 34. The reproducibility of the curve was checked for a deposition rate of 0.044μ/sec, which was the rate used in the measurements of the biangular distribution of the reflected radiation. In addition, the off-specular shift for different deposition rates is presented in Figure 34. Within the accuracy of these measurements no systematic influence of the deposition rate on the off-specular shift was found ($0.012\mu/\text{sec} \leq \dot{\tau} \leq 0.098\mu/\text{sec}$; 1×10^{-4} mm Hg $\leq p \leq 7 \times 10^{-4}$ mm Hg).

In order to further investigate the influence of the deposition rate on the formation of the water cryodeposit, biangular distributions of the radiation reflected from water cryodeposit were measured at deposition rates equal to those used before for the measurement of the off-specular shift. These distributions are given in Figure 35 for a deposit thickness of 150μ. The

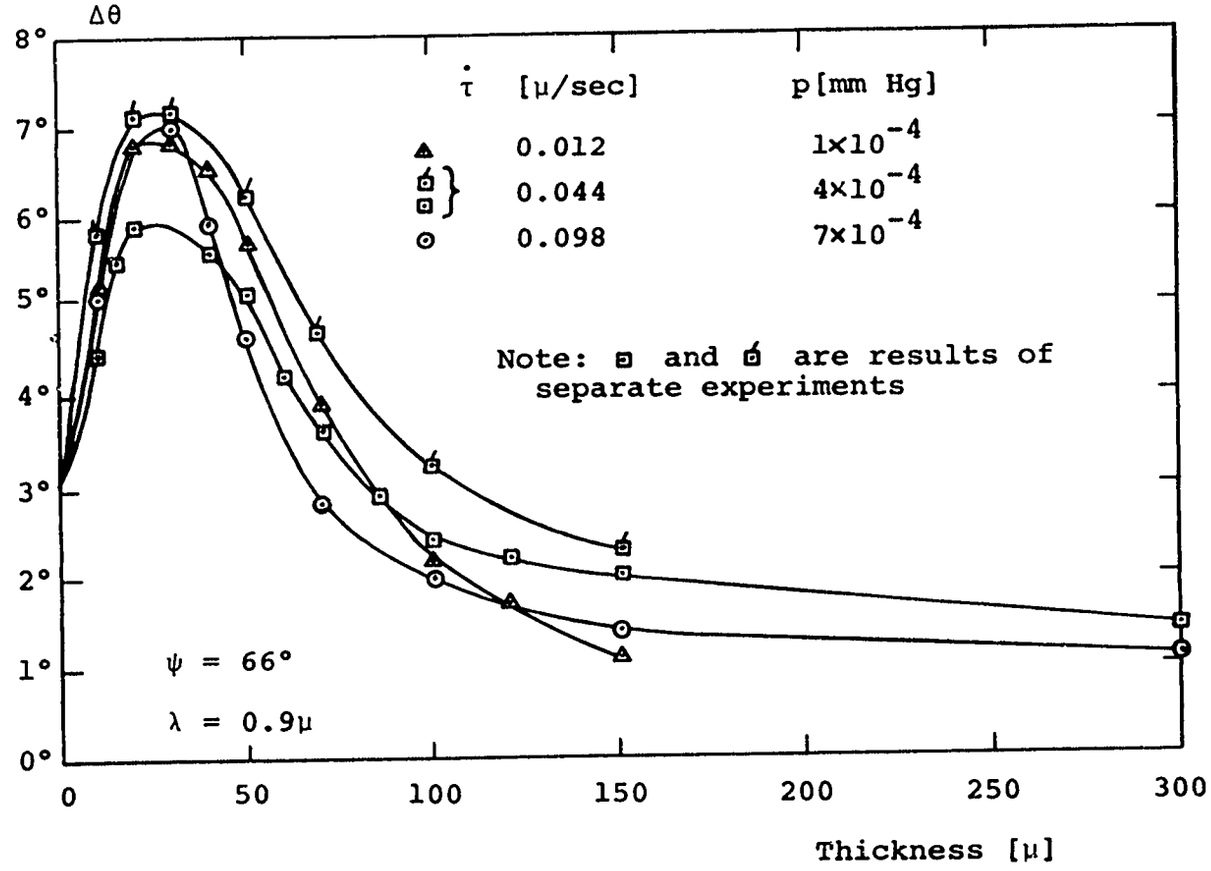

Figure 34. Off-specular shift of radiation reflected from water cryodeposit formed on a black paint substrate for $\psi = 66°$.

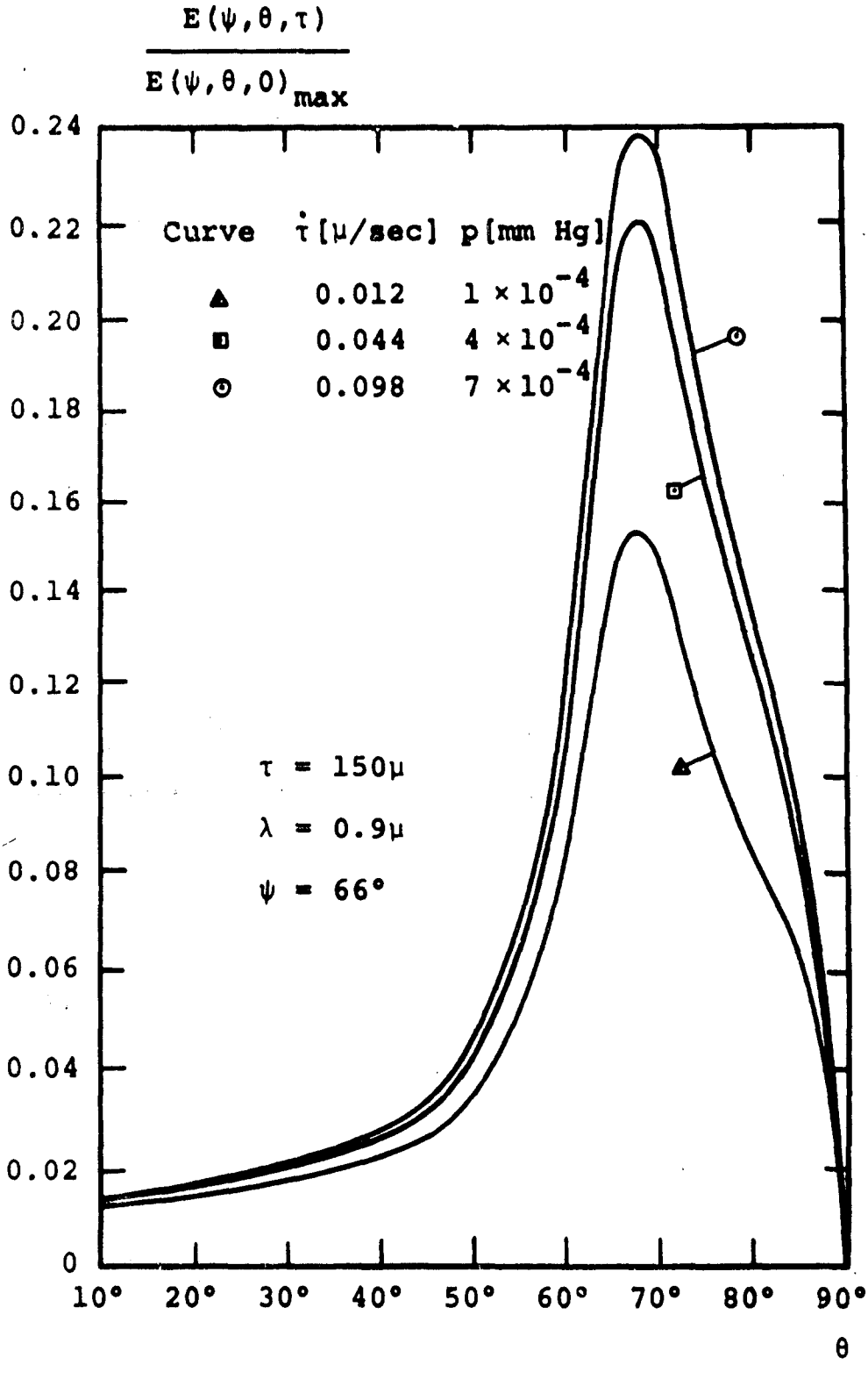

Figure 35. Biangular distribution of reflected radiation from water cryodeposit formed at various deposition rates on a black paint substrate, $\psi = 66°$.

magnitude of the peaks of the distributions, which is very sensitive to small changes of the interface roughness, is displayed in Figure 36 as a function of the deposit thickness. It is quite apparent from Figures 35 and 36 that the magnitude of the peaks of the distributions increases with increasing deposition rates. Thus, it can be concluded that with increasing deposition rate the vacuum-deposit interface is becoming smoother ($0.012\mu/\text{sec} \leq \dot{\tau} \leq 0.098\mu/\text{sec}$, 1×10^{-4} mm Hg $\leq p \leq$ 7×10^{-4} mm Hg) which can be contributed to an increasing nucleation rate and thus a grain size which decreases with increasing deposition rate. This was observed also by Thun [16] on metallic thin films.

Also the thickness of the deposit has an influence on the off-specular shift which is shown in Figure 34. With increasing deposit thickness the off-specular shift increases up to a deposit thickness of 25μ; then the off-specular shift decreases continuously with increasing thickness and assumes a very low value at a thickness of 500μ. This variation can be attributed to the relative importance of the deposit structure and the substrate determining the roughness of the vacuum-deposit interface as well as to the relative importance of the substrate and the interface on the reflected radiation. It is felt that the increase of the off-specular shift with increasing thickness below a thickness of 25μ is due to reflection

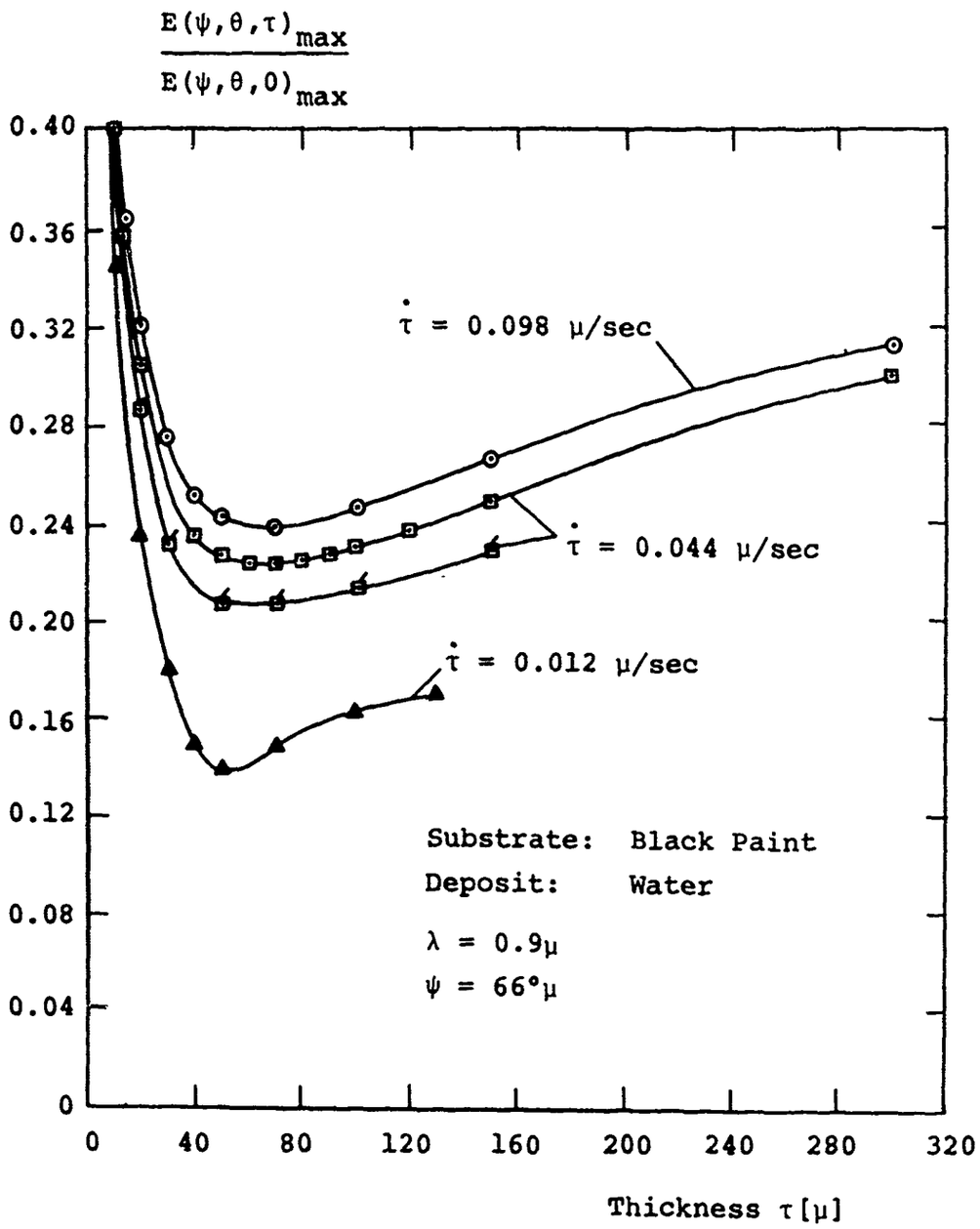

Figure 36. Normalized magnitudes of the peaks of the biangular distributions for water formed at various deposition rates on a black paint substrate.

from both vacuum-deposit interface and substrate. This can be concluded from the thin film interference patterns presented earlier which showed that at a small deposit thickness (below 2μ) the amount of radiation reflected from the water cryodeposit interface is of the same order as the amount of radiation reflected from the black paint substrate. It is felt that the decrease of the off-specular shift with increasing thickness at a thickness above 25μ is due to reflection from a vacuum-deposit interface which is becoming smoother with increasing thickness. In order to prove this statement, the distribution of the radiation reflected from the water deposit at a thickness of 500μ was compared with the distribution of the radiation reflected from the bare black paint substrate as shown in Figure 37. The distributions are normalized with the magnitude of their respective peaks. It is observed that the distribution obtained at a thickness of 500μ is much slimmer close to its peak than the distribution obtained at 0μ. Thus, it can be reasoned that the peak at a thickness of 500μ cannot be due to reflection from the rough black paint substrate, but is solely due to reflection from a very smooth interface.

In order to confirm conclusions drawn from the off-specular shift on the formation of the deposit at various deposit thicknesses, the magnitude of the peak

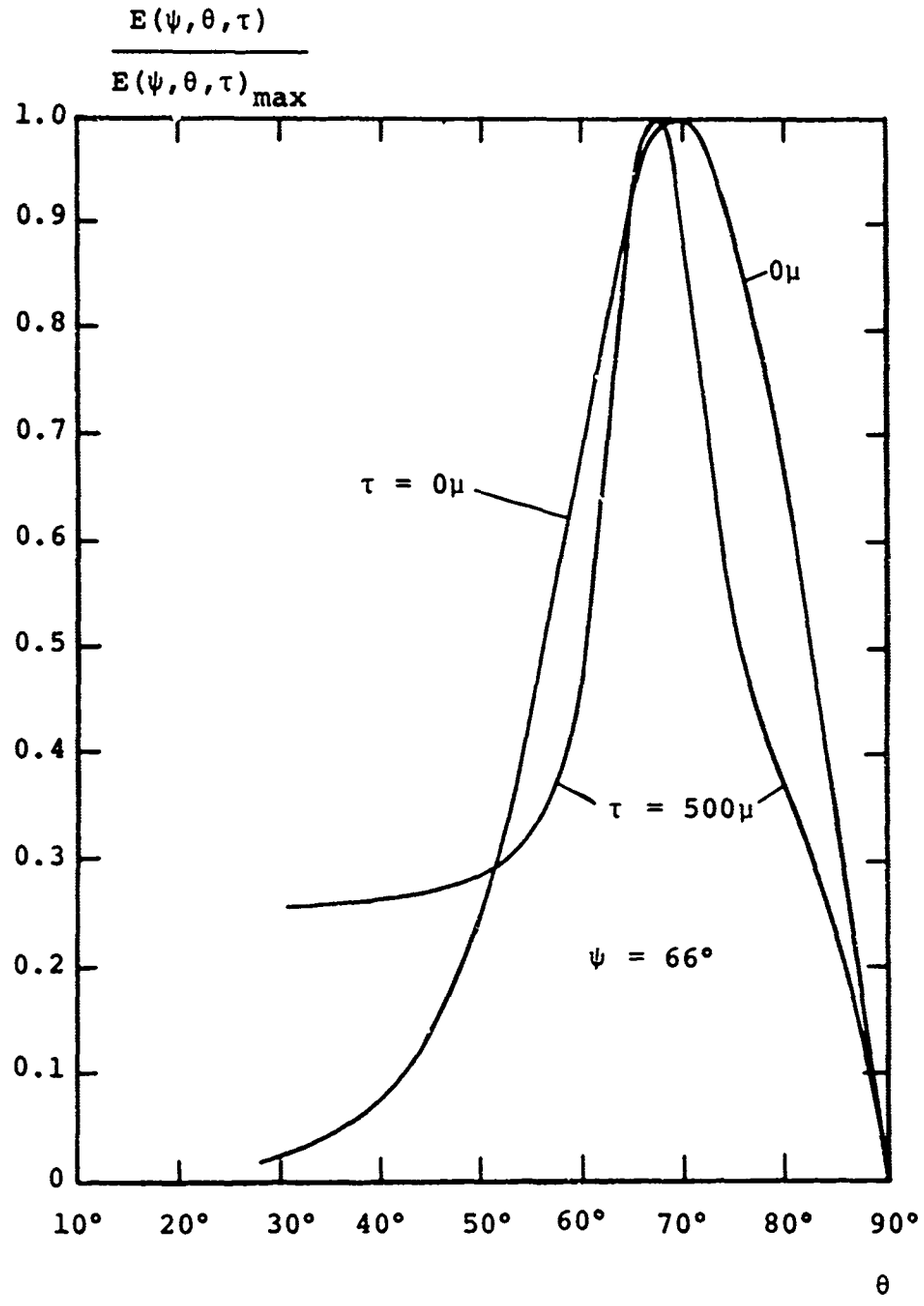

Figure 37. Normalized biangular distribution of 0.9μ wavelength radiation reflected from water deposit formed on a black paint substrate, $\psi = 66°$.

of the distributions and the diffuseness of the distributions at various deposit thicknesses were investigated. The magnitude of the peaks of the distributions rapidly decreases with increasing deposit thickness up to a thickness of about 40μ, then the magnitude of the peaks increases steadily with increasing thickness which is observed in Figure 36, page 96.

In order to show the changing diffuseness of the distributions with increasing deposit thickness, the "mid-peak width" of the distribution of the reflected radiation is defined in Figure 38. In Figure 39 the "mid-peak width" of the distributions obtained at an angle of incidence of 66° is displayed for various deposit thicknesses. It is observed that the "mid-peak width" increases initially with increasing thickness up to a thickness of about 25μ. Then the "mid-peak width" of the distributions decreases steadily with increasing deposit thickness.

These three investigations of the influence of the thickness on the formation of the deposit show that at a thickness below 25μ, the off-specular shift increases, the magnitude of the peak decreases, and the "mid-peak width" of the distribution increases with increasing deposit thickness. This diffusing effect of the cryodeposit on the distribution of the reflected radiation can be explained as follows.

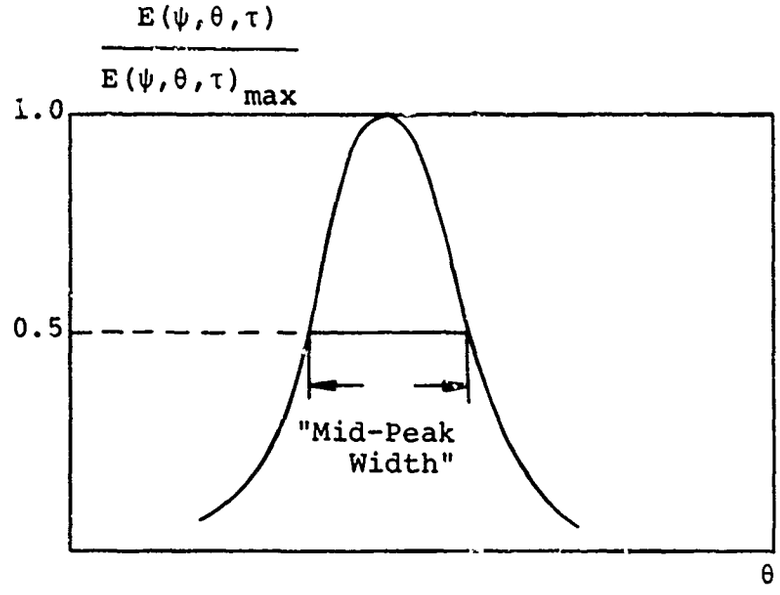

Figure 38. Definition of "mid-peak width" of biangular distribution.

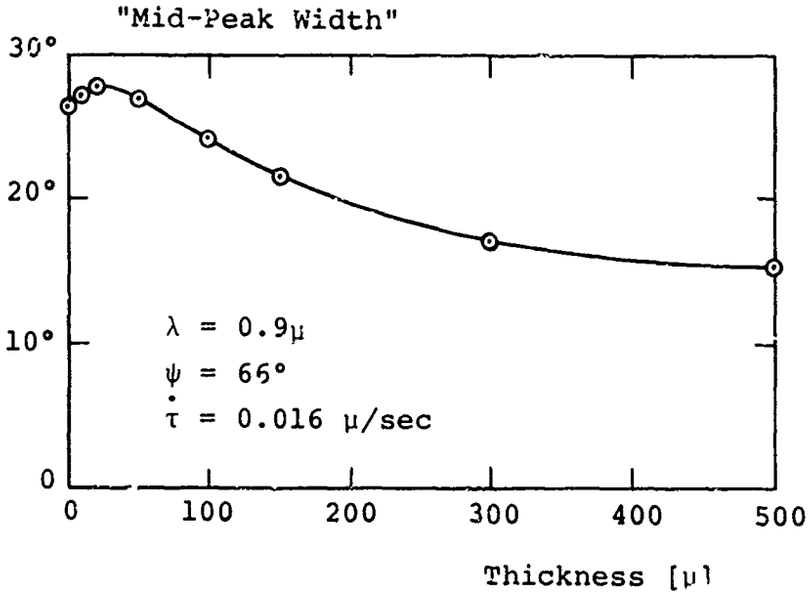

Figure 39. "Mid-peak width" of distribution of radiation reflected from water deposit formed on a black paint substrate.

In order to obtain thin film interference patterns, it is required that a thin film of uniform thickness is initially formed on the rough black paint substrate. This is evident because a variation in thickness would lead to random nature of the reflection. Therefore, the roughness of the interface and substrate is of the same order at small deposit thickness. It can be reasoned that, if these two rough faces are separated from each other, the radiation transmitted through the interface and reflected from the substrate (about half the amount of the total radiation reflected from the thin cryodeposit) becomes more diffuse than by reflection on the substrate only. The importance of this diffusing effect on the radiation reflected from the cryodeposit increases with increasing spacing between the two rough faces and hence with increasing deposit thickness.

Above a deposit thickness of approximately 25μ, the off-specular shift decreases, the magnitude of the peak of the reflected radiation increases, and the "mid-peak width" of the distribution decreases with increasing deposit thickness, so that the distribution becomes more peaked. This can be explained as follows. With increasing deposit thickness the influence of the substrate on the radiation reflected from the cryodeposit decreases, so that an increasing amount of the radiation reflected from the cryodeposit is due to reflection from the

interface, which becomes smoother with increasing thickness and is essentially a specular reflector at a deposit thickness of 500μ.

The question arises why water forms a smooth interface and why the interface of carbon dioxide is rough. A planar liquid water-ice interface at a temperature close to 0°C was observed by Bannister [17], and this was attributed by Owston [18] to the hexagonal structure of ice I[6], where the molecules are all concentrated close to planes. This structure of Ice I was observed by Burton [19] and Blackman [20] down to a temperature of about -80°C. At lower temperature, the structure changed, which was shown by x-ray and electron diffraction measurements. Burton [19] and Blackman [20] found that water vapor condensed with a cubic structure on a plate, which was cooled to a temperature between -120°C and -80°C; below -120°C, the deposit was either amorphous as shown in [19] or contained very small crystals as shown in [20]. This change of the structure with decreasing temperature is explained by Burton [19] with the migration of the molecules on the surface to positions of minimal potential energy, which are those positions favorable for crystal formation. This migration is slowed down, if the temperature is decreased below -80°C. At a temperature of

---

[6] Ice I is a phase of water which exists for very low pressures at temperatures between 0°C and -80°C.

-110°C, the migration of molecules has almost stopped, so that only small crystals can be formed or the deposit becomes amorphous.

It is also observed from these two investigations that disagreement exists about the structure of water deposit. This was attributed by Owston [18] to small amounts of different impurities in the deposit. In addition, Owston found that the structure varies with the deposition pressure. Water cryodeposit has an amorphous structure if deposited at pressures below 5×10^{-3} mm Hg at a temperature of 77°K, and it has a cubic crystalline structure at higher deposition pressures.

In this investigation only optical tests were performed. These tests lack the resolution necessary to determine the structure of the deposit. Therefore, it is not possible to decide whether the water deposit in this investigation was amorphous or crystalline. But it can be reasoned that either an amorphous structure or a structure containing small crystals forms an interface of small surface roughness. The interface of carbon dioxide deposit is rough, because carbon dioxide has a crystalline structure at a temperature of 77°K. This was found with x-ray diffraction by Graf [21], who formed the carbon dioxide deposit at a pressure of about 10^{-2} mm Hg.

6. Carbon dioxide deposit formed on a polished copper substrate. While the distributions of the radiation reflected from carbon dioxide deposit formed on a black paint substrate show off-specular shift phenomena, no off-specular shifts of the peak of the reflected radiation are observed in Figures 11 through 14, pages 55 through 58, where the deposit was formed on a polished copper substrate. However, it is apparent from Figure 14 that at a deposit thickness of 100μ a second peak emerges which occurs at a viewing angle θ greater than the angle of incidence ψ. This is confirmed by preliminary measurements of the radiation reflected from carbon dioxide deposit formed on a polished copper substrate which are reported in Figure 40. It is observed in Figure 40 that an off-specular shift occurs at the deposit thicknesses of 122.5μ and 157.5μ which are slightly greater than 100μ. However, the off-specular peaks are not pronounced which can be explained in the following way.

At a deposit thickness above 100μ the amount of radiation reflected from the vacuum-deposit interface is small compared to the sum of that reflected from the substrate and from the deposit by internal scattering. Only the reflection from the interface can result in off-specular peaks since the polished copper substrate is a specular reflector. Thus, no significant off-specular peaks are observed above a deposit thickness of 100μ.

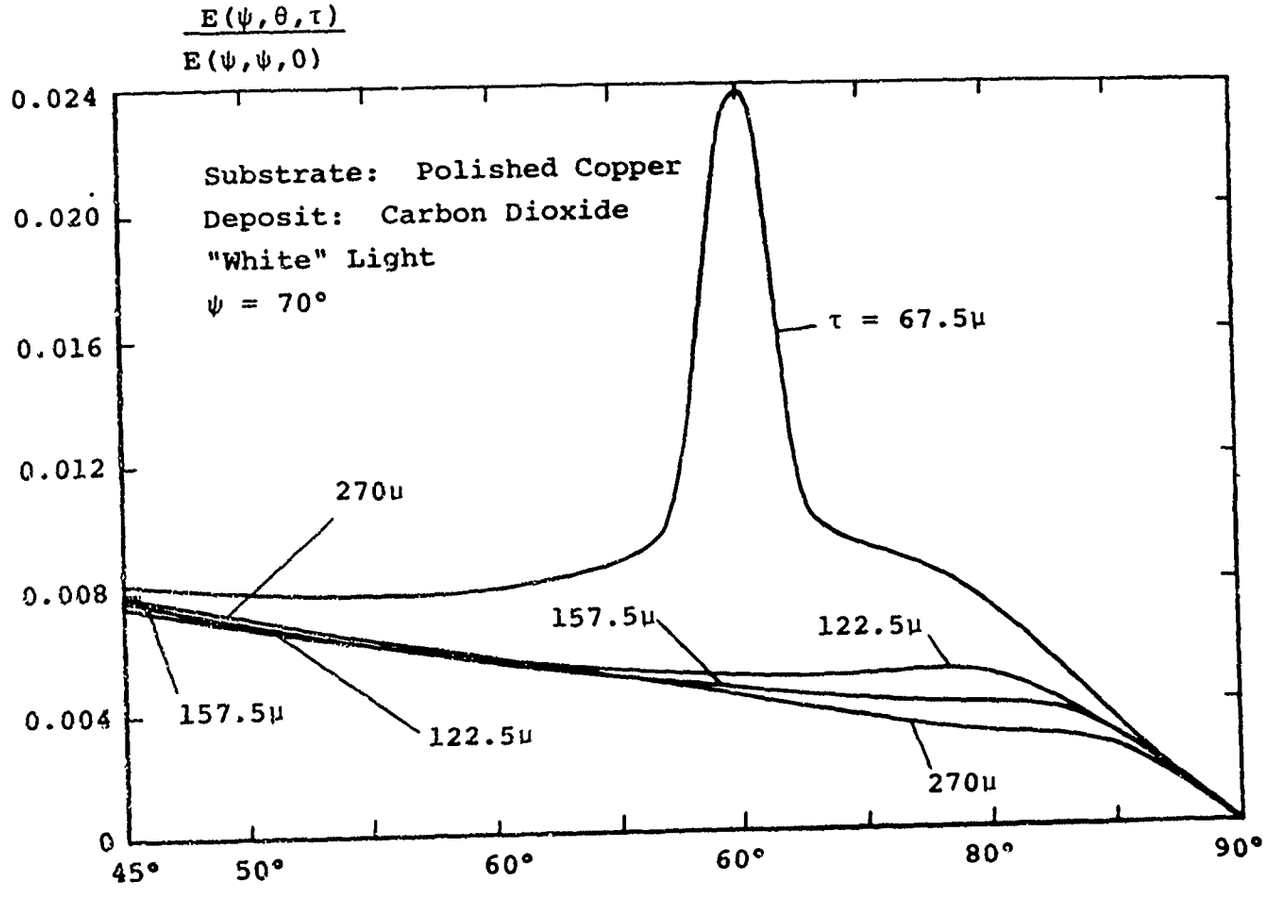

Figure 40. Off-specular maxima in the biangular distributions of "white" light reflected from carbon dioxide deposit formed on a polished copper substrate, ψ = 70° (preliminary tests).

Below a deposit thickness of 100μ no off-specular shift occurs, but this is not necessarily due to the fact that the amount of radiation reflected from the interface is much smaller than that reflected from the substrate, because specular reflection off the interface is also possible, since the interface is, for a small deposit thickness (on the order of 1μ) approximately as smooth as the polished copper substrate. This can be concluded from the relatively large amplitude of the thin film interference pattern which indicates strong reflection off the interface in specular direction. But still the peak of the distribution at the specular angle is essentially due to reflection from the polished copper at small deposit thickness. This peak decreases with increasing deposit thickness due to internal scattering inside the deposit and thus extinction of the beam transmitted through the deposit.

At a deposit thickness of 50μ, it is observed in Figures 13 and 14, pages 57 and 58, that the magnitude of the peak is smaller at an angle of incidence of 55° than at 66°. The question arises if this specular peak at an angle of incidence of 66° is still due to reflection from the substrate or if the specular peak is mainly due to reflection from the vacuum-deposit interface, since at the greater angle of incidence the path-length of the transmitted beam inside the deposit is slightly

longer. This should result in greater extinction of the transmitted beam if it is assumed that the extinction coefficient is independent of the direction of the beam inside the deposit. In order to check if this assumption is reasonable at an angle of incidence of 55° and 66°, biangular distributions obtained at a deposit thickness of 50μ and at angles of incidence of 11°, 33°, 55°, and 66° are normalized with the same factor. These distributions are shown in Figure 41. Using the assumption made before that radiation reflected far from the specular direction is mostly due to internal scattering in the deposit so that radiation reflected at viewing angles θ between -90° and +40° represents essentially internally scattered light, it can be concluded from Figure 41 that the scattering coefficient and thus the extinction coefficient is approximately equal at both angles of incidence which proves the assumption made before. Thus, it can be reasoned that the peak of the distribution of the reflected radiation at a deposit thickness of 50μ and at an angle of incidence of 66° is due to reflection from the vacuum-deposit interface.

At a deposit thickness of 67.5μ as seen in Figure 40, page 105, and at a deposit thickness of 100μ as seen in Figure 14, page 58, the specular peak is observed at a high angle of incidence. As before it can be reasoned that this peak is due to reflection from the smooth

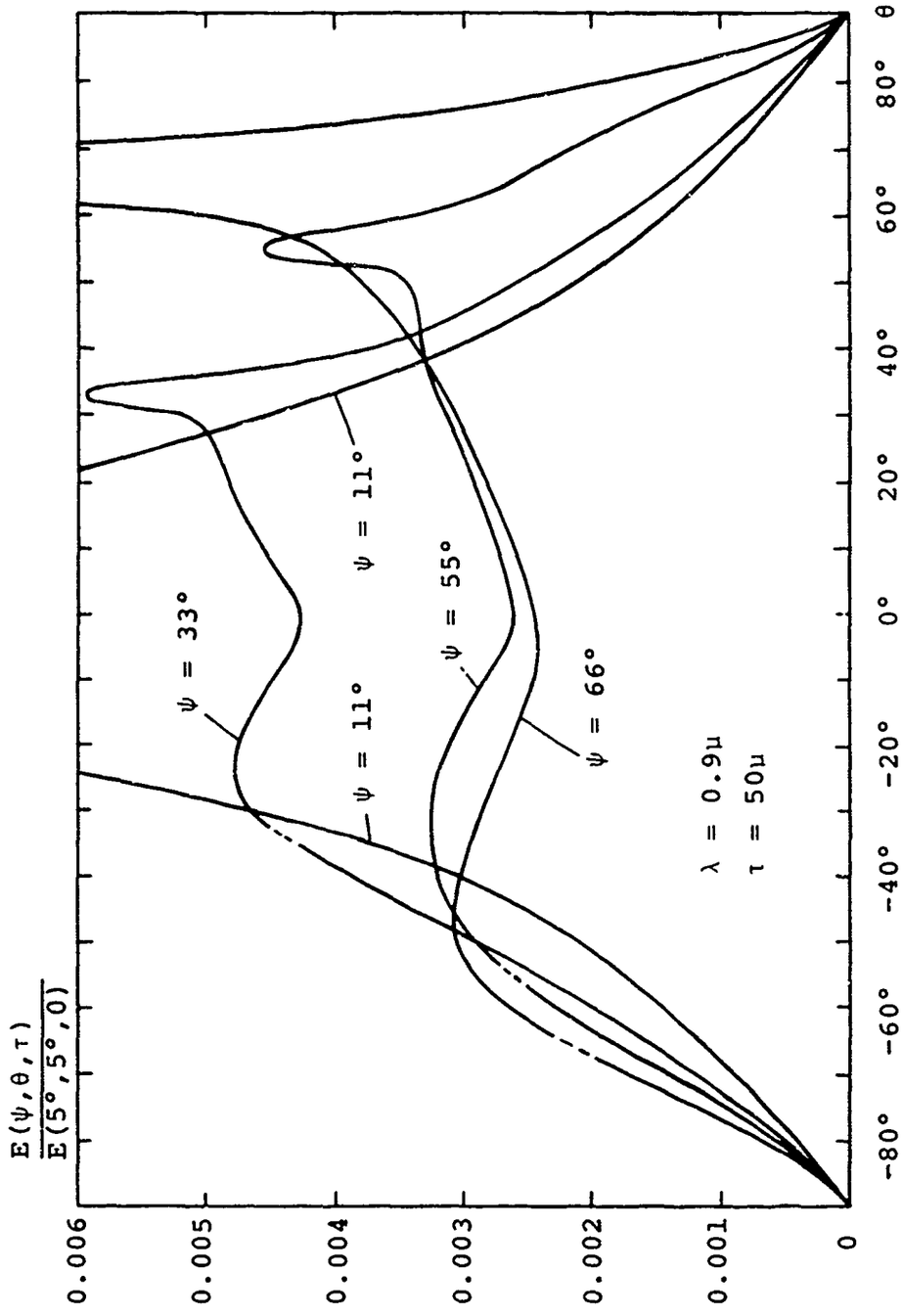

Figure 41. Biangular distributions of radiation reflected from carbon dioxide deposit formed on a polished copper substrate at various angles of incidence.

interface. Above a thickness of 100μ, the specular peak decreases quickly, and at a thickness of 122.5μ an off-specular peak appears which was mentioned before. This off-specular peak suggests that between a thickness of 100μ and 122.5μ the interface becomes relatively rough.

The smooth interface up to a deposit thickness of 100μ was not observed, when carbon dioxide was formed on the black paint substrate, even though the deposition rate and deposition pressure were equal in both cases. This was expected since, compared to the polished copper, the black paint is relatively rough; and thus the deposit interface is comparably rough even at small thickness.

7. Water deposit formed on a polished copper substrate. No off-specular shift is observed from the distributions of radiation reflected from water deposit formed on a polished copper substrate, as seen in Figures 15 through 18, pages 59 through 62, since the interface of a water deposit is very smooth at great deposit thickness as was shown before. At low deposit thickness the influence of the substrate on the reflected radiation is stronger than in the case of carbon dioxide cryodeposit because water deposit shows less internal scattering and thus less extinction of the transmitted beam through the deposit than encountered with carbon dioxide.

The influence of the wavelength on the distribution of the reflected radiation is obtained by comparison of Figure 15, page 59, with Figure 17, page 61, and Figure 16, page 60, with Figure 18, page 62. It is observed that with decreasing wavelength λ, the magnitude of the specular peak decreases. This can be explained as follows.

As stated before the radiation reflected from the cryodeposit is due to reflection from the vacuum-deposit interface, due to reflection from the substrate, and due to internal scattering in the deposit. It was found before that the amount of radiation reflected due to internal scattering decreases if λ increases which was observed from measurements of the radiation reflected from cryodeposits formed on a black paint substrate. This influence of wavelength on the radiation reflected by internal scattering is not as well shown by the measurements of the radiation reflected from cryodeposits formed on a polished copper substrate. Radiation reflected off the substrate is transmitted twice through the interface, and this radiation as well as the radiation reflected off the interface is more diffuse if σ/λ increases (λ decreases), as is shown by Müller in (15). Increasing 'diffusenses" of the distribution results in decreasing magnitude of the peak of the distribution. Hence, the magnitude of the peak of the distribution decreases if λ decreases.

CHAPTER III

CONCLUSIONS

I. MEASUREMENTS OF REFRACTIVE INDEX AND DENSITY

Measurements of the refractive index and density of cryodeposits show that the Lorenz-Lorentz law, Equation (1)

$$\frac{\mu^2 - 1}{\mu^2 + 2} \cdot \frac{1}{\rho} = \text{constant}$$

is also valid for cryodeposits. Since the deposition pressure in the tests was very low as was the partial pressure of the foreign gases, it can be reasoned that only a small amount of foreign gases was trapped by the deposit. Thus, the Lorenz-Lorentz constant of the cryodeposit at a deposition pressure of 4×10^{-4} mm Hg is that of the pure substance.

II. MEASUREMENTS OF BIANGULAR DISTRIBUTIONS OF THE RADIATION REFLECTED FROM CRYODEPOSITS

The biangular distributions of the radiation reflected from cryodeposits show that cryodeposits change the reflective properties of cold panels where they are formed. While the biangular distribution of the radiation reflected from carbon dioxide at a deposit thickness of

300μ is essentially "diffuse," the biangular distribution of the radiation reflected from water has a strong peak with a small off-specular shift at great deposit thickness (0.5 mm).

A. Carbon Dioxide Deposit Formed on a Black Paint Substrate

The off-specular shift seems to be independent of the deposition rate ($0.0011\mu/\text{sec} \leq \dot{\tau} \leq 0.016\mu/\text{sec}$; 6×10^{-5} mm Hg $\leq p \leq 4 \times 10^{-4}$ mm Hg).

The off-specular shift increases with the deposit thickness up to a thickness of approximately 50μ. Then the shift remains constant up to a thickness of approximately 160μ at an angle of incidence of 66°. Above a thickness of 160μ the distribution of the reflected radiation becomes diffuse.

B. Carbon Dioxide Deposit Formed on a Polished Copper Substrate

No off-specular shift is observed below a thickness of 100μ. It is shown that the specular reflection at a thickness between 50μ and 100μ is due to the vacuum-deposit interface which is rather smooth.

At a thickness of 100μ an off-specular peak emerges. Off-specular shift is observed between a thickness of 100μ and 150μ. Above 150μ the distribution becomes "diffuse."

C. Water Deposit Formed on a Black Paint Substrate

The off-specular shift shows no systematic influence of the deposition rate. It is felt that the change of off-specular shift due to a different deposition rate is smaller than the accuracy of the measurement.

The peak of the biangular distribution increases with increasing deposition rate. Thus the vacuum-deposit interface becomes smoother with increasing deposition rate ($0.012\mu/\text{sec} \leq \dot{\tau} \leq 0.098\mu/\text{sec}$; 1×10^{-4} mm Hg $\leq p \leq$ 7×10^{-4} mm Hg).

D. Water Deposit Formed on a Polished Copper Substrate

No off-specular shift is observed. The peak of the biangular distribution increases with increasing wavelength.

III. CARBON DIOXIDE DEPOSIT

It can be concluded that carbon dioxide forms a rough interface except at small thickness if carbon dioxide is deposited on a smooth substrate. The deposit seems to be crystalline.

IV. WATER CRYODEPOSIT

It can be concluded that water forms an interface which is rather smooth at great deposit thickness (0.5 mm). The deposit appears to be amorphous or to contain small crystals.

BIBLIOGRAPHY

1. Wood, B. E., A. M. Smith, and B. A. McCullough. "The Spectral Reflectance of Water and Carbon Dioxide Cryodeposits from 0.36 to 1.15 Microns," Arnold Engineering Development Center TR-67-131, Arnold Air Force Station, Tennessee, August, 1967.

2. Tempelmeyer, K. E., P. R. Müller, and A. M. Smith. "Angular Distribution of Radiation Reflected from Carbon Dioxide Cryodeposits Formed on 77°K Surfaces," Arnold Engineering Development Center TR-68-46, Arnold Air Force Station, Tennessee, April, 1968.

3. Tempelmeyer, K. E., B. E. Wood, and D. W. Mills, Jr. "In Situ Measurement of Thickness and Other Properties of Carbon Dioxide Cryodeposits by Optical Techniques," Arnold Engineering Development Center TR-67-226, Arnold Air Force Station, Tennessee, December, 1967.

4. Tempelmeyer, K. E., A. M. Smith, P. R. Müller, and B. E. Wood. "In Situ Angular Distribution Measurements of Visible and Near IR Radiation Reflected from CO_2 Cryodeposits Formed on LN_2-Cooled Surfaces within a Vacuum." American Institute of Aeronautics and Astronautics Paper No. 69-62, AIAA Seventh Aerospace Sciences Meeting, New York City, New York, January, 1969.

5. Born, M., and E. Wolf. Principles of Optics. Third edition. Oxford: Pergamon Press, Ltd., 1964.

6. Weast, R. C., and S. M. Selby (editors). Handbook of Physics and Chemistry. 48th edition. Cleveland: The Chemical Rubber Company, 1967.

7. Caren, R. P., A. S. Gilcrest, C. A. Zierman, W. F. Schmidt and J. P. Millard. "Experimental and Analytical Investigation of the Effect of Cryodeposits on the Radiation Properties of Plain and Extended Surfaces," Arnold Engineering Development Center TR-63-270, Arnold Air Force Station, Tennessee, December, 1963.

8. Mass, O., and W. H. Barnes. "Some Thermal Constants of Solid and Liquid Carbon Dioxide," Proceedings of the Royal Society of London, 3 (Series A): 224-244, 1926.

9. Torrance, K. E., E. M. Sparrow, and R. C. Birkebak. "Polarization, Directional Distribution, and Off-Specular Peak Phenomena in Light Reflected from Roughened Surfaces," Journal of the Optical Society of America, 56:916-924, July, 1966.

10. Wood, B. E. Private communication. Arnold Engineering Development Center, Arnold Air Force Station, Tennessee, December, 1968.

11. Dunkle, R. V., and J. T. Bevans. "An Approximate Analysis of the Solar Reflectance and Transmittance of a Snow Cover," Journal of Metereology, 13:212-216, 1956.

12. Dorsey, N. E. Properties of Ordinary Water-Substance. New York: Reinhold Publishing Corporation, 1940.

13. Blass, G. A. Theoretical Physics. New York: Meredith Publishing Company, 1962.

14. Sparrow, E. M., and R. D. Cess. Radiation Heat Transfer. Belmont: Brooks, Cole Publishing Company, 1966.

15. Müller, P. R. "Measurements of Refractive Index, Density, and Reflected Light Distributions for Carbon Dioxide and Water Cryodeposits and also Roughened Glass Surfaces," Ph.D. dissertation, University of Tennessee, June, 1969.

16. Thun, E. Structure of Thin Films. Vol. I of Physics of Thin Films. G. Hass, editor. New York: Academic Press, Inc., 1963.

17. Bannister, T. C., and B. E. Richard. "Microscopic Observation of Interfacial Phenomena." American Institute of Aeronautics and Astronautics Paper No. 69-95, AIAA Seventh Aerospace Sciences Meeting, New York City, New York, January, 1969.

18. Owston, P. G. "The Structure of Ice I, as Determined by X-Ray and Neutron Diffraction Analysis," Advances in Physics, 7:171-188, 1958.

19. Burton, E. F., and W. F. Oliver. "The Crystal Structure of Ice at Low Temperatures," Proceedings of the Royal Society of London, 153 (Series A): 166-172, 1936.

20. Blackman, M., and N. D. Lisgarten. "The Cubic and Other Structural Forms of Ice at Low Temperature and Pressure," Proceedings of the Royal Society of London, 239 (Series A): 93-107, 1957.

21. Graf, R., and J. Paulon. "Étude Radiocrystallographic de la Structure d'un Cryodepôt de CO_2." Extrait de la Recherche Aérospatiale, No. 123, March-April, 1968.

APPENDIXES

APPENDIX A

ERROR ANALYSIS OF THE MEASUREMENT OF THE REFRACTIVE INDEX AND DENSITY

The refractive index is computed from Equation (7)

$$\mu^2 = \frac{\sin^2\psi_b - \left(\frac{\Delta t_a}{\Delta t_b}\right)^2 \sin\psi_a}{1 - \left(\frac{\Delta t_a}{\Delta t_b}\right)^2}$$

This equation is differentiated implicitly.

$$\frac{\delta\mu}{\mu} = \frac{\sin\psi_b \cdot \delta(\sin\psi_b) - \sin\psi_a \cdot \left(\frac{\Delta t_a}{\Delta t_b}\right)^2 \delta(\sin\psi_a) - \sin^2\psi_a \cdot \left(\frac{\Delta t_a}{\Delta t_b}\right) \cdot \left(\frac{\Delta t_a}{\Delta t_b}\right)}{\sin^2\psi_b - \left(\frac{\Delta t_a}{\Delta t_b}\right)^2 \sin^2\psi_a}$$

$$+ \frac{\left(\frac{\Delta t_a}{\Delta t_b}\right) \delta\left(\frac{\Delta t_a}{\Delta t_b}\right)}{1 - \left(\frac{\Delta t_a}{\Delta t_b}\right)^2} \qquad (40)$$

By isolating the terms

$$\frac{\delta(\sin\psi_b)}{\sin\psi_b}, \qquad \frac{\delta(\sin\psi_a)}{\sin\psi_a}, \qquad \frac{\delta\left(\frac{\Delta t_a}{\Delta t_b}\right)}{\left(\frac{\Delta t_a}{\Delta t_b}\right)}$$

Equation (40) is written in a different form.

$$\frac{\delta\mu}{\mu}\left[1 - \left(\frac{\Delta t_a}{\Delta t_b}\right)^2\right] = \frac{1}{\mu^2}\left[\sin^2\psi_b \frac{\delta(\sin\psi_b)}{\sin\psi_b}\right.$$

$$\left. - \sin^2\psi_a \left(\frac{\Delta t_a}{\Delta t_b}\right)^2 \frac{\delta(\sin\psi_a)}{\sin\psi_a} + \frac{\delta\left(\frac{\Delta t_a}{\Delta t_b}\right)}{\frac{\Delta t_a}{\Delta t_b}}\right]$$

$$+ \left(\frac{\Delta t_a}{\Delta t_b}\right)^2 \frac{\delta\left(\frac{\Delta t_a}{\Delta t_b}\right)}{\frac{\Delta t_a}{\Delta t_b}} \qquad (41)$$

The angle of incidence is estimated to be accurate within

$$\delta\psi_b = \pm 0.25° \quad \text{at} \quad \psi_b = 55°$$

$$\delta\psi_a = \pm 0.25° \quad \text{at} \quad \psi_a = 33°$$

The magnitude of

$$\frac{\delta(\sin\psi_b)}{\sin\psi_b} \quad \text{and} \quad \frac{\delta(\sin\psi_a)}{\sin\psi_a}$$

is then computed at these angles ψ_a and ψ_b.

$$\frac{\delta(\sin\psi_b)}{\sin\psi_b} = \frac{\cos\psi_b \cdot \delta\psi_b}{\sin\psi_b} = \pm 0.00306 \text{ radians}$$

$$\frac{\delta(\sin\psi_a)}{\sin\psi_a} \quad \frac{\cos\psi_a \cdot \delta\psi_a}{\sin\psi_a} = \pm 0.00671 \text{ radians}$$

The accuracy of the measurement of $(\frac{\Delta t_a}{\Delta t_b})$ is estimated to be

$$\frac{\delta(\frac{\Delta t_a}{\Delta t_b})}{\frac{\Delta t_a}{\Delta t_b}} = \pm 0.005$$

As it is usual practice in error analysis calculations, each term in Equation (41) is squared to make it positive, so that a good estimate of the accuracy of $\frac{\delta\mu}{\mu}$ is obtained. The value of $\frac{\Delta t_a}{\Delta t_b}$ is in all measurements close to 0.76.

For water cryodeposit with a refractive index $\mu = 1.26$, it is obtained that $\frac{\delta\mu}{\mu} = \pm 0.0101$ and thus

$$\mu = 1.26 \pm 0.013$$

The refractive index of carbon dioxide deposit is close to 1.46 which leads to $\frac{\delta\mu}{\mu} = \pm 0.0097$ so that

$$\mu = 1.46 \pm 0.014$$

The deposition rate $\dot{\tau}$ is calculated from Equation (8)

$$\dot{\tau} = \frac{\lambda}{\Delta t_a \cdot 2\mu \sqrt{1 - \frac{\sin^2\psi_a}{\mu^2}}}$$

For an estimate of the accuracy of the computed deposition rate $\dot{\tau}$, it can be assumed that

$$1 - \frac{\sin^2 \psi_a}{\mu^2} \approx 1$$

even if $\psi_a = 33°$. Thus Equation (8) is simplified for further computation.

$$\dot{\tau} \approx \frac{\lambda}{2\mu \cdot \Delta t_a} \tag{42}$$

Equation (42) is differentiated

$$\frac{\delta\dot{\tau}}{\dot{\tau}} \approx \frac{\delta\lambda}{\lambda} - \frac{\delta\mu}{\mu} - \frac{\delta(\Delta t_a)}{\Delta t_b}$$

and, like in the computation of $\frac{\delta\mu}{\mu}$ before, each term of the equation is squared.

$$\left(\frac{\delta\dot{\tau}}{\dot{\tau}}\right)^2 = \left(\frac{\delta\lambda}{\lambda}\right)^2 + \left(\frac{\delta\mu}{\mu}\right)^2 + \left(\frac{\delta\Delta t_a}{\Delta t_a}\right)^2 \tag{43}$$

The wavelength λ of the peak of the filter transmission is very accurately known so that

$$\frac{\delta\lambda}{\lambda} \approx 0$$

The accuracy of the measurement of the time between two interference maxima was estimated before to be

$$\frac{\delta(\Delta t_a)}{\Delta t_a} = \pm 0.005$$

and $\frac{\delta\mu}{\mu}$ was computed before. These values are introduced into Equation (43), and it is obtained for water cryodeposit

$$\frac{\delta\dot{\tau}}{\dot{\tau}} = \pm 0.0113$$

and carbon dioxide deposit

$$\frac{\delta\dot{\tau}}{\dot{\tau}} = \pm 0.0109$$

The density of the cryodeposit is calculated from Equation (16)

$$\rho = \frac{\dot{m}}{A \cdot \dot{\tau}}$$

Differentiation and squaring of each term leads to

$$\left(\frac{\delta\rho}{\rho}\right)^2 = \left(\frac{\delta\dot{m}}{\dot{m}}\right)^2 + \left(\frac{\delta A}{A}\right)^2 + \left(\frac{\delta\dot{\tau}}{\dot{\tau}}\right)^2 \qquad (44)$$

A can be measured very accurately so that it can be assumed that

$$\frac{\delta A}{A} \cong 0$$

The accuracy of $\dot{\tau}$ was obtained before. For water vapor the flow rate $\dot{m}$ of the gas addition system is estimated to be accurate within two percent, so that

$$\frac{\delta\dot{m}}{\dot{m}} = \pm 0.02$$

The gas flow rate $\dot{m}$ of carbon dioxide is proportional to the reservoir pressure which is measured with a Wallace-Tiernan gauge. Its accuracy is estimated to be one percent.

$$\frac{\delta p}{p} = \pm 0.01$$

and thus

$$\frac{\delta\dot{m}}{\dot{m}} = \pm 0.01$$

These values are introduced into Equation (44), and it is obtained for water cryodeposit

$$\frac{\delta\rho}{\rho} = \pm 0.023$$

$$\rho = 0.81 \pm 0.017 \text{ gr/cm}^3$$

and for carbon dioxide cryodeposit

$$\frac{\delta\rho}{\rho} = \pm 0.0148 \,, \qquad \rho = 1.67 \pm 0.029 \text{ gr/cm}^3$$

APPENDIX B

EQUIPMENT USED FOR THE TESTS

Measurements on Cryodeposits

Mechanical Pump:

Duo-Seal Vacuum Pump
Serial No. 0071-97
Welch Manufacturing Company

Diffusion Pump:

Oil Diffusion Pump
Type 0162
NRC Equipment Corporation

Thermal Ionization Gauge:

Vacuum Products Division Cooke, Inc.
Norwalk, Connecticut

Alpha Radiation Ionization Gauge:

Type 530
NRC Equipment Corporation
Newton, Massachusetts

Thermocouple Gauge:

Model SV-1
Hastings Company
Hampton, Virginia

Power Supply for Xenon-Arc Lamp:

Model CXMA 6500-4S
Christie Electric Corporation
Los Angeles, California

X-Y Plotter:

Model 2DR-2A
Moseley Company
Pasadena, California

Strip-Chart Recorder:

Electronic 19
Honeywell
Industrial Products Group
Philadelphia, Pennsylvania

The black paint used as a substrate was Cat-a-lac Black, a registered trademark of Finch, Paint and Chemical Company, Torrance, California.

UNCLASSIFIED

Security Classification

DOCUMENT CONTROL DATA - R & D

(Security classification of title, body of abstract and indexing annotation must be entered when the overall report is classified)

1. ORIGINATING ACTIVITY (Corporate author)	2a. REPORT SECURITY CLASSIFICATION
Arnold Engineering Development Center ARO, Inc., Operating Contractor Arnold Air Force Station, Tennessee	UNCLASSIFIED
	2b. GROUP N/A

3. REPORT TITLE

MEASUREMENTS OF REFRACTIVE INDEX, DENSITY, AND REFLECTED LIGHT DISTRIBUTIONS FOR CARBON DIOXIDE AND WATER CRYODEPOSITS

4. DESCRIPTIVE NOTES (Type of report and inclusive dates)

October 1967 through December 1968 - Final Report

5. AUTHOR(S) (First name, middle initial, last name)

Peter R. Müller and Walter Frost, The University of Tennessee Space Institute, and A. M. Smith, ARO, Inc.

6. REPORT DATE	7a. TOTAL NO. OF PAGES	7b. NO. OF REFS
September 1969	141	21

8a. CONTRACT OR GRANT NO	9a. ORIGINATOR'S REPORT NUMBER(S)
F40600-69-C-0001	
b. PROJECT NO 8951	AEDC-TR-69-179
c. Program Element 61102F	9b. OTHER REPORT NO(S) (Any other numbers that may be assigned this report)
d	N/A

10. DISTRIBUTION STATEMENT

This document has been approved for public release and sale; its distribution is unlimited.

11. SUPPLEMENTARY NOTES	12. SPONSORING MILITARY ACTIVITY
Available in DDC	Arnold Engineering Development Center, Air Force Systems Command Arnold Air Force Station, Tennessee

37389

13. ABSTRACT

By using interference techniques, the density and the refractive index as a function of the wavelength of water and carbon dioxide cryodeposit formed at a temperature of 77°K and a deposition pressure of about 4×10^{-4} mm Hg have been measured. It is shown that the Lorenz-Lorentz constant

$$\frac{\mu^2-1}{\mu^2+2} \cdot \frac{1}{\rho} = \text{const } (\lambda)$$

at a certain wavelength computed from the refractive index and density of the cryodeposit is equal to that of the same substance at different temperature and phase, but at the same wavelength. Biangular distributions of the radiation reflected from water and carbon dioxide deposit formed at 77°K on polished copper and black paint substrates have been obtained for various deposit thicknesses and monochromatic light of $\lambda = 0.7\mu$ to 1.0μ. The influence of the deposition rate and of the wavelength of the radiation on the biangular distributions and also on the off-specular shift of the peak of the reflected radiation are investigated. Thus conclusions are drawn about the roughness of the vacuum-deposit interface of the cryodeposit. It is found that water forms a quite smooth interface, while the interface of carbon dioxide is rather rough.

DD FORM 1 NOV 68 1473

UNCLASSIFIED

Security Classification

14. KEY WORDS	LINK A		LINK B		LINK C	
	ROLE	WT	ROLE	WT	ROLE	WT
cryogenics						
refractive index						
density measurement						
reflectivity						
carbon dioxide						
water						
deposits						
wavelengths						
vacuum apparatus						

AFSC
Arnold AFS Tenn